Numerical Study of Louver Cooling Scheme on Gas Turbine Airfoils

Xuezhi Zhang

A Thesis

in

The Department

of

Mechanical and Industrial Engineering

Presented in Partial Fulfillment of the Requirements
for the Degree of Doctor of Philosophy at
Concordia University
Montreal, Quebec, Canada

June 2008

Your file Votre référence
ISBN: 978-0-494-45686-6
Our file Notre référence
ISBN: 978-0-494-45686-6

Abstract

Numerical Study of Louver Cooling Scheme on Gas Turbine Airfoils

Xuezhi Zhang, Ph.D.

Concordia University, 2008

This work presents the performance of a louver film-cooling scheme under different operating conditions. The louver cooling scheme consists of a bend by which the coolant going through the flow passage is redirected from vertical to horizontal direction before being injected into the mainstream through an expanded exit. Not only is the momentum of the coolant converted to the mainstream direction, but it is also reduced by the expanded exit before injection. The impingement of the coolant on the blade surface inside the bend also enables further cooling on the targeted surface. The louver cooling scheme was tested under a variety of conditions, from a flat plate to airfoils, from low speed incompressible flows to transonic flows, from a stationary airfoil to a rotating airfoil, and from the leading edge to the middle of an airfoil. Unsteady analysis using a DES (Detached Eddy Simulation) model was also carried out to evaluate its ability to accurately simulate film cooling by comparing with steady state analysis.

In general, the louver cooling scheme has been proved to provide enhanced cooling protection to the targeted surface in comparison with other cooling schemes in all conditions tested. At low speed incompressible flow conditions, a higher blowing ratio led to a higher cooling effectiveness. At transonic flow conditions, a moderately higher blowing ratio also proved helpful with a higher cooling effectiveness. Very high blowing ratios, however, proved to be detrimental to the cooling performance since strong

detached shock wave structures due to high blowing ratios caused boundary layer separation, rendering the coolant virtually ineffective. The rotation of blade was found to have a significant impact on the level of cooling effectiveness at the leading edge of an airfoil. With regard to the cooling performance, blowing ratio was the dominant factor at low rotational speeds and the rotational speed was the dominant factor at high blowing ratios for circular holes. For the louver scheme as jet liftoff was avoided, effectiveness increased with rotating speed. Results also showed that, unsteady analysis was not significantly more accurate than steady analysis. The unsteady analysis did capture the coolant lateral spreading better, with a high cost of computing, however.

Results in this work show that shock waves encountered on transonic airfoils had a significant impact on film cooling effectiveness on any shaped holes. Therefore, experimental data obtained under low speed test should be used with great caution in real design of turbine blade cooling. There are fundamental differences in film cooling between at the leading edge and elsewhere on an airfoil in that a slight incidence shifting due to turbine rotating speed may cause a sudden decrease in cooling effectiveness level at high blowing ratios for circular hole. This could lead to a catastrophic failure if the blade is already in a weak and stressed state. Using of shaped holes with expanded exits may prevent this from happening.

Acknowledgements

This work would never have been possible without the help of a number of people who, in one way or another, made their contributions during this journey. First of all, I would like to give my deepest appreciation to Dr. Hassan, my supervisor and mentor who has been my source of guidance, suggestion, and support in every step of the way for more than five years (including two years for M.A.Sc. study). You are not only my mentor but also one of my best friends. Without your contribution, I would not have been where I am and what I am. I am also grateful for the support from Pratt and Whitney Canada (PWC). Particularly, the discussion with Terry Lucas and Dr. Michael Papple has made the work stronger. Secondly, I would like to thank my research colleagues in the research group at Concordia University. The graduated colleagues include Ali Andaleeb, Ariane Immarigeon, Minmi Le, Patricia Phutthavong, Minh Dang, Tariq Ahmad, and Roland Muwanga and the present members Dino Bowden, Wael Fairouz, Gaber Mohamed, Rahman Hamidur Md., Ayman Megahed, Tarek Elnady, Fan Yanfeng, and Dr. Kim. It has been such a pleasure to work with you guys. A special thank goes to Dr. Kim who has helped preparing some of the figures and editing the text in Chapter 4. Finally, I would like to thank my family members including my parents and brother for their moral support in this endeavor. My wife Jane deserves a heartfelt thank for being by my side through all the ups and downs for the past ten years. Thanks also go to my elder son Songtao for his understanding of my working during some of the weekends when we should be together fishing and riding bicycles. My second son Keven was born in the last year of the study. Even the noise he made at three o'clock in the morning rendered life much more joyful.

Table of Contents

List of Figures

Nomenclature

c	Speed of sound
C	Chord length of the airfoil, (m)
C	Axial chord length of the rotor blade, (m)
C_p	Specific heat at constant pressure, (kJ/kg·K)
d	Hydraulic diameter of hole at inlet, (m)
D.R.	Density ratio, $D.R. = \frac{\rho_j}{\rho_\infty}$
E	Total energy, (J)
h	Heat transfer coefficient, (W/m^2K), $h = \frac{q''}{T_w - T_{aw}}$
h_o	Heat transfer coefficient without film cooling, (W/m^2K), $h_o = \frac{q''}{T_w - T_\infty}$
k	Turbulent kinetic energy, (m^2/s^2)
L	Distance measured along blade surface from trailing edge of hole exit, (m)
L	Distance measured along blade surface from leading edge of airfoil, (m)
m	Blowing ratio, $m = \frac{\rho_j U_j}{\rho_\infty U_\infty}$
M	Mach number
n	Normal distance to wall, (m)
p	Pitch of holes – center-to-center hole spacing, (m)
P	Pressure, (Pa)
P_r	Molecular Prandtl number

q	Q criterion, $(\|\Omega_{ij}\|^2-\|S_{ij}\|^2)/2$, $(1/s^2)$
q"	Surface heat flux per unit area, (W/m^2)
Q	Non-dimensional Q criterion, $q(d/U_\infty)^2$
R	Gas constant, (J/kg·K)
Re_D	Reynolds number based on hole diameter, $Re_D = \frac{\rho_\infty U_\infty d}{\mu_\infty}$
s	Row spacing, (m)
t	Time, (s)
T	Temperature, (K)
u	Velocity component in the x direction, (m/s)
u_i	Averaged velocity component, (m/s)
u_i'	Fluctuating velocity component, (m/s)
v	Velocity component in the y direction, (m/s)
$\vec{v}$	Velocity vector, (m/s)
U	Velocity, (m/s)
w	Velocity component in the z direction, (m/s)
x	Stream-wise coordinate, (m)
y	Vertical coordinate, (m)
y^+	Non-dimensional wall distance, $(y^+ = \frac{\rho u_\tau y_p}{\mu})$
y_p	Coordinate normal to the wall surface, (m)
z	Span-wise coordinate, (m)

Greek Symbols

ε	Dissipation rate of turbulent kinetic energy, (m^2/s^3)

η	Local adiabatic film cooling effectiveness, $\eta = \frac{T_{oaw} - T_{o\infty}}{T_{oj} - T_{o\infty}}$
θ	Non-dimensional temperature, $\theta = \frac{T - T_j}{T_\infty - T_j}$
μ	Dynamic (laminar) viscosity, (kg/m·s)
ρ	Density, (kg/m^3)
τ	Shear stress, (Pa)
τ	Non-dimensional time, tU_∞/d
ω	Non-dimensional vorticity, $\Omega d/U_\infty$
Ω	Vorticity, $\Omega_{ij} = (u_{i,j} - u_{j,i})/2$, (1/s)

Subscripts and Superscripts

aw	Adiabatic wall
eff	Effective values
f	Conditions with film cooling
j	Refers to the jet
o	Total condition
o	Conditions in the absence of film cooling
s	Static condition
w	Wall conditions
∞	Mainstream conditions

Chapter 1

Introduction

1.1 Introduction

Modern gas turbine engines typically operate at inlet temperatures of 1800-2000 K, which is far beyond the allowable metal temperature. Film cooling becomes increasingly important in the aerospace industry in the cooling of turbine blades. Many experimental and computational studies have been conducted in order to study the cooling process of gas turbine blades, understand this complex flow and heat process, and devise the best possible cooling schemes. While a large amount of coolant provides better surface coverage downstream of the jets, using too much coolant, on the other hand, can incur a severe efficiency penalty. The designer's goal is to minimize the coolant consumption, maximize the cooling efficiency, and produce acceptable temperature and thermal stress levels on the turbine blade surface. Over the past decades, significant effort has been devoted to developing effective cooling strategies to maintain the blade temperature below the melting point of alloys. As a result, various cooling strategies have been developed such as film, impingement and multi-pass cooling.

To effectively cool the turbine blades, cooler air at high pressure is diverted from the compressors of engines. The cooler air then goes through some serpentine passages inside of the turbine blades to absorb heat by convection heat transfer. Some thin pins are usually manufactured on inside walls of the blade to enhance heat transfer. At the end, the coolant is injected into the mainstream through some discrete holes on the blade

surface, Fig. 1.1. After injected into the hot mainstream, the coolant forms a thin blanket to isolate the downstream blade surface from the hot mainstream, further reducing heat transfer. The physics of film cooling seems rather simple. However, investigation of this phenomenon proved that this was not the case. There are so many factors that could have a significant impact on film cooling performance, among which are film surface angle, hole shaping, blowing ratio, density ratio, Reynolds number, turbulence intensity level, surface roughness, blade curvature, compressibility of the working fluid, etc.. Despite decades of intensive research into this phenomenon, it has not yet been fully understood.

Film cooling has been heavily investigated during the last three decades. Publications on film cooling consist of nearly 2700 manuscripts (Bunker [1]), the majority of which have appeared in the period between 1970 and the present. All the research papers on this subject roughly fall into two categories, experimental studies and computational studies. A majority of the early studies are experimental. Only during the last two decades did ever increasingly more powerful computers in combination with turbulence modeling development make computational study more accessible. Currently, there are more CFD (Computational Fluid Dynamics) studies of film cooling than its experimental counterpart in the literature.

Experimental studies of film cooling can be categorized as measurement techniques, hole shaping, surface roughness, hole arrangements. Earlier measuring technique is mostly thermocouples which were used to measure the surface temperature when deployed on the targeted area downstream of the jet exits, Goldstein et al. [2], Sen et al. [3], Shinha et al. [4]. Later, other measuring techniques were developed for more detailed local resolution, such as mass-heat transfer analogy, Goldstein and Jin [5], Pedersen et al.

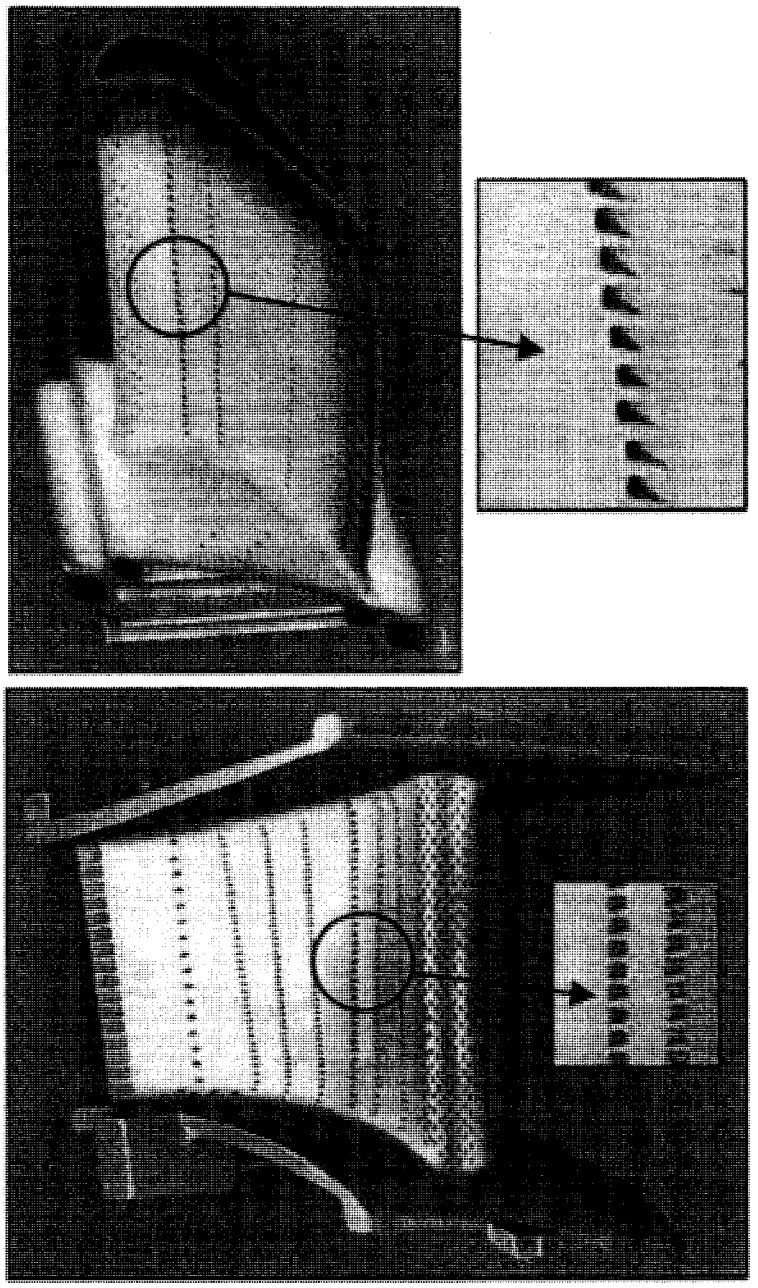

Fig. 1.1 Modern film cooled blade and vane (Bunker [1]).

[6], Cho et al. [7]; TLC (Thermochromic Liquid Crystals) technique, Sargison et al. [8], Chen et al. [9], Ahn et al. [10]; transient measurement technique, Vogel et al. [11], Ekkad and Han [12]; film cooling flow visualization, Lee et al. [13], Jung et al. [14], Jessen et al. [15]; pressure sensitive paint technique, Ahn et al. [16], Mhetras et al. [17], Gao et al. [18]; Infrared thermography technique, Schulz [19], Baldauf et al. [20]. Studies of alternatives other than using air as coolant include Li et al. [21], Li and Wang [22], Nasir et al. [23]. Hole shaping studies were done by Dittmar et al. [24], Colban et al. [25], Colban and Thole [26], Miao and Wu [27], Gritsch et al. [28], Sargison et al. [29], Taslim and Khanicheh [30], and Okita and Nishiura [31]. Other aspects of film cooling study include, but not limited to, effects of surface roughness, Rutledge et al. [32], Guo et al. [33]; surface curvature effect, Li and Wang [34], Waye and Bogard [35]; effects of turbulence intensity, Ethridge et al. [36], Al-Hamadi et al [37], Mayhew et al. [38], Saumweber et al. [39]; effect of jet pulsing, Coulthard et al. [40]; aerodynamic losses due to film cooling; Jackson et al. [41]; turbulence modeling of film cooling, Medic and Durbin [42], Garg [43], Keimasi and Taeibi-Rahni [44]; LES (Large Eddy Simulation), Guo et al. [45], Rozati and Tafti [46], Renze et al. [47]; DES (Detached Eddy Simulation), Martini et al. [48].

1.2 Motivations, objectives, and organization

Demand for higher fuel efficient engines and reliability pushes for more effective cooling designs for turbine blades. The focus of research on film cooling has been shifting from circular holes to shaped holes and from flat plate ideal cases to more realistic curved surface cases during the last two decades. Among the recently proposed cooling schemes

are laterally diffused holes Bell et al. [49], forward and lateral shaped holes Yu et al. [50], straight fan-shaped holes Dittmar et al. [24], forward-lateral-diffused holes Taslim and Khanicheh [30], Fig. 1.2, all of which have been proved to have superior cooling performance than the traditional circular holes.

An advanced louver cooling scheme was first introduced by Immarigeon and Hassan [51] as shown in Fig. 1.3. With the concept of the proposed new cooling scheme, a greater portion of the airfoil is protected. The film hole was designed in such a way that the coolant must go through a bend before exiting the blade, thus impinging on the blade material. Finally, the flow exits very close to the blade surface, minimizing aerodynamic losses. In Immarigeon and Hassan [51], the cooling performance of the louver cooling scheme was compared with a circular hole. However, due to some unfair test conditions, the advantages of the louver cooling scheme were masked. Some critics mentioned that the louver scheme had sharp corners which could cause high stress concentration and failure. In addition, four pedestals and three small inlet holes make the cooling scheme very complicated to manufacture. In the subsequent studies by Zhang and Hassan [52,53], Fig. 1.4, the louver scheme was refined, simplified, and retested under comparable conditions. The four pedestals were removed since numerical results in Immarigeon and Hassan [51] showed that the effect of pedestals on the level of film cooling effectiveness downstream of jet exit was insignificant. The three inlet holes were merged into one to make the louver cooling scheme simpler. Sharper corners were also eliminated from the design. After the redesign, and numerically tested under comparable conditions, the louver cooling scheme showed its clear advantages in the numerical predictions over other different cooling schemes proposed in recent years. This drew

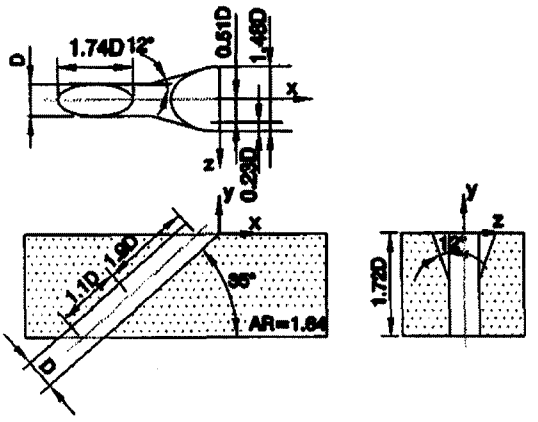

a. Laterally diffused hole,
Bell et al. [49]

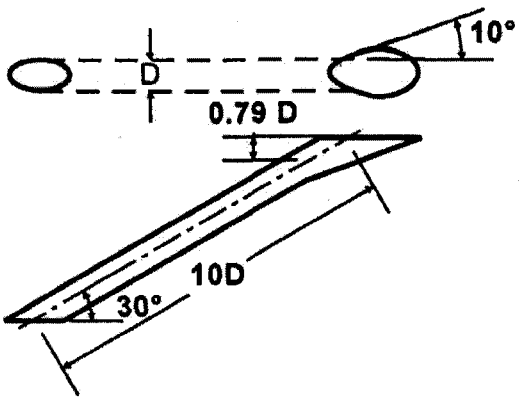

b. Forward and lateral shaped hole,
Yu et al. [50]

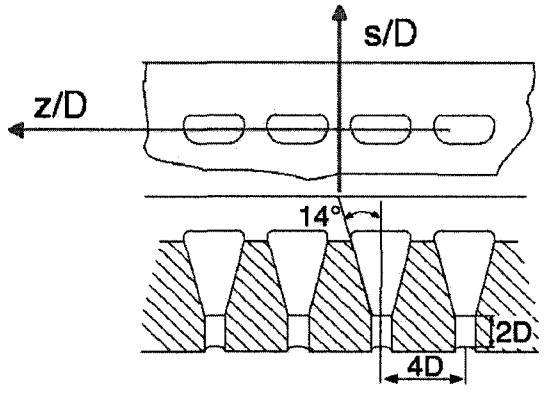

c. Straight fan-shaped holes,
Dittmar et al. [24].

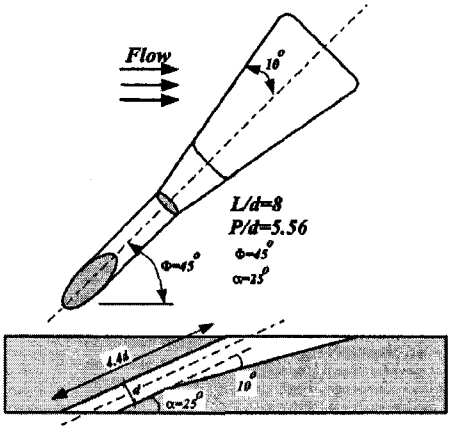

d. Forward-lateral-diffused hole,
Taslim and Khanicheh [30].

Fig. 1.2 Different cooling schemes proposed recently in the literature.

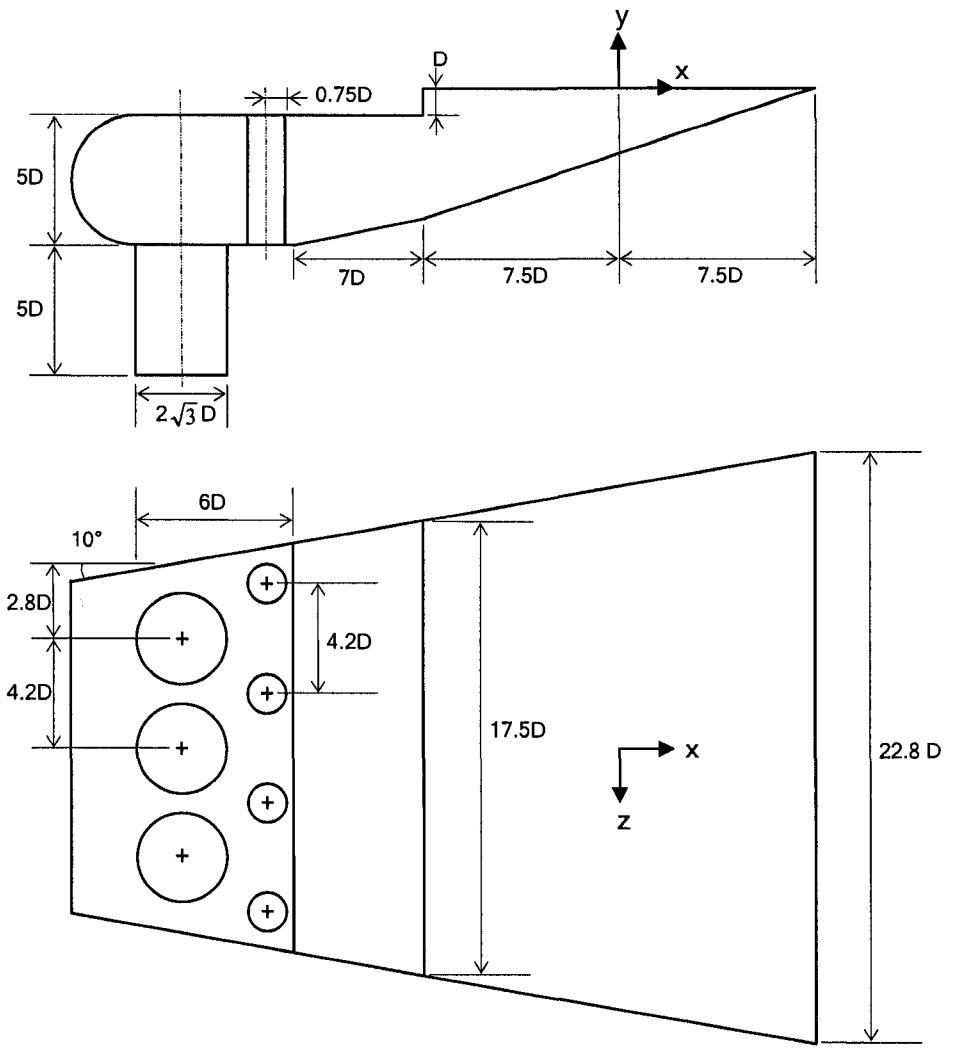

Fig. 1.3 First proposed louver cooling scheme (Immarigeon and Hassan [51]).

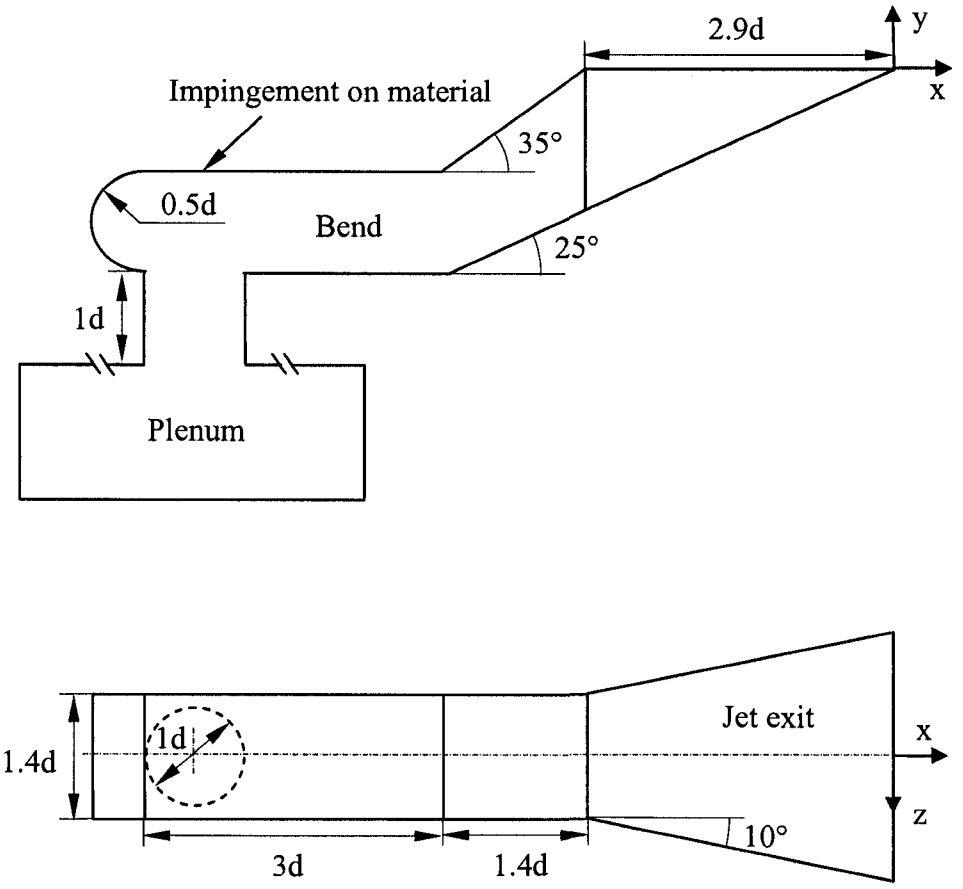

Fig. 1.4 The refined louver cooling scheme (Zhang and Hassan [52]).

wide interest in this novel cooling design in the technical community. Thus far, study of this novel cooling scheme has been limited to highly idealized conditions, i.e., a single row of holes on a flat plate under low speed conditions. Therefore, the motivation of this work is to study the refined louver cooling scheme under different and more realistic conditions. The objectives of this study are:

- To study the performance of the louver cooling scheme in multiple rows with different arrangements on a flat plate.
- To carry out an unsteady analysis of the louver cooling scheme using DES (Detached Eddy Simulation) model on a flat plate.
- To investigate the cooling performance of the louver cooling scheme on a curved surface under transonic flow conditions.
- To investigate the cooling performance of the louver cooling scheme on a rotating turbine blade at the leading edge.

Chapter 2 presents the literature review which is divided into four sections according to the objectives: multiple rows on a flat plate, unsteady analysis of film cooling, transonic film cooling, and film cooling on a rotating blade. Based on the four objectives outlined above, each section of the literature review focuses on a specific topic. Chapter 3 shows the mathematical modeling. Only the principal equations were mentioned in this chapter. More case-specific equations and modeling details were given in the corresponding chapters that follow. Nonetheless, effort was made to make as much information as possible available in each sections, from steady state modeling, unsteady

modeling, low speed incompressible flow modeling, compressible transonic flow modeling, to modeling rotating frame, in case somebody would like to reproduce the results using a different Commercial CFD code or an in-house code. Chapters 4, 5, 6, 7 present the results for each topics outlined as the objectives, i.e., multiple rows on a flat plate, unsteady analysis of the louver scheme, transonic film cooling, and film cooling on a rotating turbine blade, respectively. Finally, conclusions and recommendations are presented in chapter 8.

Chapter 2

Literature Review

In this chapter the literature survey was focused on four topics, i.e., multiple rows on a flat plate, unsteady analysis of film cooling, transonic film cooling on an airfoil, and film cooling on a rotating turbine blade, according to the objectives outlined in the proceeding chapter. As film cooling was heavily investigated, by no means is the survey exhaustive. Only articles most relevant to a specific topic were cited here. Preference was also given to the most recent publications. A summary was provided at the end.

2.1 Multiple rows on a flat plate

The majority of studies of film cooling focused on circular holes with simple or compound orientation angles. Only recently, in the last 10 to 15 years, have shaped holes received much attention. Schmidt et al. [54] and Thole et al. [55] documented that jets with expanded exits significantly reduce jet penetration and produce an improved lateral spread of the film cooling jets. Compound angles lead to increased lateral spreading of injectant. Those findings were later confirmed by Bell et al. [49] and Taslim and Khanicheh [30]. Yu et al. [50] showed that shaped holes resulted in a lower and more uniform heat transfer coefficient as compared with cylindrical holes. In contrast, Sen et al. [3] reported significantly increased heat transfer levels at high blowing ratios in holes with a large compound angle, resulting in poorer overall performance despite higher effectiveness. Lee et al. [13] recommended that the forward expanded hole be adopted in

combination with a compound angle orientation as shaped holes with simple angles do not provide substantial improvement in film cooling performance. Gritsch et al. [56] showed that laterally averaged film cooling effectiveness was found to show only limited sensitivity to variations of hole geometry and that a compound angle has some detrimental effects at high blowing ratios.

Makki and Jakubowski [57], Cho et al. [7], and Rhee et al. [58] have studied rectangular shaped holes. The rectangular holes with expanded exits reduce momentum of coolant and promote lateral spreading like two dimensional slots with an overall pronounced improvement in film cooling effectiveness over the circular holes. Saumweber et al. [39] showed that for shaped holes, the heat transfer level was highly sensitive to the blowing ratios when turbulence intensity was raised, in contrast to low sensitivity for cylindrical holes. Sargison et al. [29] studied a converging slot-hole or a console. Although the thermal performance of a console was similar to the fan shaped hole, the console had a greater advantage in terms of aerodynamic performance with the aerodynamic loss significantly less than that for shaped or circular holes.

Computational studies of shaped holes include Giebert et al. [59], Hyams and Leylek [60], and Bohn et al. [61]. Giebert et al. [59] performed simulation for a circular hole and a hole with laterally expanded exit, and a hole with forward-laterally expanded exit using a three dimensional Navier-Stokes code together with the standard k-ε model with wall function approach. Satisfactory numerical results for shaped holes with forward-laterally expanded exits in terms of the adiabatic film-cooling effectiveness was achieved. This could be a result of the absence of jet liftoff and subsequent reattachment. Hyams and Leylek [60] numerically studied five distinct film cooling configurations, circular hole,

forward-diffused hole, laterally diffused hole, inlet shaped hole, and cusp-shaped hole. It was shown that the laterally diffused hole provides the best coverage and highest cooling effectiveness and that forward diffused holes perform well along the centerline, but do not spread well laterally. Bohn et al. [61] performed numerical simulations for a circular hole and a shaped hole. It was concluded that secondary flows in the cooling jets were the main reason for the degradation of the cooling performance of a film-cooled blade. Results demonstrated that fan-shaped configurations were up to three times more effective than cylindrical configurations.

Jubran and Maiteh [62] studied two staggered rows of circular holes in different arrangements, including a combination of one row of simple angle holes with another row of compound angle holes and both rows of compound angle holes, were tested in an open suction-type wind tunnel. It turned out that the effect of row arrangement was very much dependent on the relative position of the compound and simple injection rows. Staggered arrangements of compound angle holes for two rows provide better cooling protection than inline compound angle holes. Similar trend was also found for simple angle injection rows. Ligrani et al. [63] investigated two rows of compound angle holes in a wind tunnel. The two rows of holes were in staggered arrangement with a three diameter spanwise spacing, a 35 degrees inclination angle with respect to the test surface when projected to the streamwise plane, and a 30 degrees angle with respect to the test surface when projected to the spanwise plane. It was shown that compound angle injection configurations provided significantly improved protection as compared with simple angle configurations.

Ahn et al. [10] carried out an experimental study of two rows of holes with opposite orientation angles. Four film hole arrangements either inline or staggered were considered. The holes were positioned six diameters apart and row spacing was set at four diameters. All holes had a 35 degrees surface angle. The hole arrangements were put into an open subsonic wind tunnel to be tested under four blowing ratios of 0.5, 1.0, and 2.0. Results showed that at the low blowing ratio of 0.5 the coolant was centered near the surface regardless of configuration with a higher cooling effectiveness level. At higher blowing ratios of 1.0 and 2.0, the downwash flow at the hole exit made the coolant well attached to the wall to yield a high cooling effectiveness level, while the upwash flow deteriorated the cooling effectiveness. Yuen and Martinez [64,65] investigated experimentally rows of circular holes with streamwise angles of 30, 60, and 90 degrees on a flat plate. They concluded that staggered rows of holes improved the span-wise uniformity in cooling effectiveness, but the heat transfer levels were higher than those of the inline rows with the same pitch ratio.

Maiteh and Jubran [66] did an experimental investigation into the effect of pressure gradient on film cooling effectiveness from two rows of circular holes. The injection configurations included five arrangements. Each consisted of two rows of holes arranged either staggered or inline. All holes were 13 mm in diameter with a simple 35 degrees surface angle. In addition, some holes had a 30 degrees compound angle when compound angle holes were involved in the test. The presence of a favorable pressure gradient tended to increase the dilution of the injected coolant, leading to a reduction of cooling effectiveness over the surface. As other studies, the two staggered rows arrangement provides a better and more uniform cooling protection than that of the two inline rows.

Dittmar et al. [24] compared the performance of double rows of circular hole and slots both in staggered arrangement against that of single row of fan-shaped hole with and without a compound angle. The experiments were conducted in an open loop wind tunnel and the Reynolds number was 7,330 based on the injection hole diameter. It was found that all configurations showed similar film cooling effectiveness at low blowing ratios. At high blowing ratios, fan-shaped hole showed a higher cooling effectiveness level. Double rows of discrete slots provided better effectiveness at high blowing ratios than circular holes. Double rows configurations also showed decreased heat transfer levels.

Bergeles et al. [67] conducted an investigation into double-row discrete-hole cooling arrangements. Holes of 19.05 mm inner diameter were machined on the test plate with a 30 degrees surface angle. The lateral and streamwise distance between adjacent hole centers were 2.67 and 3.5 diameters, respectively. The test plate was then installed in an open circuit wind tunnel to be tested. It was demonstrated that the mean effectiveness downstream of holes increased monotonically as the blowing ratio was raised up to one due to the fact that the stream-wise vorticity field created by the leading row of jets kept the second row of jets impressed on the surface. Numerical simulation was also carried out using a three-dimensional finite-difference code that embodied a semi-elliptic treatment of the flow field in conjunction with a two-equation turbulence model. For low blowing ratios, the film cooling effectiveness levels were well predicted even beyond about 10 diameters behind the leading row of holes. However, the discrepancies between the prediction and the experimental data became apparent as the blowing ratio was increased.

Amer et al. [68] did a computational study of film cooling from two rows of holes using different turbulence models. The capability of four turbulence models in the prediction of cooling effectiveness were evaluated against experimental data, including a k-ε model, a modified version of k-ε model, a k-ω model, and a modified k-ω model. The results showed that the ability of any turbulence model to predict satisfactorily the film cooling effectiveness and velocity profiles for two rows of holes was heavily dependent on the blowing ratio in question as well as on the distance downstream from the injection holes. It was suggested that in the case of two rows of round holes, the two-equation turbulence models did not work well for film cooling, especially in the vicinity of the holes and at high blowing ratios due to the fact that the flow near the holes was disturbed and unsteady.

2.2 Unsteady analysis of film cooling

The research into the fundamental problem of circular hole on a flat plate was still being carried out since this jet-in-a-crossflow was still not fully understood. Most of the numerical studies were about steady state simulation based on RANS (Reynolds averaged Navier-Stokes) approach. As unsteady state simulations are very computationally intensive, almost all the studies related to the unsteady simulation were carried out within the last 10 to 15 years thanks to the ever increasing computing power making the numerical calculation practical.

The majority of the numerical studies on film cooling have been based on the assumption that the flow field was steady state. However, experimental results by Fric and Roshko [69] revealed that the flow field associated with jet-in-a-crossflow was

highly unsteady and complex with at least four different types of vortices. Therefore, the assumption of steady state, at the best, is a rough approximation. It was widely accepted that the mixing processes downstream of the hole were highly anisotropic since the turbulent diffusion is much stronger in the transverse direction than in the streamwise direction. This was possibly the cause of under-prediction of jet spreading by the isotropic turbulence models.

Roy et al. [70] performed numerical simulations using a finite volume based parallel solver called Cobalt with a Spalart-Allamaras based detached eddy simulation (DES) which makes no such assumption of isotropy downstream of the hole. The film cooling geometry modeled was based on Sinha et al. [4], a circular hole with a 35 degree surface angle spaced three diameters apart in the spanwise direction. To reduce the computing time, only a half hole was simulated. The multi-block computational grid consisted of approximately 1,300,000 cells, which was probably fine enough. Cells clustering at walls ensured a y^+ value of less than one on all solid walls. The case was run for a 1,200 hours period on a cluster of 256 parallel processors on a supercomputer. However, the prediction by DES in comparison with experimental data proved to be no more accurate than that of RANS (Reynolds averaged Navier-Stokes) model solution, which was attributed to the use of symmetry boundary condition in the simulation since the symmetry boundary might have inhibited the growth of three-dimensional asymmetric instability deterring further mixing. In another paper by Kapadia et al. [71], the symmetry boundary condition was abandoned and periodic boundary condition was adopted with a full computational domain of one period in an effort to capture the asymmetric vortical flow patterns. The mesh used in the study contained a single block of 2,109,440 cells for

the whole period, which was no finer than the previous one for the half hole case. Using the same computational facility, the total computing time was approximately 4,000 hours, which was almost three times as much as for the half hole case. Improved cooling effectiveness prediction was achieved and the DES solution was more realistic as it captured the asymmetric features in temperature and velocity distribution.

Claiming the existing two-equation models failed to resolve the anisotropy and the dynamics of the highly complex flow field created by the jet-crossflow interaction based on the literature, Tyagi and Acharya [72] studied film cooling using large eddy simulation (LES) where the dynamics of the larger scales in the flow were directly resolved. Momentum equations were solved using a projection method, while the temporal differencing was done with an explicit second-order Adams-Bashforth scheme. The spatial descretization was done using a fourth-order central finite-difference scheme. All terms in energy equation were differenced using fourth-order central differences. A uniform grid of 172×102×62 was used to mesh the computational domain of the size of 17D×5D×6D with periodic boundary conditions used in the spanwise direction on the domain including one single hole. The velocity predictions at both blowing ratio of 0.5 and 1 were generally in good agreement with experimental data. The agreement of cooling effectiveness between predictions and experimental data was also good at low blowing ratio of 0.5. Coherent structures were extracted using positive isosurfaces of the Laplacian of the pressure field. It was shown that the cooling effectiveness was intrinsically linked to the dynamics of the hairpin structures. All previously reported vortical structures were identified and all the discrepancies were attributed to the

insufficient averaging of time-dependent fields and the uncertainties associated with boundary conditions.

Wegner et al. [73] used the large eddy simulation (LES) methodology to investigate how turbulent mixing can be enhanced by varying the angle between the jet and the oncoming cross-flow. In the LES model, all scales of motion and mixing smaller than a given filter width were removed by filtering the governing equations, while large scales were explicitly computed. All governing equations were integrated into a three dimensional finite volume CFD code called FASTEST-3D. A geometry-flexible block structured mesh with boundary-fitted grid was employed. Second-order central schemes taking into account grid non-orthogonality by multi-linear interpolating were used for spatial discretization. For time discretization, second-order implicit Crank-Nicolson method was utilized. A total grid size of 430,000 cells was used at the blowing ratio of 0.5 with a circular jet on a flat plate since the jet does not penetrate far into the crossflow and hence a large number of points in the wall-normal direction may not be necessary to achieve an adequate flow field resolution. It was demonstrated that the LES can capture the flow and mixing features in jets-in-a-crossflow well at low blowing ratio conditions in comparison to experimental data. In addition, the angle between the jet and the cross-flow influenced the secondary flow features which in turn had an effect on the coolant-mainstream mixing process.

Holloway et al. [74] studied the jet-in-crossflow by considering new unsteady physics. A new in-house unsteady RANS-based turbulence model was developed and tested with other models against experimental data. They determined that current steady RANS turbulence models tended to under-predict jet-crossflow mixing. Therefore, it was

believed that inclusion of unsteady mechanisms should enhance predicted mixing rates and improve results. The grids were created with a multi-block unstructured approach. The y^+ values on all walls were kept below one so that viscous sub-layers could be resolved. The meshes consisted of around 2 million finite volumes and 15 iterations per time step proved to be adequate. The cases were run using a pressure-correction solver with the SIMPLE algorithm and convective terms were discretized with a second-order upwind scheme to reduce the effects of numerical viscosity. A SUN Ultra 6500 with 20 CPUs and 20 GB of RAM was used for the computation. The unsteady simulation required approximately 4,000 CPU hours or 10 days of running time, which was an order of magnitude more time than needed for a steady simulation. In contrast to the steady simulations of film cooling which indicated a significant overprediction of adiabatic effectiveness at high blowing ratios, especially in the near hole region, the new approach did lead to an improvement in the effectiveness prediction in that the dramatic overprediction in the near hole region was eliminated by the unsteady approach. The unsteady simulation led to some downstream coolant lateral spreading that could not be predicted with a steady simulation. There was still some quantitative disagreement with the experimental data for this case, however.

Guo et al. [75] performed LES simulations of a jet in a crossflow problem to investigate the turbulent flow structures and vortex dynamics in film cooling on a flat plate. The jet-in-a-crossflow of two inclination angles of 30 or 90 along with two lowing blowing ratios of 0.1 and 0.48 was analyzed using a filtered Navier-Stokes equations solver. Viscous terms in the governing equations were approximated by a central scheme. An explicit five-step Runge-Kutta time stepping scheme was used for temporal

integration. These schemes resulted in an overall approximation of second-order accuracy in space and time. The final grid used was 721×113×33, which led to an approximately 2.7 million mesh. The results showed that a large vortex region was observed on the windward side of the jet in the perpendicular injection case. No separation along the leading edge of the jet hole was found in the stream-wise inclined injection cases since all the blowing ratios tested were low. In comparison with the perpendicular injection case at the same blowing ratios, the starting position of the counter-rotating vortex pair (CVP) in the stream-wise inclined injection case was shifted downstream of the jet exit and its strength was reduced. The results have to be dealt with caution due to a lack of comparison with experimental data.

2.3 Transonic film cooling on an airfoil

Early studies on film cooling concentrated on circular holes on a flat plate under incompressible flow conditions. Although there are quite a few studies of film cooling on a curved surface in the literature within the last 10 years, most of them are under incompressible flow conditions [24,32,36,76-82]. Only a few studies of film cooling involve a high speed test at Mach number higher than 0.5 [33,83-84] when compressibility of fluid can not be neglected.

Ito et al. [76] tested a row of circular holes on a gas turbine blade using a mass transfer technique. A linear cascade of six turbine blades was used, four solid and two hollow. One of the hollow blades had a row of holes with a 35 degrees surface angle on the suction side and the other had a row of holes with a 35 degrees surface angle on the pressure side. The experiment was conducted in a low velocity wind tunnel at room

temperature. It was shown that the effect of blade wall curvature on film cooling effectiveness was significant. On the convex wall, the jet was pushed towards the wall by the static pressure force around the jet. At low blowing ratios, this resulted in a higher level of cooling effectiveness compared with that on a flat plate. At higher blowing ratios, the jet would move away from the curved surface leading to a lower level of cooling effectiveness on the convex wall. On the concave wall, the effect of curvature on cooling effectiveness was the opposite of those for the convex wall.

Guo et al. [83] employed a thin-film technology to measure heat transfer and cooling effectiveness over a heavily film cooled nozzle guide vane (NGV). The cooling configuration consisted of 14 rows with a total of 350 holes, including both circular and fan-shaped holes. Mach number varied between 0.04 and 0.96 in the flow passage. The test section of the tunnel was an annual cascade of 36 NGVs and the test lasted typically 3 to 5 seconds in a blow-down facility. It was demonstrated that on the pressure surface the injection of coolant generally increased the heat transfer coefficient. The heat transfer coefficient was largest in the shower-head region near the leading edge and fell progressively towards the back of the suction surface. Fan-shaped hole resulted in a lower heat transfer coefficient compared to circular hole, either on the pressure side or suction side. Despite the large number of holes near the leading edge, effectiveness level was quite low due to either high blowing ratios or stagnation region. Fanning the hole resulted in a significant improvement of cooling effectiveness. In another study by Guo et al. [33] on the same test facility, attention was paid to the influence of surface roughness on heat transfer and effectiveness for the fully film cooled NGV. He concluded that roughness

generally did not greatly influence the film cooling effectiveness while it was shown to increase the heat transfer coefficient significantly.

Drost and Bolcs [84] did a thorough investigation of film cooling effectiveness and heat transfer on a gas turbine airfoil using transient liquid crystal technique. Tests were conducted in a linear cascade at exit Mach number of 0.33, 0.62, and 0.8 at two mainstream turbulence intensities of 5.5 and 10 percent. The film cooling configurations consisted of a single compound angle row on the pressure side and a single or a double row on the suction side. Tests were conducted for blowing ratios of 0.23 to 2.3 on the suction side and 0.55 to 7.3 on the pressure side. The effectiveness was found to be significantly higher in the near hole region on the suction side while variations in Mach and Reynolds numbers changed the film hole performance on the suction side due to the flow acceleration and/or changed boundary layer thickness. A double row of film cooling holes provided superior heat load reduction over a single row at medium to high coolant mass flow rate due to an improved film coverage and delayed jet liftoff at high blowing ratios on the suction side.

Ethridge et al. [36] investigated film cooling performance on the suction side of first stage turbine vane. Two different mainstream turbulence intensity levels of 0.5 and 20 percent were tested. The row of film cooling holes was located in a position of both strong curvature and strong favorable pressure gradient. A linear cascade of three vane leading edges and two main flow passages was instrumented in a closed-loop low-speed wind tunnel. It was found that high mainstream turbulence had little effect at low blowing ratios when jets remained attached to the surface but reduced cooling effectiveness at higher blowing ratios due to a higher level of mixing between detached jet and

mainstream of high turbulence. Also film cooling effectiveness was greatly enhanced comparison with hole over a flat plate, which was attributed to the surface curvature.

Lakehal et al. [80] studied film cooling at the leading edge of a symmetrical turbine blade model under low speed incompressible flow. Film cooling effectiveness of lateral and non-lateral injection from one row of circular holes placed on each side near the leading edge was computed with a three dimensional finite volume method on multi-block grids. Various versions of k-ε turbulence model were used in the simulations. The laterally spreading was under-predicted leading to a too low average effectiveness although reasonable agreement with measurement was obtained for film cooling on a flat plate. A limited improvement was achieved by modifying the turbulence model.

Colban et al. [25] measured film cooling on a stator vane with fan-shaped holes in incompressible flow regime. The test was carried out in a low speed closed loop wind tunnel. A contoured endwall was incorporated to accelerate the flow in the low speed simulation. It was shown that upstream blowing increased the cooling effectiveness of the second row as turbulence generated by the first row blowing tended to disperse the downstream jet onto the vane surface, making it more effective to cool the surface. In addition, high curvature on the suction side caused jet easily separated from the surface while on the pressure side concave curvature caused jet impingement on the surface after 20d down stream. Suction side was particularly hard to cool because of the jet separation from the convex curvature. In the following study by Colban et al. [81] computational study was done and comparisons of fan-shaped film cooling on a turbine vane surface between computational and experimental results were made to evaluate turbulence models' capability in film cooling simulation. Both RNG (renormalization group) k-ε and

v^2-f turbulence models were used for the CFD simulations. Around 2.2 million unstructured tetrahedral cells were used to mesh the computational domain. The CFD predictions did not agree well with the experimental data with a discrepancy of 50 to 100% which was attributed to turbulence modeling.

Rutledge et al. [32] studied the degradation of film cooling performance on a turbine vane suction side due to surface roughness under low speed flow condition. Tests of a three-vane linear cascade were conducted in a closed loop wind tunnel. All holes were circular with a diameter of 4.11 mm. Surface roughness was found generally to cause a significant decrease in adiabatic effectiveness and a doubling of heat transfer coefficient due to the increased mixing within the boundary layer. At extremely high blowing ratios, however, the increased mixing helped bring separated coolant back to the vane surface, leading to an increased cooling effectiveness. The effect of roughness was decreased with the adding of showerhead blowing.

Among the transonic film cooling studies, Reiss and Bolcs [85] did an experimental study of showerhead film cooling on a cylinder. Experiments were conducted for circular holes and two types of shaped holes in a free jet test facility at Mach numbers of 0.14 and 0.26. Blowing ratios ranged from 0.6 to 1.5. The holes of all five rows were oriented 45 degrees toward the cylinder axis and inclined 30 degrees toward the circumferential direction. It was found that film cooling effectiveness was slight lower for high Mach number with the onset of flow separation occurring at smaller blowing ratios. It was proposed that an increased Mach number reduced the boundary layer thickness, which in turn caused a stronger jet penetration and a smaller quantity of coolant remaining in the boundary layer while a bigger portion of the coolant was lost to the free stream.

Furthermore, holes with widened exits clearly enhanced the overall cooling performance comparing to the circular holes, whereas laterally expanded holes gave only slight performance enhancement.

Gritsch et al. [28] measured film cooling effectiveness for shaped holes under supersonic flow conditions with mainstream Mach number up to 1.2. The three single holes studied were, a circular hole, a fan shaped, and a laid-back fan-shaped hole, all inclined 30 degrees toward the mainstream. It was found that for the circular hole, the laterally averaged film cooling effectiveness was hardly affected by the mainstream Mach number for the subsonic test cases of Mach numbers of 0.3 and 0.6. For supersonic cases of Mach of 1.2, however, the laterally averaged effectiveness increased in comparison to the subsonic cases. This was because the jet liftoff was impeded by the shock-induced pressure field, particularly at high blowing ratios. For the expanded holes, the penetration into the mainstream was not as pronounced as for the circular holes. Due to the test section being a flat plate, the effect of surface curvature was not addressed.

Study of the effect of shock-wave interaction on supersonic film cooling was done by Juhany and Hunt [86]. The mainstream supersonic flow was generated by forcing air through a converging-diverging nozzle in a continuous supersonic wind tunnel. Coolant was injected at Mach numbers of approximately 1.3 and 2.2 into a mainstream of Mach 2.4 through a slot parallel to the mainstream. A two dimensional oblique shock wave was induced by placing a variable angle wedge on the top wall of the test section. By changing the wedge angle, the desired shock strength could be achieved. Contrary to the Gritsch et al. [28] study, shock impingement was found to decrease film cooling effectiveness.

Ligrani et al. [87] studied shock wave interactions with film cooling from a row of three cylindrical holes with a 30 degrees inclination angle toward the mainstream on a flat plate. All holes had a diameter of 5 mm with a pitch/diameter ratio of 4 and a length/diameter ratio of 6. Free-stream Mach numbers of 0.8 and 1.12 were used and it was demonstrated that the cooling effectiveness was generally higher when shock waves were present. Strong oblique shock waves were found to form at the immediate vicinity of the film hole exits and reflect back and forth between the top the bottom walls. The configurations, locations, and character of these oblique shock waves varied significantly as the blowing ratio was changed. The static pressure could increase by as much as 50% after strong shock waves, which, coupling with mainstream flow deflections, forced larger quantities of cooling film near the surface compared to a situation without shock waves.

2.4 Film cooling on a rotating turbine blade

Study of film cooling on a flat plate in terms of measuring techniques, field visualization, hole shaping, was already state-of-the-art. As results of film cooling on a flat plate are not completely equivalent to those on a curved surface such as a turbine blade, more research was being directed to the investigation of turbine blade film cooling, either in the incompressible, subsonic, transonic, or supersonic flow regimes.

Few studies were done on film cooling on a rotational turbine blade. Dring et al. [88] studied single holes with a 30 degree angle in the streamwise direction on a rotor blade in a five feet diameter rotating rig with a $1^1/_2$ stage turbine model. As it was a low speed test facility, the axial chords of the airfoils in each row of the turbine model were

approximately 6 inches, or five times engine scale. Two holes were positioned one at ten percent axial chord on the suction surface and the other 16 percent axial chord on the pressure surface. Each hole was inclined at an angle of 30 degrees in the stream-wise direction with no radial component. Flow visualization results showed that suction surface film coolant trace was narrow and straight while on the pressure side it was much wider with a strong radial displacement, almost 30 degrees outward in the radial direction. The radial component of the film coolant trajectory was found to have a strong impact on the film cooling effectiveness distribution. Film cooling effectiveness on the suction side was very similar to the data on a flat plate. On the pressure side, very low levels of cooling effectiveness was measured with a much faster decay of the cooling effectiveness than did the flat plate data, which was attributed to both curvature and redial flow. It was also observed that centrifugal effects and Coriolis forces had no significant impact on film cooling trajectory.

Abhari and Epstein [89] conducted an experimental study of film cooling in a rotating transonic turbine. The experiments were carried out in a short-duration (0.3 s) blowdown turbine test facility. The 0.5 meter diameter turbine model was a single stage 4:1 pressure ratio transonic machine with the NGV exit Mach number of 1.18. The holes in all rows were circular except for the holes in the first row, which were D-shaped at the exits. The time averaged data were compared to uncooled rotor data and cooled linear cascade measurement made on the same profile. Compared to the uncooled rotor data, heat transfer to the film cooled rotor was reduced by as much as 60 percent, but little effect was felt on the pressure surface. On the suction surface of the turbine blade, heat transfer was lower in the rotor than in the linear cascade. High blowing ratios were shown to

provide much less cooling than lower ones due to jet liftoff at higher blowing ratios. Overall, film cooling was effective on the rotor suction surface in reducing heat transfer while little reduction in heat transfer was observed on the rotor pressure surface.

Takeishi et al. [90] studied film cooling effectiveness on a rotating blade in a one stage turbine model using a heat-mass transfer analogy. The test was carried out in a 559 mm diameter rotating rig at room temperature with the density ratio around 1. There were 32 vanes for the first vane and 72 blades for the first blade. Only two of the blades were film cooled and instrumented whereas the remaining blades were solid. Each cooled blades had three rows of holes at the showerhead, a single row of holes on the suction surface, and two rows of holes on the pressure surface. All holes were circular. For each row of holes, the blowing ratio ranged from 0.6 to 1.0. It was found that film cooling effectiveness on the suction surface agreed well with that on the stationary blade, while on the pressure surface effectiveness was 30% lower than that of stationary cascade data, possibly due to the effect of radial flow and strong mixing on the pressure surface. In addition, film cooling effectiveness decreased with increasing blowing ratio due to jet penetration to the mainstream.

Numerical study of film cooling on a rotating turbine blade was done by Weigand and Harasgama [91]. A 3D-Navier-Stokes code with an unstructured adaptive grid methodology was employed to simulate a whole rotor blade with film holes on pressure and suction surfaces. The equations solved were the fully three dimensional Reynolds-averaged Navier-Stokes equations expressed in conservation form in combination with a low Reynolds number k-ε model. A first coarse grid of 17×46×29 consisting of about 73, 000 tetrahedral cells was refined to a fine grid of 358, 169 cells for the grid independent

solution. Considering the big computational domain of a whole blade from hub to tip with several holes and the number of cells used, the flow field might not be adequately resolved although the authors claimed the aerodynamics as well as mass flow rate were preserved quite well.

Other numerical studies of film cooling on a rotating blade were done by Garg [92-94]. The rotor blade had either 83 holes, all circular, in five rows [92], or 93 holes, including both circular and D-shaped, in five rows [93], or 172 holes, all circular, in eight rows [94]. A three dimensional Navier-Stokes code was used to simulate the film cooling flow. In all these cases, the film cooling holes were represented by boundary patches on the blade surface instead of real hole with a finite lengths and plenums. Thus, meshing the hole interior and plenum was avoided and mesh size reduced. Different velocity and temperature profiles were specified at the exit patches on the blade surface. The cases were run on a 16 CPUs supercomputer with a grid around two million cells. Adiabatic cooling effectiveness was shown to be higher for a rotating blade in comparison with that for a stationary blade. In all these studies, a whole rotor blade from hub to tip with scores of holes was simulated with only around two million cells, which seems far from enough to fully resolve the detailed local flow field. The approach of using variable profiles on film hole exit patches on the blade surface to represent real three dimensional holes might have compromised the accuracy of the final solutions.

Experimental study of film cooling on a rotating blade at the leading edge was done by Ahn et al. [16,95]. Film cooling effectiveness was measured on the leading edge of the first stage rotor blade in a three stage gas turbine test facility using a pressure sensitive paint technique. Tests were conducted for three rotational speeds at three blowing ratios

each. The Mach number at inlet and outlet of the rotor blade was 0.1 and 0.3, respectively. During the tests, the temperatures of the mainstream air, coolant, and the test section as well as the rotating speed were maintained in steady state conditions. When two rows of holes were tested [16], there were 16 film cooling holes in two rows, pressure side row and suction side row from the stagnation. The two rows were in a staggered arrangement. All holes were circular with a 30 degrees surface angle and oriented to the span-wise direction. Images showed that the location of the stagnation line moved from the pressure side to the suction side as the rotational speed increased. In general, the overall film cooling effectiveness levels decreased as the rotational speed increased, which was attributed to severe mixing due to increased unsteady turbulent wake effect. At high rotating speed cooling effectiveness decreased slightly as blowing ratio increased while it was insensitive to blowing ratio at low speeds. When three rows of holes were tested [95], 15 film holes in three rows were positioned around the leading edge of the rotor blade, pressure side, suction side, and center row. Each row had five film cooling holes and the center row holes were staggered to the pressure side holes and suction holes. All holes were circular with a 20 degrees surface angle and oriented to the span-wise direction. Results showed that different rotation speeds significantly changed the film cooling behavior with the average film cooling effectiveness in the leading edge region slightly increasing with blowing ratio. The coolant traces downstream of cooling hole at higher blowing ratios decayed faster in comparison to lower blowing ratios because of more mixing between the mainstream and coolant flow and possibly liftoff phenomenon at higher blowing ratios.

2.5 Summary

Numerical studies of shaped holes in multi-row arrangements seem to be rare. This was partly because the jet-in-a-cross phenomenon was not well understood, and partly because even with the simplest one circular jet numerical simulations failed to capture the jet liftoff effect in terms of cooling effectiveness at high blowing ratios (Leylek and Zerkle [96], Walters and Leylek [97]). Consequently, the accuracy of the numerical results was left in doubt. A methodology was established and improvement in predicting the right level of cooling effectiveness and heat transfer was achieved. The methodology was extended to study the louver cooling scheme in multiple rows. In particular, the performance of the louver cooling scheme with two and three rows would be presented and compared with other cooling schemes.

The literature survey showed that the jet-in-a-crossflow was a very complicated mixing process between the jet and the mainstream. Counter-rotating vortex shedding is a dominating mechanism in determining the downstream cooling effectiveness. Therefore, the mixing process is highly unsteady and the steady state assumption in the RANS approach may undermine the accuracy of its solutions. That may partly explain the discrepancies between the numerical predictions and the experimental data in a number of studies. In this study, numerical simulations using a DES turbulence model would be performed for film holes on a flat plate, including the louver scheme. It should be pointed out that all work done to this louver cooling scheme up to date have been steady state numerical simulations. This will be the first effort of unsteady state simulation of this louver scheme using DES turbulence model.

The flow behaviors and performance of film cooling in supersonic mainstream flow are significantly different from those when the mainstream flow is subsonic. Both film cooling and shock wave interaction have been studied heavily in the literature. However, combined studies of the two are rare. To the author's knowledge, the only two of these are Juhany and Hunt [86] and Ligrani et al. [87] both of which are experimental studies. A combined numerical study of the two has not been done. If carried out properly, a numerical study could shed new light on this phenomenon as it affords us to examine the solution in greater detail than an experimental study would permit. The performance of a louver cooling scheme on a transonic airfoil would be presented. The effects of curvature and compressibility of the working fluid on the performance of different film cooling schemes would be examined. Specifically, film cooling behaviors under the mainstream flow condition of Mach number greater than 1 would be analyzed from a gasdynamics perspective.

Based on the literature survey, there are only a few studies of film cooling on a rotational airfoil. All the numerical studies of film cooling on a rotating blade considered only the rotor domain. By including both the stator and rotor domains in the numerical model, more realistic results are expected, which could lead to further understanding of the flow field. In addition, turbine blade at the leading edge is exposed to a high level of heat load. Study of flow field in this particular region is important for better cooling designs and blade durability. Numerical investigation of film cooling at the leading edge of a rotor blade in a complete turbine stage, including both stator and rotor blades, would be carried out. Particular attention would be paid to the effects of rotational speed on film cooling performance. The prediction capability of CFD in simulating a rotational blade

was evaluated and validated. Also, the performance of the louver cooling scheme was studied and compared with a circular hole.

In this work, a comprehensive numerical study of the louver cooling scheme was conducted. Computational study of the louver cooling scheme in a single row was already done by Immarigeon and Hassan [51] and Zhang and Hassan [52,53]. Study of the louver cooling scheme in multiple rows is an extension of these studies. Unsteady analysis of film cooling, either using LES or DES modeling, has attracted attention in recent years due to faster computers and deficiencies in the traditional Reynolds averaged Navier-Stokes approaches in capturing lateral spreading of coolant in film cooling simulations. An unsteady analysis of the louver cooling scheme may provide more realistic results, particularly on the aspect of lateral coolant spreading. Therefore, simulation of the louver cooling scheme using a DES model was carried out. These two parts are studies of the louver cooling scheme on a flat plate. Finally, the louver cooling scheme on airfoils was studied, firstly on a stationary transonic airfoil, then on a rotating airfoil in a complete turbine stage. Among these four parts of the study, the geometry and boundary conditions are becoming progressively more realistic. Each part has its own focus and, in a sense, independent from one another, however. The combination of all four parts will give us a comprehensive picture of film cooling performance of the louver cooling scheme.

Chapter 3

Mathematical Modeling

In this study, a variety of film cooling flows was analyzed, from incompressible to high speed compressible flow, and from steady to unsteady analysis. Therefore, the equations involved and models used were different from one case to another. For example, in steady analysis all the partial derivatives with respect to time in the Navier-Stokes equations disappear. Only the most general equations were presented in this chapter. More details regarding mathematical modeling and boundary conditions were provided in each individual chapter.

Although the flows involved are different from case to case, they all have one thing in common, i.e., they all obey the fundamental laws of physics. The assumptions made for the flow were based on experimental test conditions, and are as follows: a. three-dimensional; b. viscous; c. turbulent; d. single phase air; e. no source of fluid or heat generation in the domain; f. negligible gravitational force. The flow is governed by the Navier-Stokes conservation equations, and under the above assumptions, the conservation equations of continuity, momentum and energy become

Continuity:

$$\frac{\partial \rho}{\partial t} + \nabla \cdot (\rho \vec{v}) = 0, \tag{3.1}$$

Momentum:

$$\frac{\partial}{\partial t}(\rho \vec{v}) + \nabla \cdot (\rho \vec{v} \vec{v}) = -\nabla P + \nabla \cdot \left(\mu \left[\left(\nabla \vec{v} + \nabla \vec{v}^{T} \right) - \frac{2}{3} \nabla \cdot \vec{v} I \right] \right), \tag{3.2}$$

Energy:

$$\frac{\partial}{\partial t}(\rho E)+\nabla\cdot[\vec{\upsilon}(\rho E+P)]=\nabla\cdot\left[k_{eff}\nabla T+\left(\mu_{eff}\left(\left(\nabla\vec{\upsilon}+\nabla\vec{\upsilon}^{T}\right)-\frac{2}{3}\nabla\cdot\vec{\upsilon}I\right)\cdot\vec{\upsilon}\right)\right]. \tag{3.3}$$

where

$$E=h-\frac{P}{\rho}+\frac{\upsilon^2}{2} \tag{3.4}$$

Transonic flows, with Mach number approaching unity, are typically found in gas turbine stage rendering compressibility effects significant. Mach number is defined as,

$$M=\frac{V}{c}, \tag{3.5}$$

where V is the magnitude of gas velocity. In the present study, compressibility of the gas was considered by assuming that the air is an ideal gas. Thus, according to the ideal gas law the density is given by

$$\frac{P}{\rho}=RT. \tag{3.6}$$

where R is the gas constant.

As turbulent flows are characterized by fluctuating fields of small scale and high frequency, which are computationally expensive, the instantaneous governing equations – Eq. (3.1), (3.2), and (3.3) – have been time-averaged to remove the small scales. As a result, new unknown variables due to the time-averaging have been created. These unknown variables have been defined differently in terms of known quantities, and have given rise to various turbulence models. When considering all types of problems, no single turbulence model is deemed superior over the others.

The literature survey indicates that the jet-in-cross flow is quite complicated. Consequently, the simulations usually do not agree very well with the experimental data. In many efforts to evaluate the performance of different turbulence models in film cooling applications, numerical errors were usually too large to allow clear conclusions to be drawn. In this study, a methodology which has proved to be very successful in the prediction of film cooling effectiveness will be used to carry out the numerical simulation with the realizable k-ε model (Shih et al. [98]) provided by the commercial software FLUENT 6.3.

3.1 The realizable k-ε model

The realizable k-ε model (Shih et al. [98]) is a semi-empirical two-equation model based on the Boussinesq approximation of Reynolds stresses. Two additional scalar variables, the turbulent kinetic energy k and the turbulence dissipation rate ε, are solved in order to model the turbulence effects. The k and ε transport equations are

$$\frac{\partial}{\partial t}(\rho k)+\frac{\partial}{\partial x_j}(\rho k u_j)=\frac{\partial}{\partial x_j}\left[\left(\mu+\frac{\mu_t}{\sigma_k}\right)\frac{\partial k}{\partial x_j}\right]+G_k+G_b-\rho\varepsilon-Y_M \tag{3.7}$$

$$\frac{\partial}{\partial t}(\rho \varepsilon)+\frac{\partial}{\partial x_j}(\rho \varepsilon u_j)=\frac{\partial}{\partial x_j}\left[\left(\mu+\frac{\mu_t}{\sigma_\varepsilon}\right)\frac{\partial \varepsilon}{\partial x_j}\right]+\rho C_1 S_\varepsilon-\rho C_2\frac{\varepsilon^2}{k+\sqrt{\nu\varepsilon}}+C_{1\varepsilon}\frac{\varepsilon}{k}C_{3\varepsilon}G_b \tag{3.8}$$

where G_k represents the generation of turbulence kinetic energy due to the mean velocity gradients, and G_b is the generation of turbulence kinetic energy due to buoyancy. Y_M represents the contribution of fluctuating dilatation in compressible turbulence to the dissipation rate. σ_k and σ_ε are the turbulent Prandtl numbers for k and ε respectively, where C_2 and $C_{1\varepsilon}$ are constants. The turbulent viscosity is computed from

$$\mu_t = \rho C_\mu \frac{k^2}{\varepsilon}. \tag{3.9}$$

Based on the concept of Reynolds's analogy to turbulent momentum transfer, the energy equation or turbulent heat transfer is given by,

$$\frac{\partial}{\partial t}(\rho E) + \frac{\partial}{\partial x_i}[u_i(\rho E + P)] = \frac{\partial}{\partial x_j}\left(k_{eff} \frac{\partial T}{\partial x_j} + u_i(\tau_{ij})_{eff} \right), \tag{3.10}$$

where k_{eff} is the effective thermal conductivity. $(\tau_{ij})_{eff}$ is defined as

$$(\tau_{ij})_{eff} = \mu_{eff}\left(\frac{\partial u_j}{\partial x_i} + \frac{\partial u_i}{\partial x_j} \right) - \frac{2}{3}\mu_{eff} \frac{\partial \mu_i}{\partial x_i}\delta_{ij}. \tag{3.11}$$

The effective thermal conductivity is given by

$$k_{eff} = k + \frac{c_p \mu_t}{\mathrm{Pr}_t}. \tag{3.12}$$

The presence of the wall significantly affects turbulent flow field. In the near wall region, the solution variables such as velocities and temperatures have large gradients, and the accuracy of the final numerical solution primarily depends on how successfully the near wall boundary layers are modeled. Unfortunately, most current turbulence models, including the realizable k-ε models, are only valid for turbulent core flows far from walls. In order to render these models suitable for wall-bounded flows, a series of empirical functions are introduced in order to resolve the boundary layers. Since the wall function approach does not need to resolve viscosity-affected near wall region, it saves computational resources substantially. In addition, it has become popular due to its economy, robustness, and reasonable accuracy.

The standard wall functions were proposed by Launder and Spalding [99]. The formulas or law-of-the-wall for mean velocity are

$$U^* = \frac{1}{k}\ln(Ey^*), \tag{3.13}$$

where

$$U^* \equiv \frac{U_P C_\mu^{1/4} k_P^{1/2}}{\tau_w / \rho},$$

and

$$y^* \equiv \frac{\rho C_\mu^{1/4} k_P^{1/2} y_P}{\mu}.$$

According to the Reynolds' analogy between momentum and energy transport, a similar logarithmic law for mean temperature is given as

$$T^* \equiv \frac{(T_w - T_P)\rho c_P C_\mu^{1/4} k_P^{1/2}}{\dot{q}} = \begin{cases} \Pr\, y^* + \dfrac{1}{2}\rho \Pr \dfrac{C_\mu^{1/4} k_P^{1/2}}{\dot{q}} U_P^2 & (y^* < y_T^*) \\ \Pr_t \left[\dfrac{1}{\kappa}\ln(Ey^*) + P\right] + & \\ \dfrac{1}{2}\rho \dfrac{C_\mu^{1/4} k_P^{1/2}}{\dot{q}} \left[\Pr_t U_P^2 + (\Pr - \Pr_t) U_c^2\right] & (y^* > y_T^*) \end{cases} \tag{3.14}$$

where

$$P = 9.24\left[\left(\frac{\Pr}{\Pr_t}\right)^{3/4} - 1\right]\left(1 + 0.28e^{-0.007\Pr/\Pr_t}\right).$$

The thermal boundary layer thickness y_T^* is computed from the intersection of the linear and logarithmic profiles. In the simulation, the wall temperature T_w or heat flux is computed from the above equations.

The turbulence variables, the production of k and its dissipation rate ε, are computed from

$$G_k \approx \tau_w \frac{\partial U}{\partial y} = \tau_w \frac{\tau_w}{\kappa \rho C_\mu^{1/4} k_P^{1/2} y_P}$$

and

$$\varepsilon_P = \frac{C_\mu^{3/4} k_P^{3/2}}{\kappa y_P}$$

At the wall, the boundary condition for k is

$$\frac{\partial k}{\partial n} = 0 \tag{3.15}$$

where n is the local coordinate normal to the wall. The production of k is assumed to be equal to its dissipation rate ε in the wall-adjacent control volume. Note that the solution variables including mean velocity, temperature, species concentration, k, and ε are all computed from the wall functions. More information about the Realizable k-ε model and wall functions can be found in the Fluent Documentation [100].

3.2 Methodology

Systematic benchmark studies were performed in Zhang [101] to find the most appropriate turbulence model in film cooling application, which turned out to be the mentioned realizable k-ε model. Structured meshes were created to fully resolve the features of the flow field with most of the cells concentrated in areas of large variable gradients, since a hexahedron is more efficient to fill a volume than a tetrahedron. When unstructured meshes are used, it is very difficult to efficiently concentrate cells in the near hole and wall regions to resolve the wake of recirculation and boundary layers. Particular attention was paid to the boundary layers. The present Reynolds-Averaged turbulence models are empirical, or semi-empirical, and are only valid for the turbulence

core flow far away from the walls. In order to render these models suitable for wall-bounded flows, a series of empirical functions are introduced to resolve the boundary layers with some near wall mesh requirements attached which have to be satisfied to reach an appropriate solution. Therefore, whenever the parameters such as blowing ratio change, the y^+ value will change and the near wall mesh has to be changed accordingly.

The methodology was very reliable and could yield accurate results over a wide range of blowing ratios and density ratios. When used appropriately, this method successfully captured the jet liftoff effect in traditional circular jet-in-cross flow over a flat plate. Figure 3.1 shows that the current methodology yields a prediction much closer to the experimental data than previous studies. Figure 3.2 shows that the realizable k-ε model outperforms all the other turbulence models tested. Therefore, in the present work, the realizable k-ε model has been selected to perform the simulations by solving the Reynolds-averaged Navier-Stokes equations. The wall functions approach was chosen to avoid using a very fine mesh close to walls to resolve the boundary layer. Thus, smaller meshes can be used with more efficient computation and faster and better convergence.

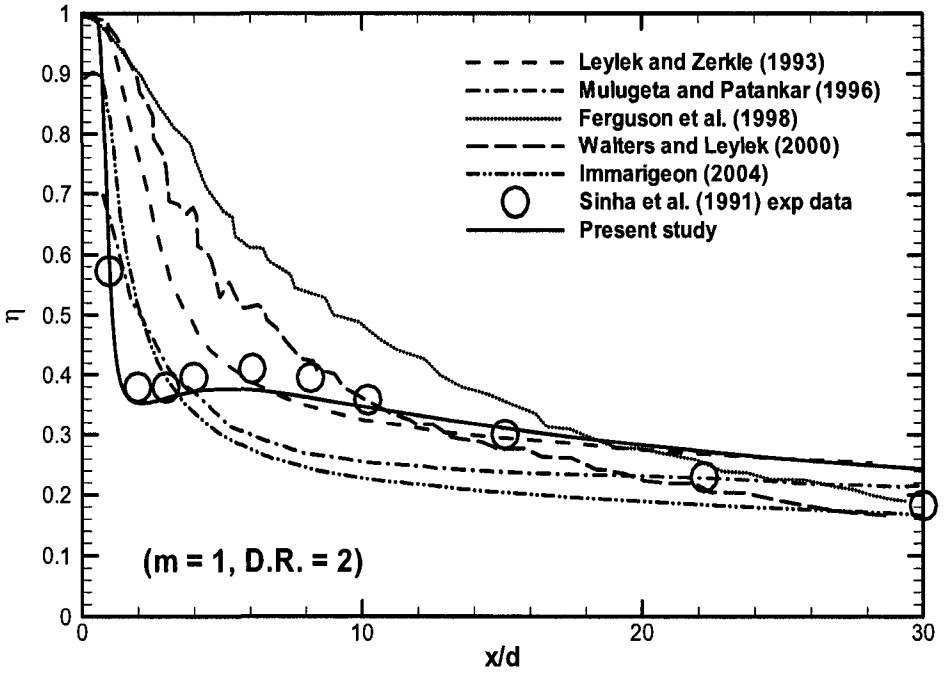

Fig. 3.1 Present and previous predictions (Zhang and Hassan [52]).

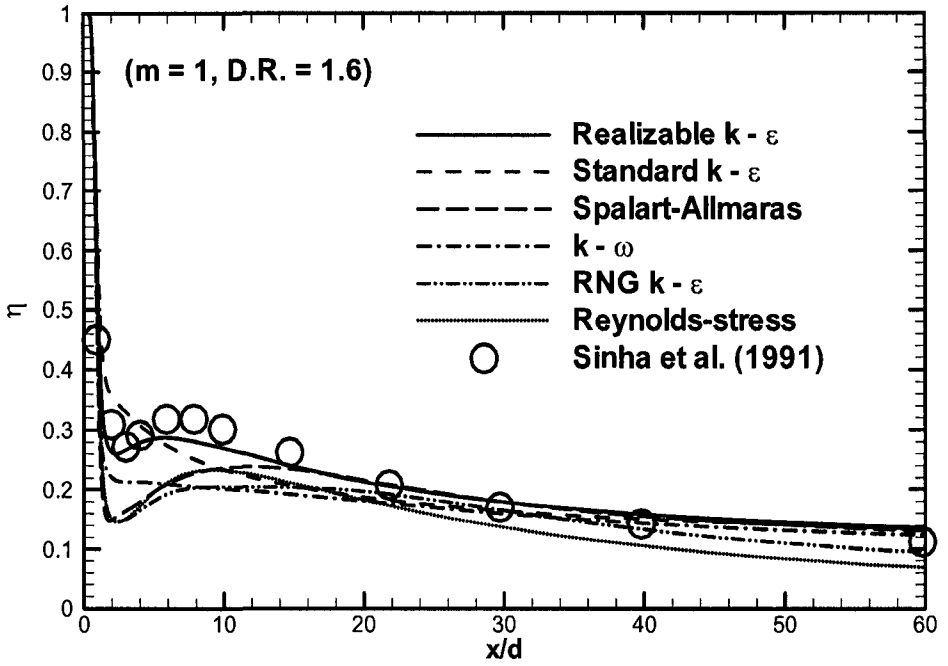

Fig. 3.2 The performance of turbulence models (Zhang and Hassan [52]).

Chapter 4

Louver Cooling Scheme on a Flat Plate – Multiple Rows

In this chapter, the louver cooling scheme in two and three rows was studied. Both staggered and inline arrangements of the louver cooling scheme were presented, specifically, two inline rows, two staggered rows, and three staggered rows. The performance of the louver cooling scheme was evaluated against other cooling schemes in the literature in terms of adiabatic film cooling effectiveness and heat transfer coefficient.

4.1 Simulation details

Three configurations of the louver cooling scheme shown in Fig. 4.1 were studied, namely, two inline rows of holes, two staggered rows of holes, and three staggered rows of holes equally distanced in the span-wise direction, Fig. 4.1. The computational domain and boundary conditions were based on the assumption that the louver scheme was tested in a wind tunnel with the characteristic length of d = 12.7 mm at low turbulence intensity of less than 3% and with a mainstream velocity of 20 m/s corresponding to Reynolds number of 16,000. This assumption was made only for comparison purposes, because in most of the experimental studies different cooling schemes were tested in a wind tunnel with low mainstream velocities. In the adiabatic cooling test the density ratio was assumed to be 2, while in the heat transfer test the density ratio was set at 1.

The computational domain includes one whole period from center to center. Assume infinite rows of film cooling holes on a flat plate, so that the end-wall effects can be neglected. At the upstream inlet, a constant velocity normal to the inlet boundary was applied with the free-stream turbulence being 0.2%. At the outlet, a pressure boundary condition was imposed. The domain extends 20d from the bottom test surface, far enough such that a free slip boundary condition or zero shear stress may be applied. Symmetry boundary conditions were imposed on the two faces in the span-wise direction. At the bottom wall, an adiabatic wall was specified when cooling effectiveness was calculated and constant heat flux boundary condition when heat transfer was calculated. On all the other walls, an adiabatic wall boundary condition with no-slip was imposed. The temperatures at the mainstream and plenum inlets were specified at 300K and 150K, respectively, which gives a coolant to mainstream density ratio of 2. All these boundary conditions were based on Sinha et al. [4]. Different meshes were used at the beginning to determine the optimum grid size and to ensure a grid independent solution. The grids contained between 0.4 and 1 million cells which took roughly one full day of computing time to reach convergence using a workstation with a CPU speed of 3 GHz and a RAM of 1 GB. The previous study by Zhang and Hassan [52] has shown that a structured mesh yields more accurate predictions than its unstructured counterpart. In this work, as the geometry is more complicated than a simple circular jet, a multi-block structured mesh was used, therefore, a structured mesh was created wherever possible. A typical mesh for the two rows of staggered holes arrangement is shown in Fig. 4.2. Due to the large number of cells, only half of the domain was shown to make the mesh structure more visible.

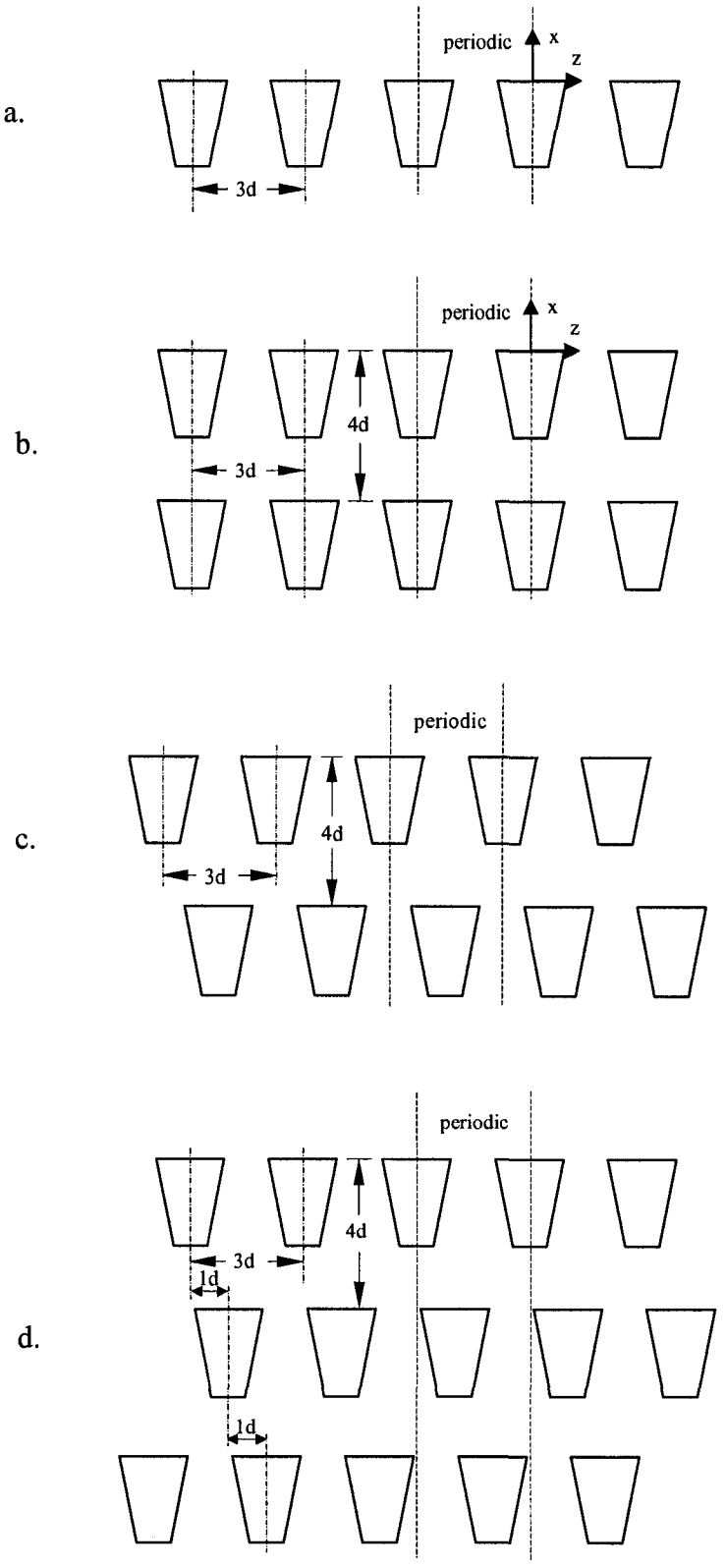

Fig. 4.1 Hole configurations: a. single row; b. two inline rows; c. two staggered rows; d. three staggered rows.

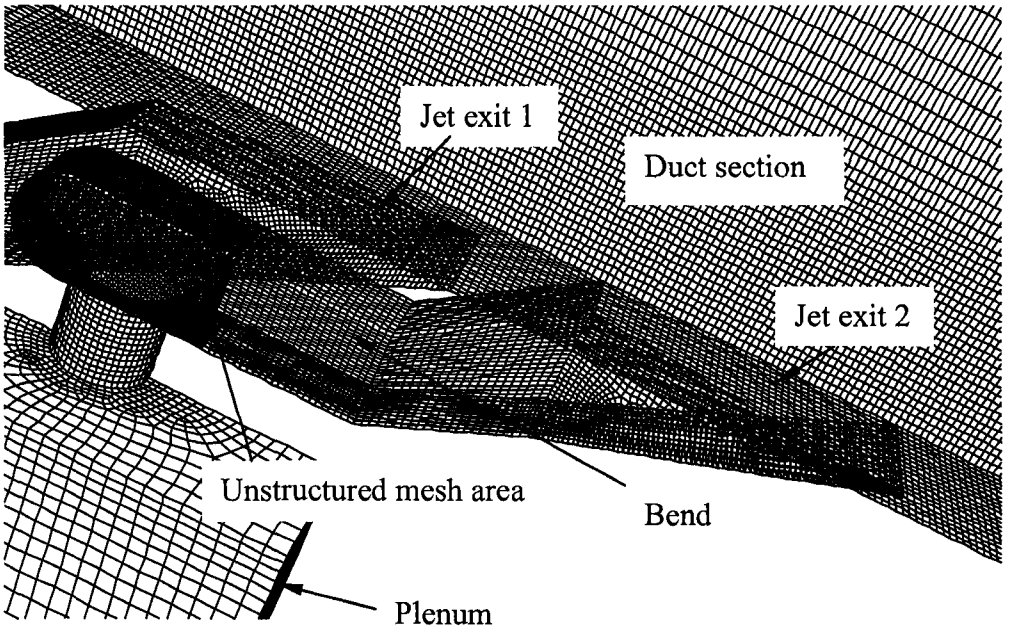

Fig. 4.2 A typical mesh – multi-block structured (two staggered rows).

After convergence is reached, the adiabatic effectiveness η can be calculated as,

$$\eta = \frac{T_{aw} - T_{\infty}}{T_j - T_{\infty}} \quad . \tag{4.1}$$

In this study, the same method from previous experimental work will be used to calculate the heat transfer coefficient. A first case was run until convergence, and the heat transfer coefficient with film cooling was determined from

$$h_f = \frac{q''}{T_w - T_{aw}} \quad , \tag{4.2}$$

where $T_{aw} = T_{\infty}$ because the temperature of coolant is forced to be equal to that of the mainstream. Since this study used a multi-block structured mesh, a second case was run with the jet and plenum sections removed, and the heat transfer coefficient without film cooling was determined from

$$h_o = \frac{q''}{T_w - T_{\infty}} \quad . \tag{4.3}$$

In either case, the constant heat flux boundary condition was applied on the bottom wall of the test section: downstream of injection, as in most experiments. It should be noted that the effect of impingement cooling on the blade material was not taken into account due to the fact that either adiabatic or constant heat flux boundary condition was applied on the test section only, downstream of the jet exits, for comparison purposes.

4.2 Results and discussion

4.2.1 Grid independence

Figure 4.3 and Fig. 4.4 show the grid independence for the cases of a single row of circular holes and the louver scheme of two rows of staggered holes, respectively. In

order to capture the fine features of the jet liftoff effect for a circular hole at high blowing ratio a mesh requires a minimum of 200×10^3 cells. Although more cells may lead to an improved solution, the computing time increases exponentially. A mesh of between 300×10^3 to 600×10^3 cells is appropriate to reach an acceptable accuracy with a reasonable running time. For the louver scheme, as jet liftoff does not occur at high blowing ratios, much fewer cells are needed to reach a result with reasonable accuracy. If jet liftoff is not present with associated flow separation and recirculation in the flow field, the same number of cells could produce results with a higher level of accuracy.

4.2.2 Adiabatic cooling effectiveness

Comparisons of laterally averaged cooling effectiveness for the new louver cooling scheme with two rows of holes and other schemes are presented in Fig. 4.5 and Fig. 4.6. At low blowing ratios, shown in Fig. 4.5, jets in all the different schemes stay attached to the wall after injection. The prediction of the louver scheme is slightly higher or at least at the same level than the experimental data of other schemes. Reducing the pitch ratio results in a higher level of laterally averaged effectiveness because less protected surface area shares the same amount of coolant. At high blowing ratios, Fig. 4.6 shows that the louver scheme consistently provides a higher effectiveness than other schemes such as circular holes with compound angles (Ahn et al. [10]) and discrete slots (Dittmar et al. [24]). Comparison between the dashed line and the square symbols shows that at the same pitch and spacing ratio for the two staggered rows, the louver scheme offers an effectiveness twice that of circular holes with compound angles because the circular holes lift off of the surface at high blowing ratios in spite of compound angles. The advantages

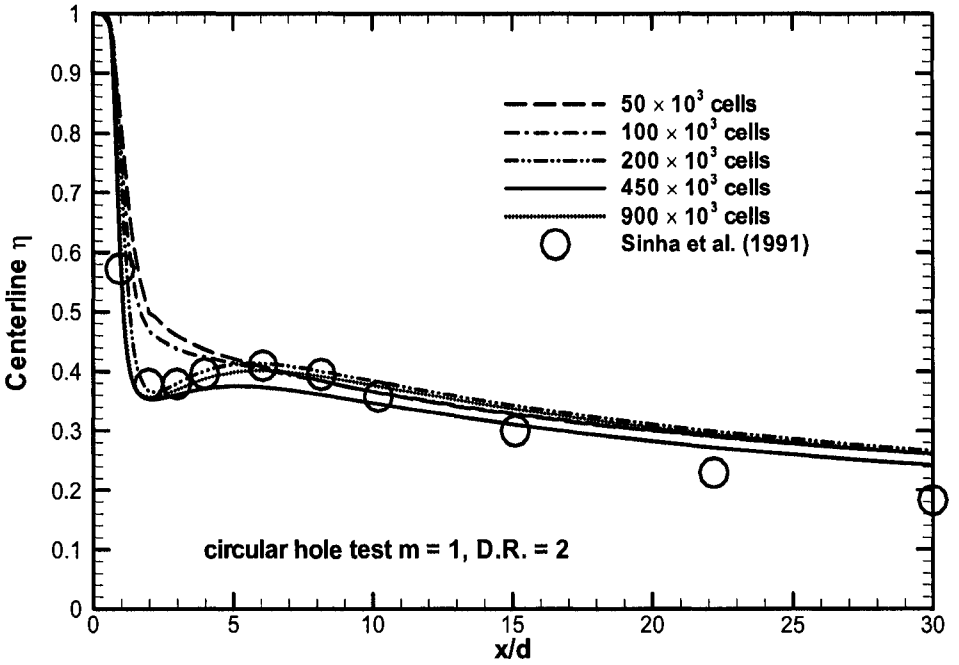

Fig. 4.3 Grid independence test for the circular hole.

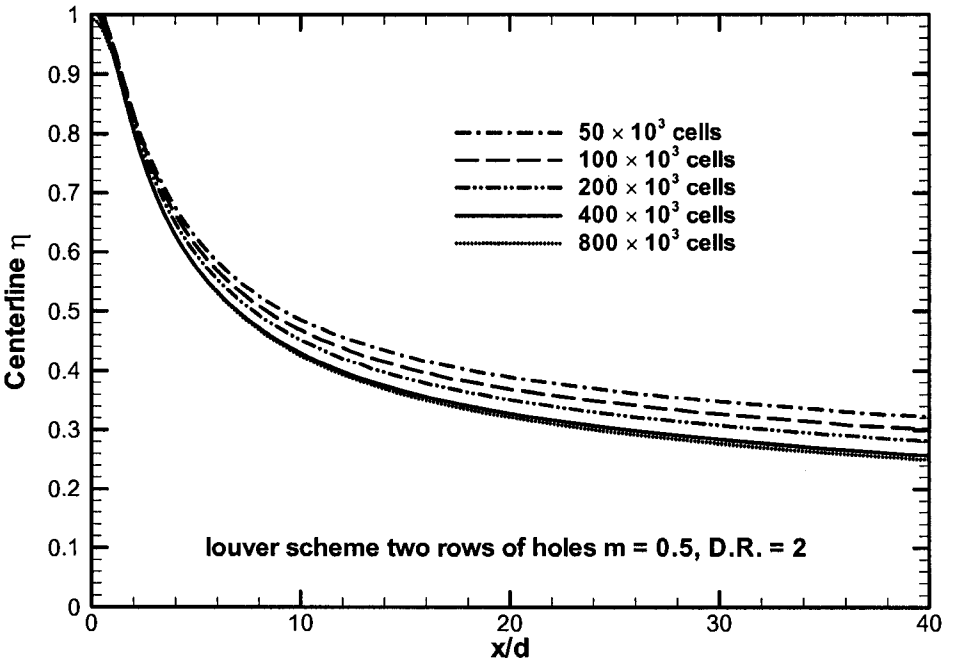

Fig. 4.4 Grid independence test for the louver scheme.

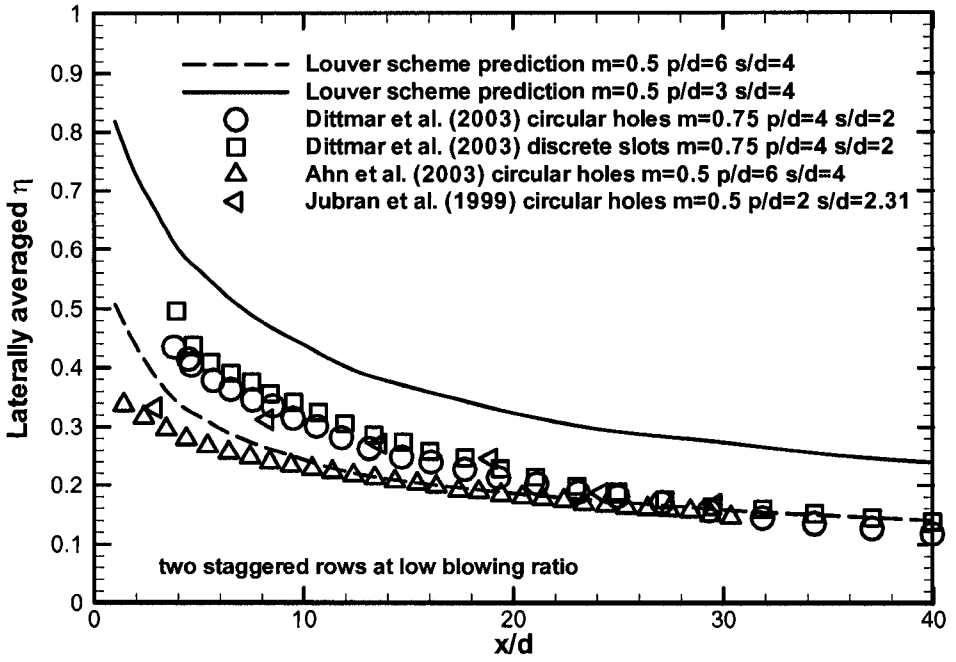

Fig. 4.5 Comparison of laterally averaged η for holes in two rows at low blowing ratios.

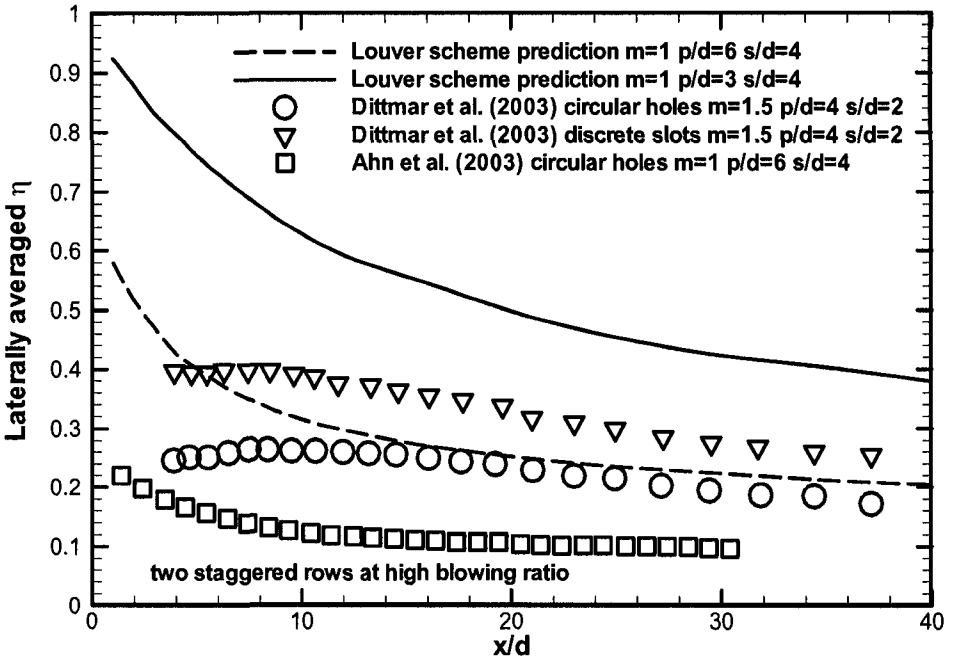

Fig. 4.6 Comparison of laterally averaged η for holes in two rows at high blowing ratios.

of the louver scheme can also be seen in Fig. 4.7, in which comparisons with other shaped holes were made for a single row of holes. These comparisons were made due to a lack of experimental data of shaped holes in more than one row arrangements.

As the blowing ratio increases, the coolant momentum also increases, which causes a greater interaction between jets and mainstream. In the circular holes with a certain angle, usually 30° - 60° to the stream-wise direction, the interaction between jets and mainstream creates a counter-rotating secondary flow within jet trajectory. At high blowing ratios, high jet velocity produces a low pressure region at the trailing edge immediately after injection, which sucks in hot mainstream air with the aid of secondary vortices. Ensuing flow separation and recirculation cause a serious deterioration of protection. A high pressure region at the leading edge of the jet due to impingement of the mainstream on the jet, coupled with a low pressure region at the trailing edges, causes the jet to bend toward downstream. After a certain distance downstream of the exits, turbulence causes part of the coolant to be dissipated into the mainstream, thereby reducing its momentum. This reduction allows the mainstream to push the jet back to the wall and reattachment occurs. In the louver scheme, a sudden reduction of the jet momentum occurs after the coolant enters the bend. This is due to a sudden increase in cross sectional area size. Additionally, the bend changes the momentum of the jet from upward to the stream-wise direction. Further downstream towards the exit, the flow path area increases gradually and the coolant momentum was further reduced, therefore enlarging the coverage area. All these factors contribute to enhancing surface protection by eliminating flow separation and recirculation. With this louver scheme, the jet liftoff phenomenon is avoided and the effectiveness increases monotonically with blowing ratio.

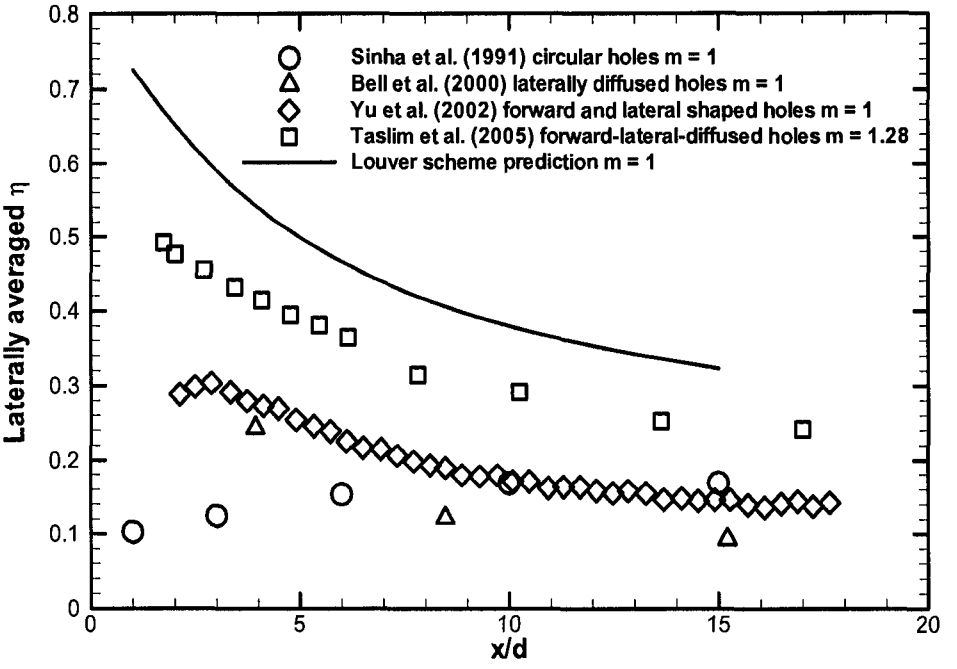

Fig. 4.7 Comparison of laterally averaged η between the louver scheme and other cooling schemes in one row of holes.

Figure 4.8 shows comparisons of arrangements with two rows of holes. The staggered arrangement provides a higher level of laterally averaged effectiveness than the inline arrangement, consistent with that of circular hole results from the literature. Since the coolant does not spread well in the span-wise direction for the inline arrangement, much of the coolant is quickly diffused into the mainstream, resulting in a lower laterally averaged effectiveness. On the other hand, the staggered arrangement covers the protected surface more uniformly. Consequently, the use of coolant is more efficient since the neighboring jets can easily coalesce at the mid-span. Also shown in this figure is the behavior of one, two, and three rows of holes for the new louver scheme. It can be seen that two rows of holes provide higher effectiveness than the one row of holes and the three rows of holes yield higher effectiveness than the two rows of holes, as expected. Nevertheless, the increase in effectiveness from two to three rows is less than half of the increase from the one to two rows. This indicates that a further increase in the number of rows beyond two only gains limited increase in cooling effectiveness. Thus, it is of major importance to have the surface covered with coolant. However, surface coverage by additional coolant layers from more than two neighboring jets yields a less efficient use of the coolant.

Figure 4.9 shows the contours of adiabatic cooling effectiveness at the wall for the three configurations. Figure 4.9a demonstrates that the two inline rows do not provide uniform lateral coolant spreading with the high cooling effectiveness area concentrated mainly around the centerline, leaving the mid-span unprotected. Shaping reduces the momentum of the jet significantly, resulting in very weak vortices, and the expanded exit stretches the coolant thin after the injection. The span-wise momentum component of the

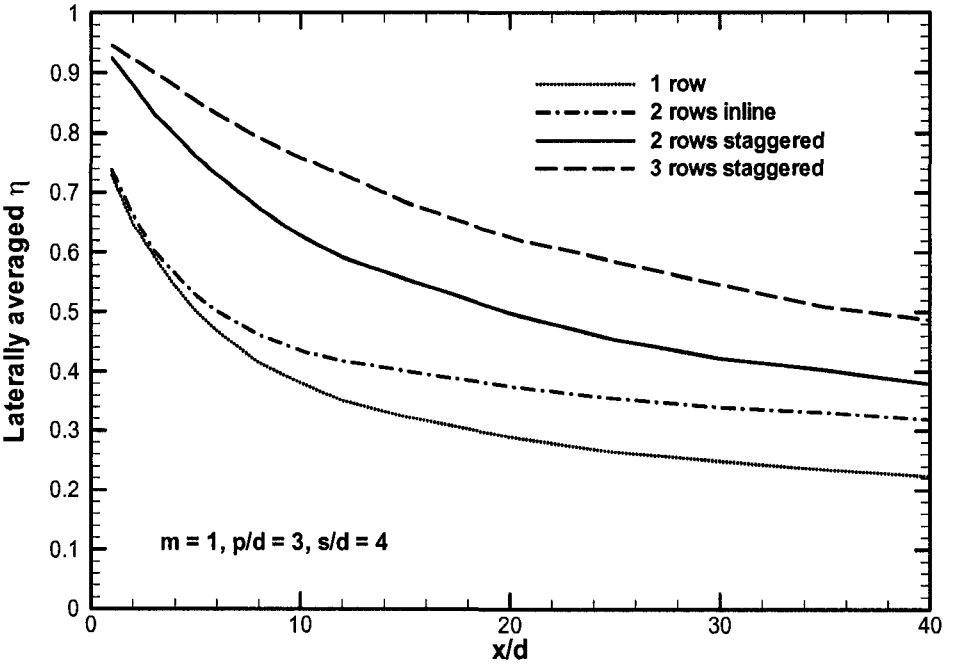

Fig. 4.8 Comparison of laterally averaged η between 1, 2, and 3 rows of the louver scheme.

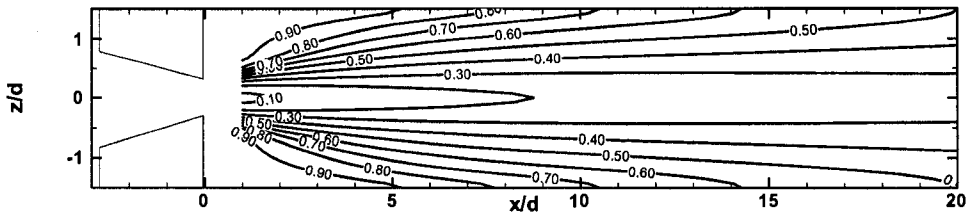

a. Two inline rows

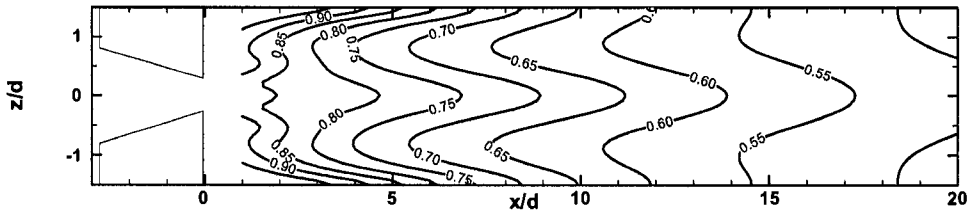

b. Two staggered rows

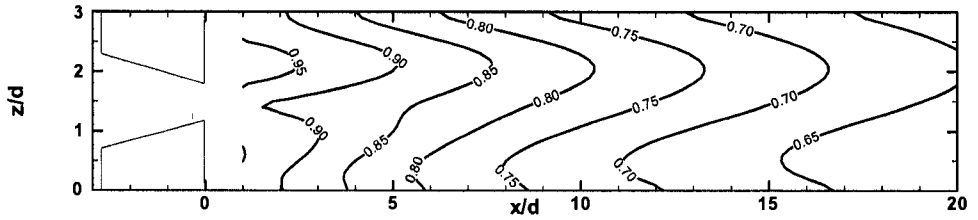

c. Three staggered rows

Fig. 4.9 Contours of η on the test surface.

jets from the laterally expanding exits is too weak to spread coolant in the span-wise direction under the strong influence of the mainstream. At high blowing ratios, the mainstream is strong enough to break into the jet at the leading edge of the exit prior to the injection. The two staggered rows provide more even protection, as shown in Fig. 4.9b, simply because the jets are better positioned causing more uniform distribution of the coolant after injection. The three staggered rows provide slightly higher cooling effectiveness, compared with two rows, but the coverage is no more uniform, as shown in Fig. 4.9c.

4.2.3 Mean velocity and turbulence characteristics

Figure 4.10 shows the normalized stream-wise velocity profiles on the central plane at the blowing ratio of 1. The thickness of boundary layer increases downstream after injection, as can be seen from the comparison of velocity profiles at different locations. The velocity gradually increases further away from the wall, signifying that the coolant stays close to the wall without penetration. At x/d = 1, the injection of the jets causes a large disturbance to the boundary layer, particularly for the two inline rows arrangement, as shown in Fig. 4.10a. This disturbance is relaxed quickly after x/d = 4. The thickness of the coolant layer at the central plane for two staggered rows is substantially thinner than that of two inline rows at all locations after injection. Therefore, coolant accumulates at the centerline of the two inline rows arrangement after the injection of the second jet, resulting in poor spreading. Although the three rows arrangement has roughly the same coolant layer thickness as the two inline rows, this is only because it has 50% more coolant to distribute on the wall.

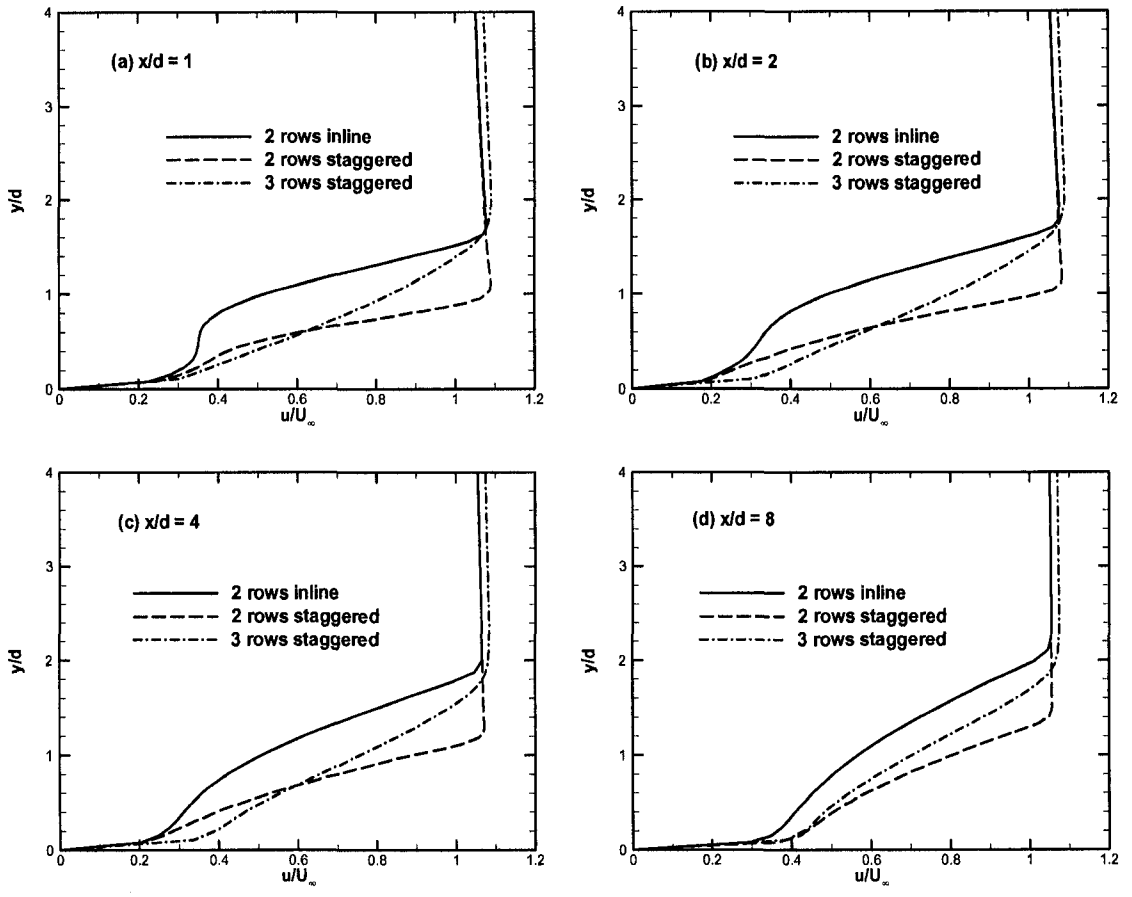

Fig. 4.10 Profiles of the stream-wise velocity on the central plane for m = 1 at (a) x/d = 1, (b) x/d = 2, (c) x/d = 4, and (d) x/d = 8.

Figure 4.11 shows the turbulence kinetic energy profiles along the centerline at the blowing ratio of 1. Among these three configurations, the two inline rows generate the highest level of turbulence, while three staggered rows have the lowest turbulence level. The accumulation of coolant on the wall after injection pushes the maximum level of turbulence further from the wall with two inline rows as compared with two or three staggered rows. It is also observed that the area of high turbulence in the two inline rows arrangement is larger than two staggered rows counterpart. This causes greater coolant mixing with the mainstream. Consequently, there is a lower level of laterally averaged effectiveness with the inline arrangement. The three staggered rows create a larger area of turbulence in the vertical direction than the two row configurations. However, its turbulence level is considerably lower with subsequent lower mixing and higher effectiveness.

4.2.4 Heat transfer coefficient

Figure 4.12 and Fig. 4.13 shows heat transfer coefficient of the louver scheme in comparison with other cooling schemes published in recent years. It was determined that at a low blowing ratio, Fig. 4.12, the louver scheme yields nearly the same level of heat transfer as other schemes. At a high blowing ratio, Fig. 4.13, a lower level of heat transfer compared to previous cooling schemes is predicted because the louver scheme prevents jets from penetrating into the mainstream, resulting in less mixing with the mainstream and better coverage. Figure 4.13 also demonstrates the prediction of two inline rows and three staggered rows. The inline arrangement provides higher heat transfer levels since coolant builds up along the centerline after injection of the second jet, as compared with

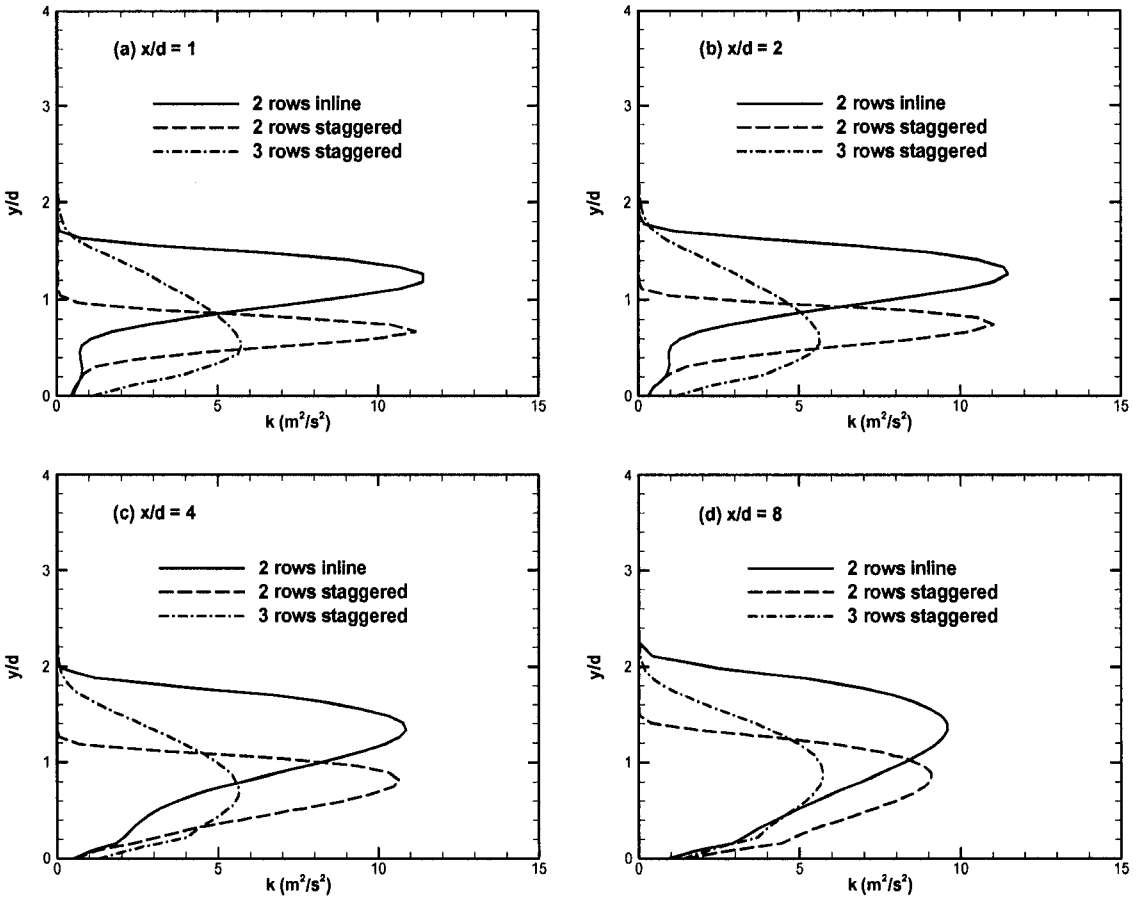

Fig. 4.11 Profiles of the k on the central plane for m = 1 at (a) x/d = 1, (b) x/d = 2, (c) x/d = 4, and (d) x/d = 8.

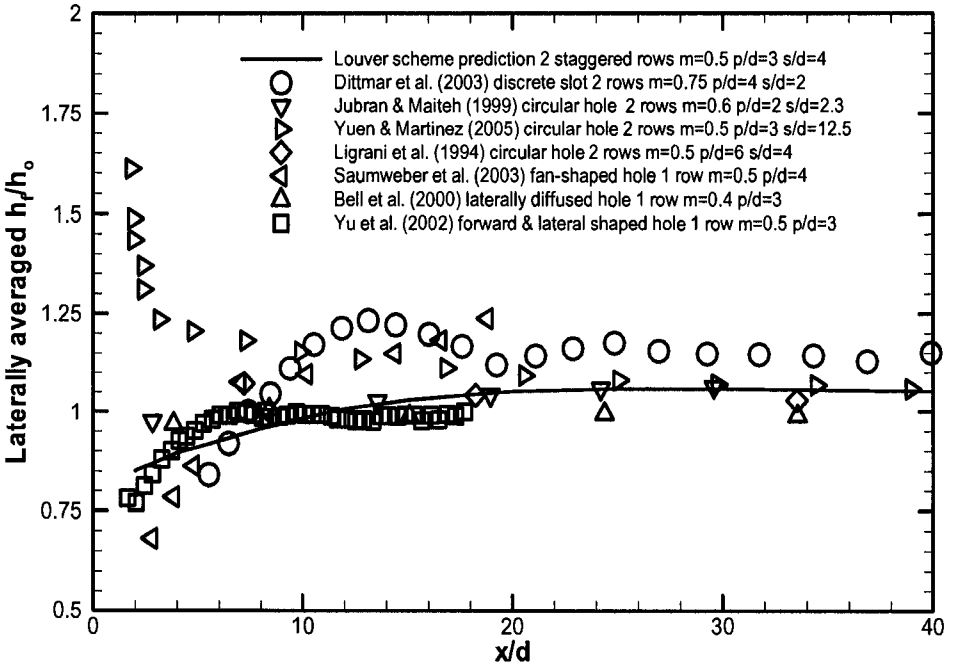

Fig. 4.12 Comparison of laterally averaged h_f/h_o for holes at low blowing ratios.

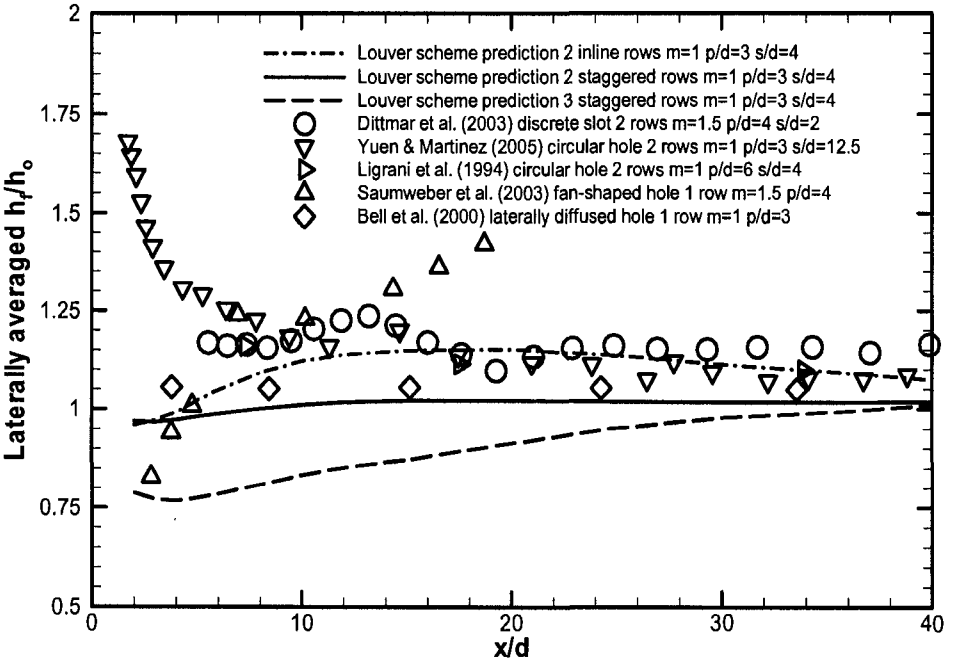

Fig. 4.13 Comparison of laterally averaged h_f/h_o for holes at high blowing ratios.

the staggered arrangement, giving rise to poor coverage of the surface. Three rows of holes offer a lower level of laterally averaged heat transfer than two rows. Interesting here is that three rows provide a heat transfer level considerably lower than two rows of holes while the heat transfer level of two rows of holes lingers around 1. This is caused by additional coolant being injected by the three rows arrangement. Hence, a thicker coolant boundary layer reduces heat transferred to the protected surface. Comparison of heat transfer levels for the louver scheme between high and low blowing ratios shows that the heat transfer value is insensitive to the blowing ratios, lingering around one. This is in contrast to the circular holes scheme in which the heat transfer level increases with blowing ratio since high blowing ratio causes higher levels of mixing and penetration. Therefore, high blowing ratios can be used with the louver scheme to generate more protection without concern about raising heat transfer levels.

4.3 Summary

A methodology with high fidelity developed and validated in a number of benchmark cases in previous studies has been applied to the louver scheme with two and three rows of holes. In order to make the results of predictions of the louver scheme comparable to those of the other schemes from the experimental works in the literature, the dimension of the louver scheme was scaled appropriately. Due to a lack of available experimental data for multiple rows of holes, either shaped or circular, some comparisons were made between the predictions of the louver scheme and experimental data of other schemes under different parameters, such as pitch ratio, blowing ratio, and row spacing. After all the differences were considered, the following conclusions emerged.

1. The proposed cooling scheme can prevent jets from lifting off the surface at high blowing ratios and provides the highest cooling effectiveness among the schemes compared. The new cooling scheme also produces a considerably lower heat transfer coefficient in the near hole region, as compared with circular hole. This is particularly true at high blowing ratios when coolant jets from circular holes undergo liftoff.

2. The two staggered rows of holes provide much better surface protection than two inline rows. The staggered arrangement offers much higher laterally averaged cooling effectiveness with a slightly lower heat transfer coefficient. In addition, in the staggered arrangement, both the cooling effectiveness and heat transfer results are more uniform.

3. Three staggered rows give slightly higher cooling effectiveness than its two rows counterpart but with considerably lower heat transfer results. From the viewpoint of surface cooling, two staggered rows are highly recommended when row spacing is small, since three rows of holes offer only 10% increase in cooling effectiveness with a 50% coolant increase.

4. Reducing the pitch ratio in half from 6 to 3 roughly doubles the laterally averaged cooling effectiveness partly because the jet liftoff effect at high blowing ratios is avoided leading to more uniform coverage of the protected surfaces and partly because jets 6d apart are too far from each other to coalesce easily after injection leaving the mid-span unprotected.

5. The heat transfer results for the two rows of holes, whether inline or staggered or at different pitch ratios, are insensitive to blowing ratios with the normalized averaged heat transfer coefficient lingering around 1. This is a desirable characteristic since high blowing ratios can be used to generate a higher cooling effectiveness.

Chapter 5

Unsteady Analysis of the Louver Cooling Scheme

In this chapter, unsteady analysis of the louver cooling scheme was carried out using a DES (Detached Eddy Simulation) model. Only film holes on a flat plate was simulated. As unsteady analysis is computational intensive, only one hole was considered in the computational domain with periodic boundary condition. Code validation was done with a widely used benchmark experimental study in the open literature. Care was taken to ensure convergence and simulation accuracy, including the time step size study, number of inner iterations between time steps, and effects of computational domain – whether a half hole or a whole hole. Particular attention was paid to unsteady flow chrematistics. Fast Fourier Transform (FFT) was also performed in an effort to understand the vortical structures and mixing process of the jet-in-a-crossflow from the perspective of turbulent frequency spectrum.

5.1 Simulation details

The test conditions were based on Sinha et al. [4] study, in which experiments were conducted in a closed-loop low speed wind tunnel facility. The test section is a flat plate made of polystyrene foam to reduce the conduction errors during the test. Cooler air was issued from a row of holes, each 1.27 cm in diameter and spaced 3 diameters apart laterally. Thermocouples were positioned on the test surface to obtain the cooling effectiveness data. The mainstream flow conditions were kept constant, free stream

velocity 20 m/s at the inlet and turbulence level about 0.2 percent. Different blowing ratios were achieved by changing the plenum inlet mass flow rate. The louver cooling scheme were tested under the same conditions numerically. The film cooling hole configurations are shown in Fig. 5.1a and Fig. 5.1b, the circular hole and the louver cooling scheme, respectively.

The Reynolds number based on the hole diameter is 16200. Therefore, turbulent flow prevails. The flow is governed by conservation equations of continuity, momentum, and energy. In addition, a turbulence model is needed to reach a mathematical closure. In this study, the Realizable k-ε based DES model provided by FLUENT Inc. was selected to carry out the simulations. In the DES turbulence modeling, the unsteady RANS models are employed in the near wall regions while the same filtered models are utilized in any other regions away from walls. The transport equations for k and ε in the Realizable k-ε model were given in Chapter 3.

Figure 5.1c shows the computational domain and boundary conditions for the louver cooling scheme. Assume infinite rows of film cooling holes on a flat plate, so that the end-wall effects can be neglected. At the upstream inlet, a constant velocity of 20 m/s normal to the inlet boundary was applied with the free-stream turbulence being 0.2% as in the experimental work. At the outlet, a pressure boundary condition was imposed. The domain extended 20d from the bottom test surface, far enough such that a free slip boundary condition or zero shear stress may be applied. If the computational domain was only half of a period, symmetry boundary conditions were imposed at both the central plane and at the 1.5d plane in the stream-wise direction. If a full domain was employed, a periodic boundary condition would be applied. At the bottom wall, as well as the other

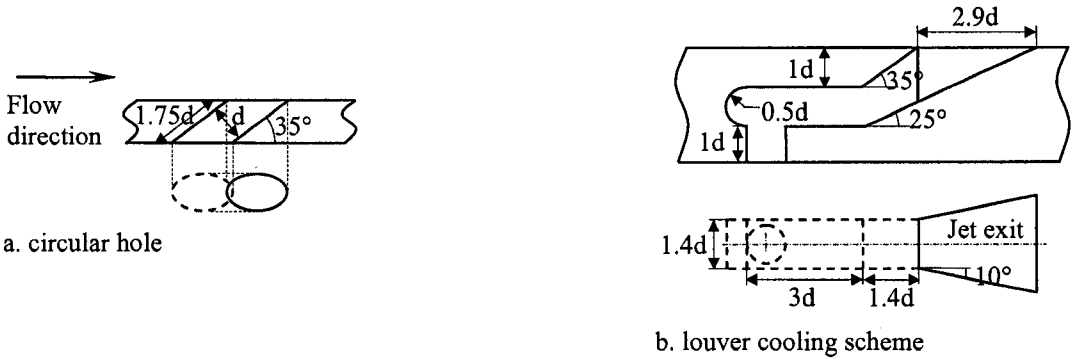

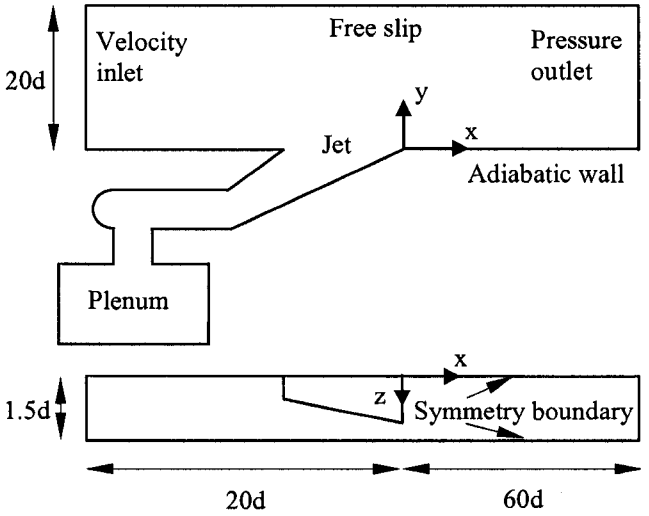

c. computational domain and boundary conditions

Fig. 5.1 Film cooling configurations and computational domain with boundary conditions (not to scale).

walls, an adiabatic wall boundary condition with no-slip was imposed. The temperatures at the mainstream and plenum inlets were specified at 300K and 150K, respectively, which gives a coolant to mainstream density ratio of 2. All these boundary conditions were based on Sinha et al. [4].

Multi-block mostly structured meshes, Fig. 5.2, were created to fully resolve the features of the flow field with most of the cells concentrated in areas of large variable gradients. The grids contain between 0.3 and 0.8 million cells depending on whether it is a half or full meshed domain. The cases were firstly run on a workstation for the steady state solution with a CPU of 3 GHz and a RAM of 3 GB. It took around 2000 iterations to reach convergence, approximately 20 hours of computing time. The case and data files were subsequently transferred to a super-computer – an HPC cluster – for further computation. After being switched to unsteady state simulation with the steady state results as the initial solution, the simulation continued to run parallel on 16 nodes with 16 GB memory on the cluster. The iterations were stopped to check whether a statistically steady state was reached. If the answer is positive, data sampling for time statistics will be launched for more iterations to calculate the time averaged results. It took two weeks of intensive parallel computing on 16 nodes on the cluster to get one sound solution.

5.2 Results and discussion

5.2.1 Time step size and number of sub-iterations

The time step size in an unsteady analysis affects the maximum frequency that can be resolved in the flow field. For finding the more appropriate time step size under the flow condition four different time steps from $\Delta t = 1\times10^{-4}$s to $\Delta t = 1\times10^{-6}$s have been tested, as

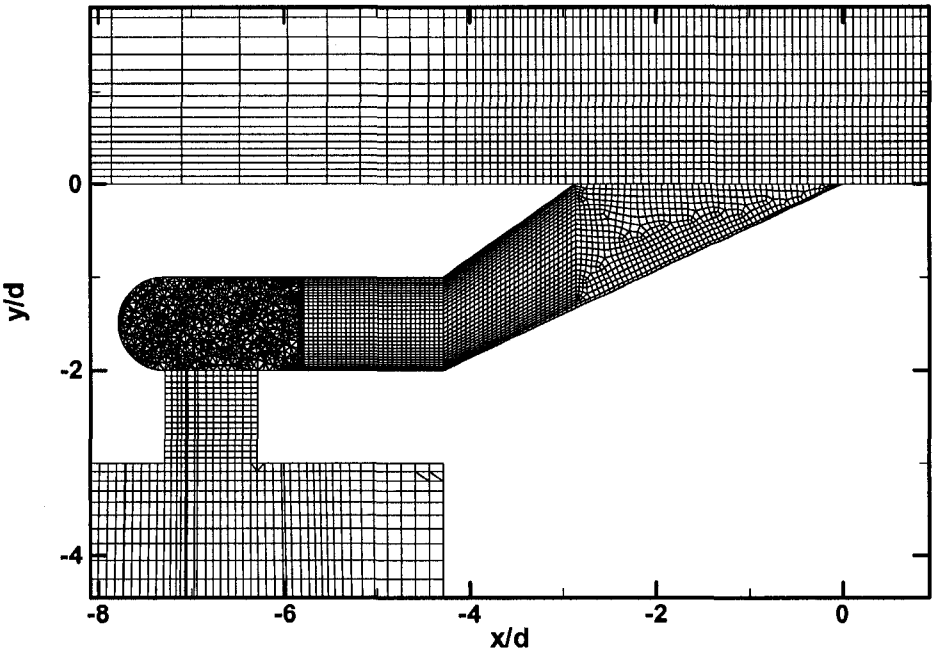

Fig. 5.2 A typical multi-block mostly structured mesh.

shown in Fig. 5.3. The amplitude, frequency and mean value of the velocity fluctuations for different time step sizes were compared. It turned out that $\Delta t = 1\times10^{-5}$s is capable of capturing the unsteady features of the flow and was deemed sufficient (Kim et al. [102]). The number of sub-iterations at each time step also has a big impact on the final results. Therefore, it is very important to ensure that convergence is reached at one time step before marching to the next time step. Otherwise, the errors caused by insufficient number of iterations at each time step – a not fully converged solution at each time step – will add up and eventually contaminate the final solution. In this study, different numbers of sub-iterations were tested and Fig. 5.4 shows the result. In addition, at each time step the solution residuals dropped at least three orders of magnitude. After comparing the results by different numbers of sub-iterations, it was concluded that the number of 30 iterations per time step is adequate.

5.2.2 Effect of computational domains

When a half domain was used, the symmetry boundary conditions were imposed on the center plane and z/d = 1.5 plane. The use of the symmetry boundary condition can be considered as a limitation of the unsteady simulation as it prevents the possibility of capturing the unsteady asymmetric vortical flow patterns in the spanwise direction. To evaluate the effects of domain size, unsteady simulations using both a half domain with the symmetry boundary conditions and a full domain with a periodic boundary condition have been performed.

Instantaneous temperature contours and the corresponding velocity vector distributions at x/d = 5 plane are shown in Fig. 5.5. Both sides of the symmetric line are plotted to

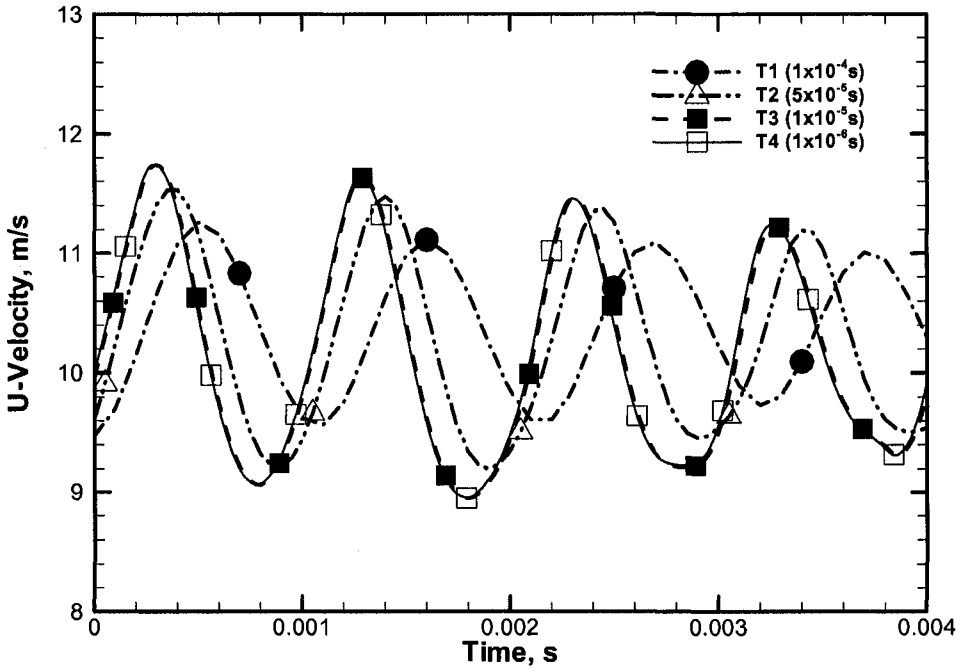

Fig. 5.3 Time step size test – velocity time histories at point (2d, 0.4d, 0.08d) for the cylindrical jet.

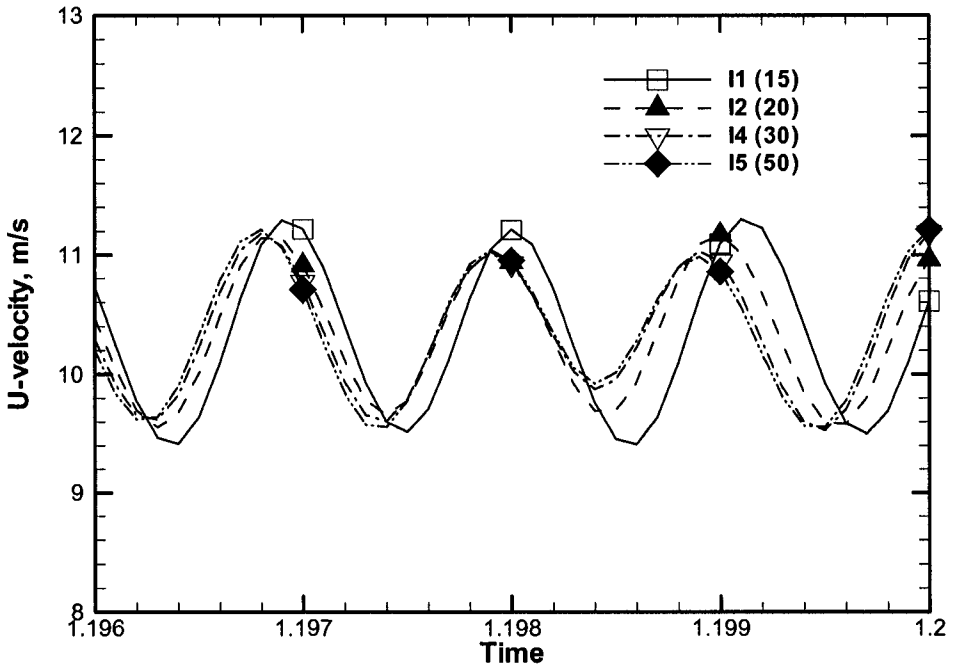

Fig. 5.4 Test of number of sub-iterations – velocity time histories at point (2d, 0.4d, 0.08d) for the cylindrical jet.

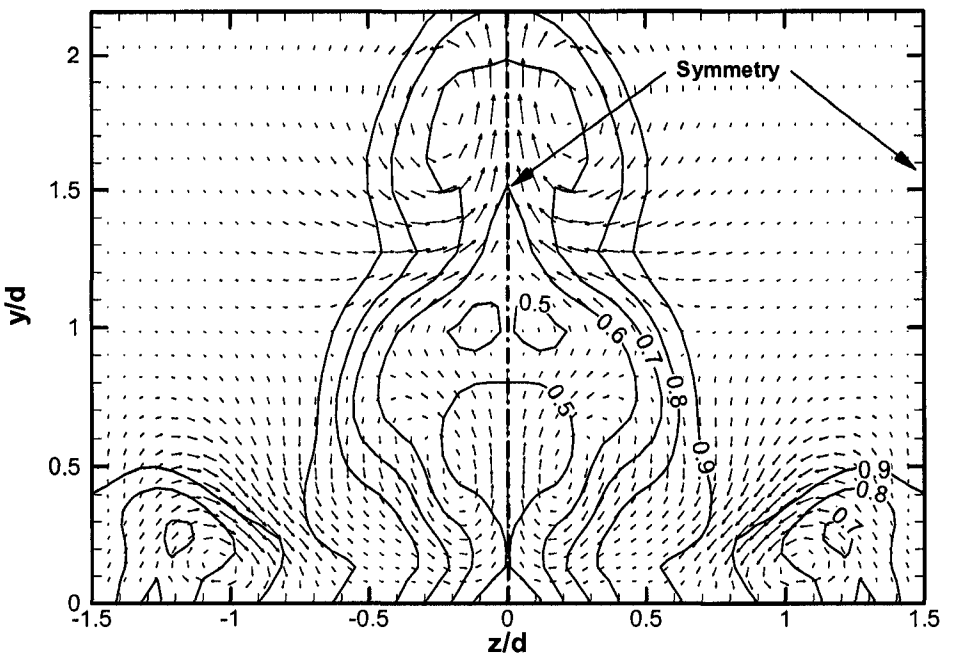

(a) Half domain with symmetric boundary conditions

(b) Full domain with periodic boundary conditions

Fig. 5.5 Instantaneous temperature (θ) contours and velocity vectors at x/d = 5 plane for the louver scheme.

depict the dominant bound vortical structures for the case with a half domain, Fig. 5.5a. In contrast to the case with a half domain, Fig. 5.5b shows asymmetric distribution in nature from the full domain computation. The coolant of the case with a full domain exhibits unsteady spanwise fluctuations, whereas the computation with a half domain could not capture the full fluctuation in the spanwise direction. The unsteady simulation with a full domain is, thus required to accurately predict lateral spreading of the coolant for a film cooling flow as well as for unsteady three dimensional flow structures. Hence a full computational domain with periodic boundary conditions was used throughout the remaining computations.

5.2.3 Comparison with experimental measurement

Figure 5.6 shows the comparison between experimental and computational data of film cooling effectiveness along the centerline for the cylindrical jet at the blowing ratio of 1. At high blowing ratios, the coolant jets lift off from the surface. The steady predictions of other researchers, Leylek and Zerkle [96], Mulugeta and Patankar [103], Ferguson et al. [104], and Walters and Leylek [97], failed to capture the jet liftoff phenomenon near and downstream of the injection hole, Fig. 5.6, possibly due to either inadequate grid density or turbulence modeling. In Ferguson et al. [104] and Walters and Leylek [97], unstructured meshes were employed which prevents adequate grid concentration at the jet exit area. Even when the grid concentration was adequate, the standard k-ε model completely missed the jet liftoff as shown in [52] and the standard k-ε model was used in [96,97,103]. However, the present DES prediction showed a greater rate of decrease in effectiveness immediately downstream of the injection hole, due to the jet liftoff and hot

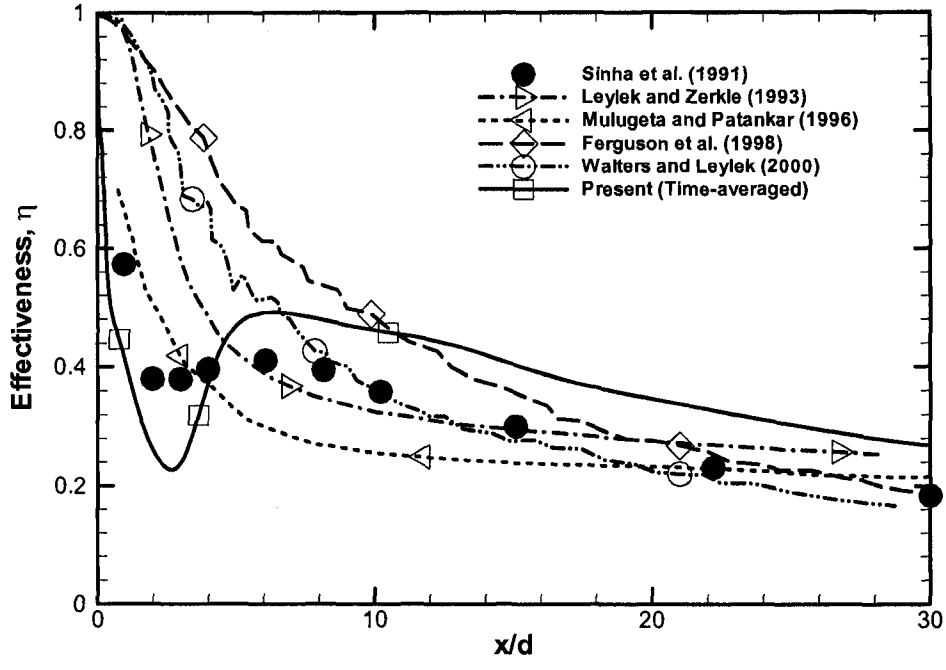

Fig. 5.6 Comparison of centerline η between experimental and computational values for the cylindrical jet (symbols used on lines for distinguishing).

entrainment flows. The time-averaged distribution of the laterally averaged film-cooling effectiveness is shown in Fig. 5.7. Also shown are the experimental data of Sinha et al. [4] and other numerical results at the same blowing ratio and with the same geometry. The present RKE based DES simulation gives an improved prediction, compared to the S-A based DES result of Roy et al. [70], Fig. 5.7. The ability of DES simulation to capture the jet liftoff and unsteady behaviors is desirable.

5.2.4 Time averaged film cooling characteristics

Unsteady simulations for the louver cooling scheme have been performed in this study using the Realizable k-ε based DES model for the blowing ratios of 0.5 and 1.0. A comparison between the steady and unsteady time-averaged results, and the experimental data of the traditional cylindrical hole and forward and lateral shaped holes was made. The present time-averaged data was obtained from a computation of 15,000 time steps.

Figure 5.8 and Fig. 5.9 show the centerline effectiveness for the louver scheme at the blowing ratios of 0.5 and 1.0, respectively. The difference of cooling effectiveness between the steady and unsteady time-averaged results can be seen. Also shown are the experimental data of the traditional cylindrical holes by Sinha et al. [4] and forward and lateral shaped holes by Yu et al. [50]. For the blowing ratio of 0.5, Fig. 5.8, the centerline effectiveness is at the same level for both the traditional cylindrical hole and the louver cooling scheme since both jets stay attached to the surface after injection. The unsteady fluctuation of the coolant jet for the blowing ratio of 0.5 is relatively weak. Consequently, the time-averaged centerline effectiveness is almost same as the steady result. For the blowing ratio of 1.0, Fig. 5.9, the jets in Sinha et al. [4] case lift off from the surface

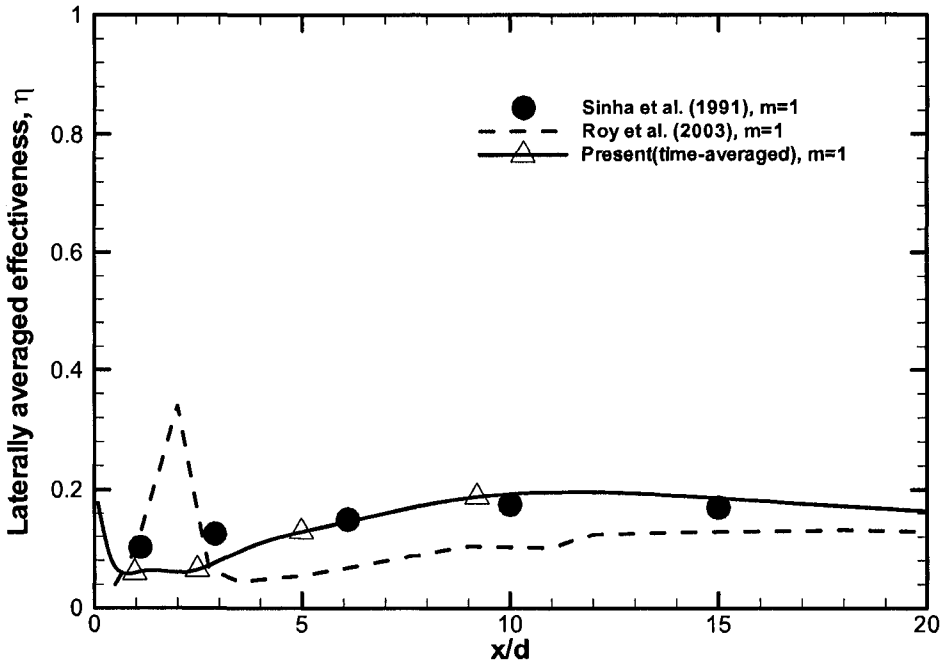

Fig. 5.7 Comparison of laterally averaged η between experimental and computational values for the cylindrical jet.

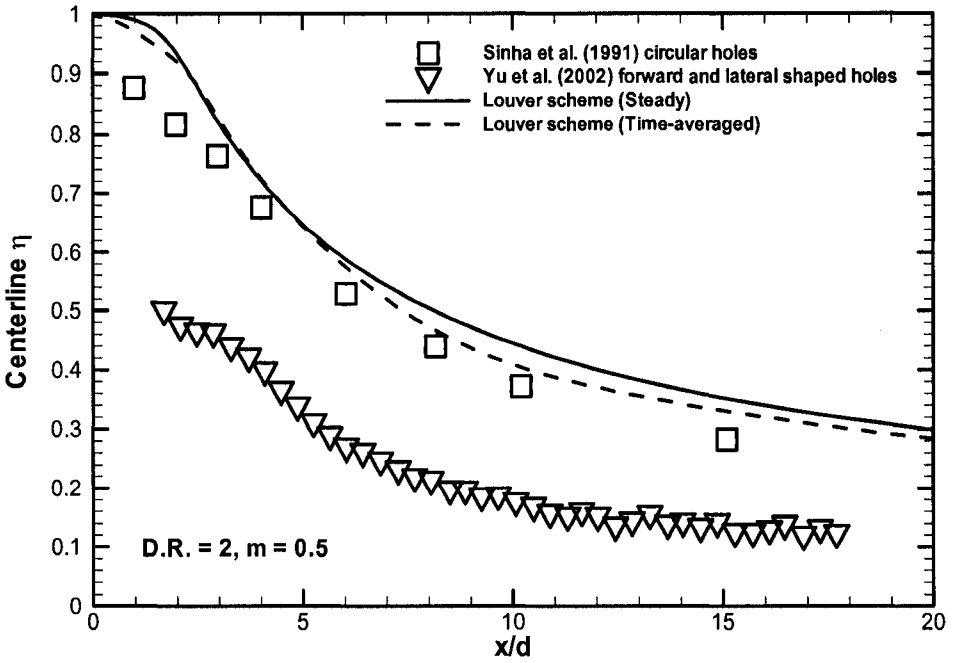

Fig. 5.8 Centerline η for the louver scheme at low blowing ratio of 0.5.

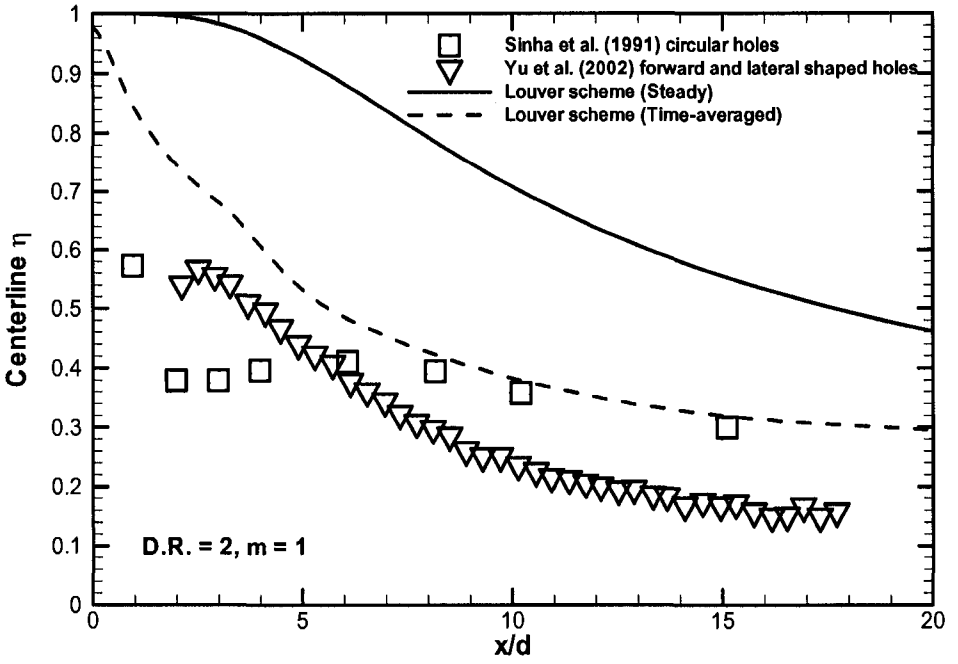

Fig. 5.9 Centerline η for the louver scheme at high blowing ratio of 1.

causing a sharp drop in effectiveness immediately downstream of the injection. However, in the louver scheme the jets remain attached to the surface and the effectiveness gradually decreases in the streamwise direction. The time-averaged centerline effectiveness is lower than that of steady prediction, in contrast to the case of the blowing ratio 0.5. A higher unsteady fluctuation of the coolant jet in spanwise direction occurs, causing a wider spreading of coolant and a lower level of centerline effectiveness than that of the steady result.

The effect of the unsteadiness in spanwise direction on the film cooling effectiveness can be seen easily in Fig. 5.10 and Fig. 5.11, which show the effectiveness distribution in the spanwise direction at blowing ratio of 0.5 and 1, respectively. At the blowing ratio of 0.5, Fig. 5.10, the effectiveness of both steady and unsteady (time-averaged) predictions is almost the same in the central region. Only a little more spread of the coolant is observed at time-averaged results. In the case of a blowing ratio of 1.0, Fig. 5.11, the time-averaged local effectiveness of the louver scheme is much lower than that of steady prediction in the central region, whereas it is higher in the outer region. The time-averaged effectiveness of the louver scheme is still higher than that of the cylindrical jets. Moreover, the time-averaged effectiveness of the louver scheme along the x/d = 15 line is almost uniform, which is considered more realistic.

Figure 5.12 and Fig. 5.13 show the comparison of laterally averaged effectiveness between different cooling schemes, namely, the traditional circular holes by Sinha et al. [4], forward diffused holes by Bell et al. [49], both forward and lateral shaped holes by Yu et al. [50], straight fan-shaped holes by Dittmar et al. [24], fan-shaped holes by Saumweber et al. [39], and forward-lateral-diffused holes by Taslim and Khanicheh [30].

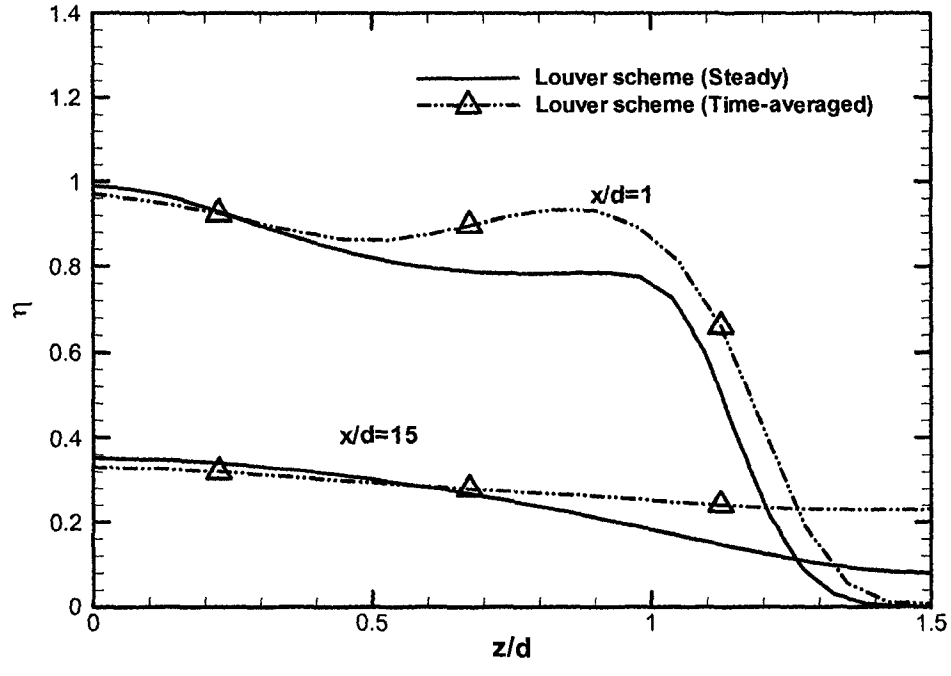

Fig. 5.10 Comparison of local η for the louver scheme at blowing ratio of 0.5.

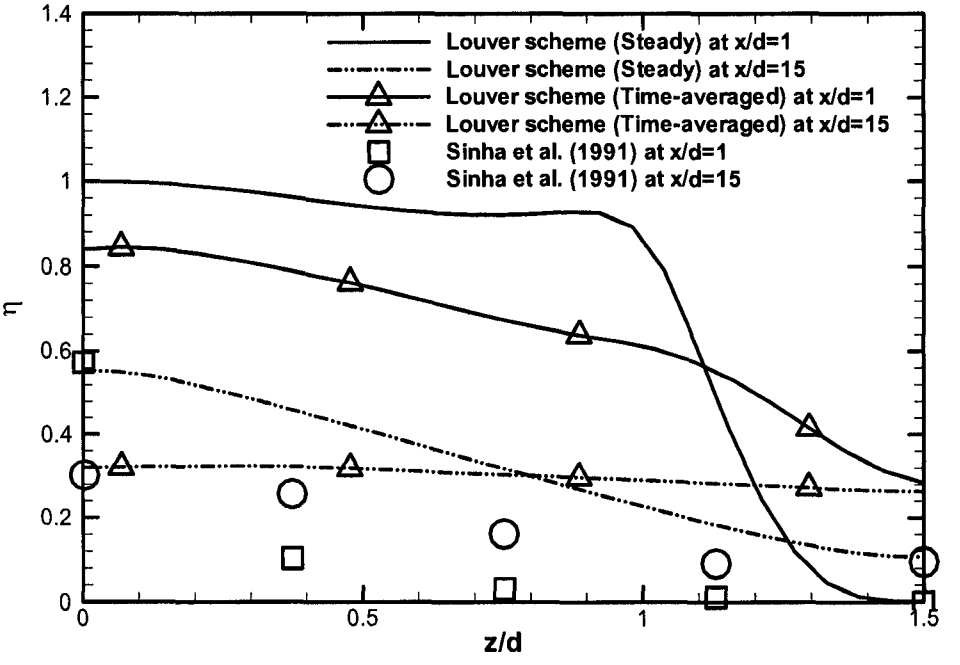

Fig. 5.11 Comparison of local η between the louver scheme and the cylindrical jet of Sinha et al. [4] at blowing ratio of 1.

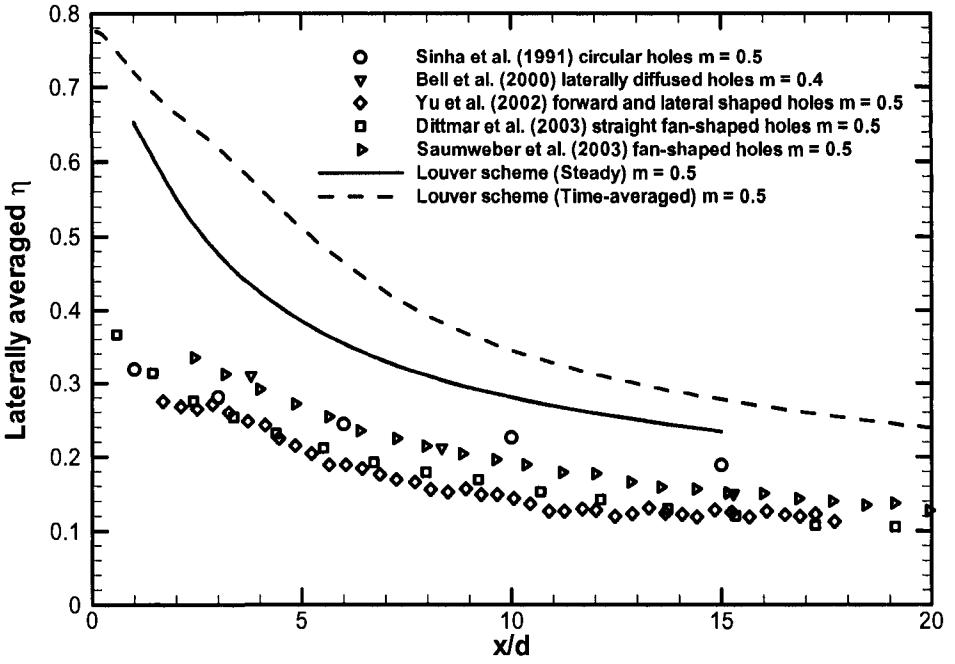

Fig. 5.12 Comparison of laterally averaged η between the louver scheme and other cooling schemes at low blowing ratios.

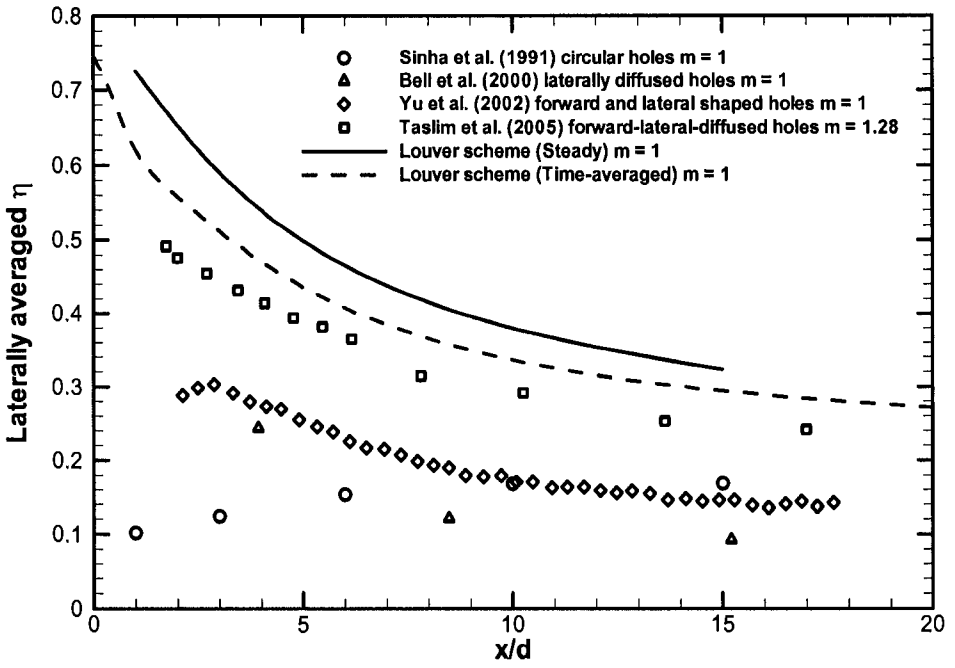

Fig. 5.13 Comparison of laterally averaged η between the louver scheme and other cooling schemes at high blowing ratios.

The DES time-averaged result shows a lower effectiveness distribution at high blowing ratios and a higher effectiveness at low blowing ratios than that of steady result, possibly the result of a wider spreading of the coolant in the span-wise direction in the DES unsteady solution, Fig. 5.12 and Fig. 5.13. The decay of adiabatic film cooling effectiveness of the steady simulation seems to be over-predicted on the test surface. The unsteady DES simulation may provide more reasonable predictions, especially for high blowing ratios, Fig. 5.13. The time-averaged result of laterally averaged cooling effectiveness of the louver scheme is still the highest, when some cooling schemes such as the circular holes undergo liftoff at the high blowing ratio of 1.

5.2.5 Unsteady flow characteristics

The non-dimensional temperature distributions, including the instantaneous, unsteady-state time-averaged, and steady state results, at the center plane in the wake region for both the cylindrical jet and the louver cooling scheme are presented in Fig. 5.14 and 5.15, respectively. The instantaneous picture shows a highly unsteady mixing layer, Fig. 5.14a and 5.15a. The hot spot immediately downstream of the jet exit, caused by a coolant jet liftoff and hot entrainment flows, can be seen for the cylindrical jet, Fig. 5.14a. A comparison between Fig. 5.14a and 5.15a reveals that under the same blowing ratio the coolant-mainstream mixing process in the shear layer is more intense for the cylindrical than for the louver scheme. Most of the mixing takes place before x/d of 10 after which the coolant is mostly settled, especially for the louver scheme. The unsteadiness enhances the mixing process in the wake region and enlarges the mixing layer for the louver scheme. Contrary to the steady temperature distribution with a relatively thinner coolant

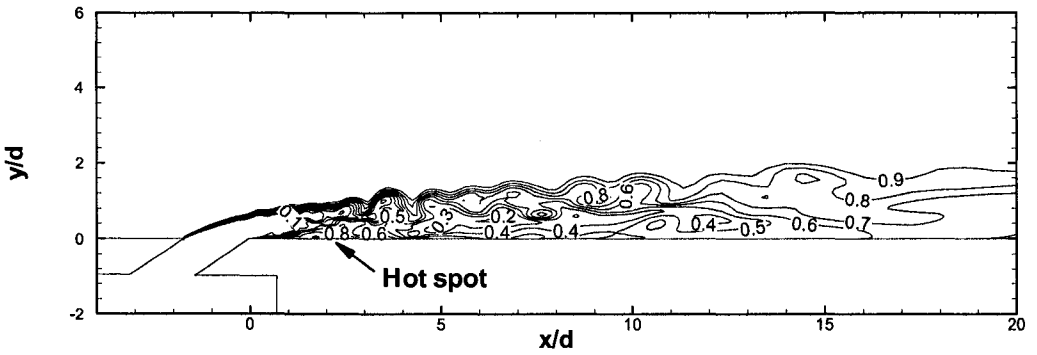

(a) Instantaneous

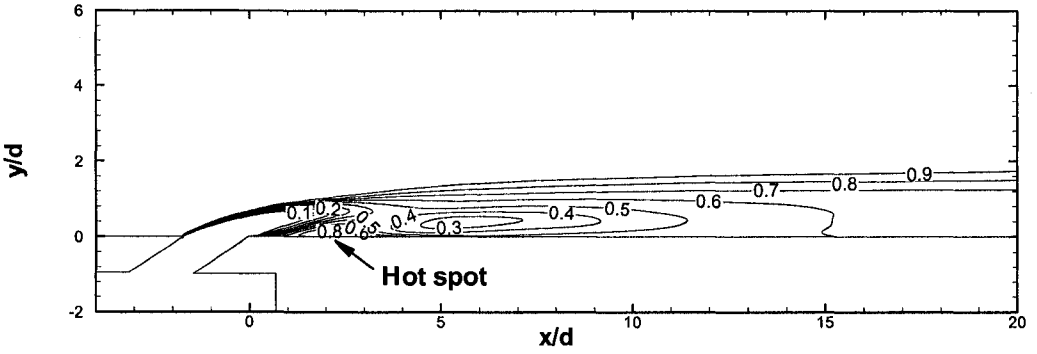

(b) Time-averaged

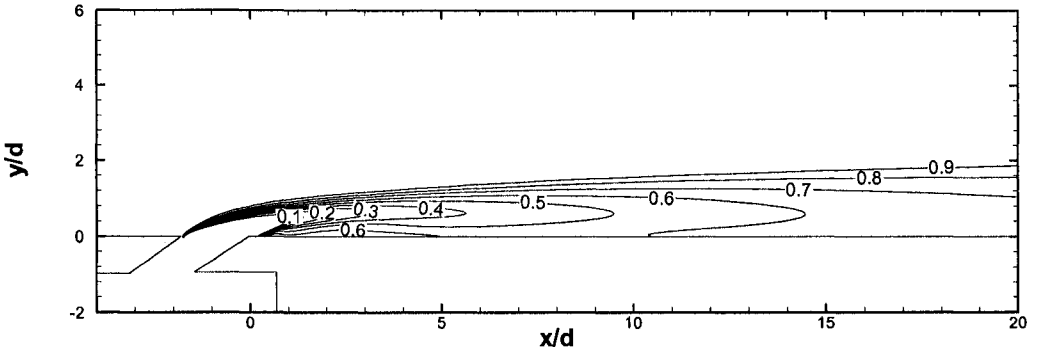

(c) Steady

Fig. 5.14 Instantaneous, time-averaged and steady nondimensional temperature (θ) distributions at centerplane (m = 1) for the cylindrical jet.

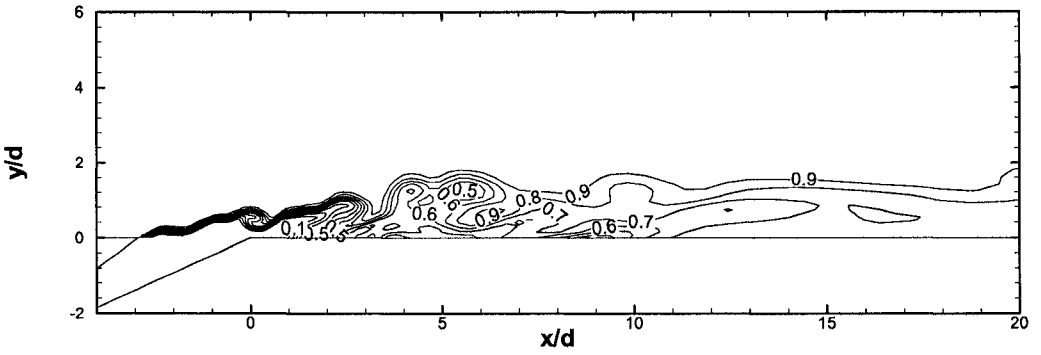

(a) Instantaneous

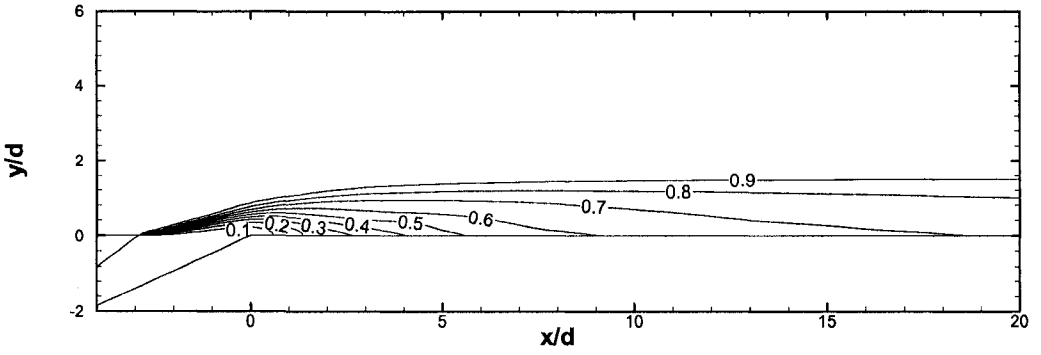

(b) Time-averaged

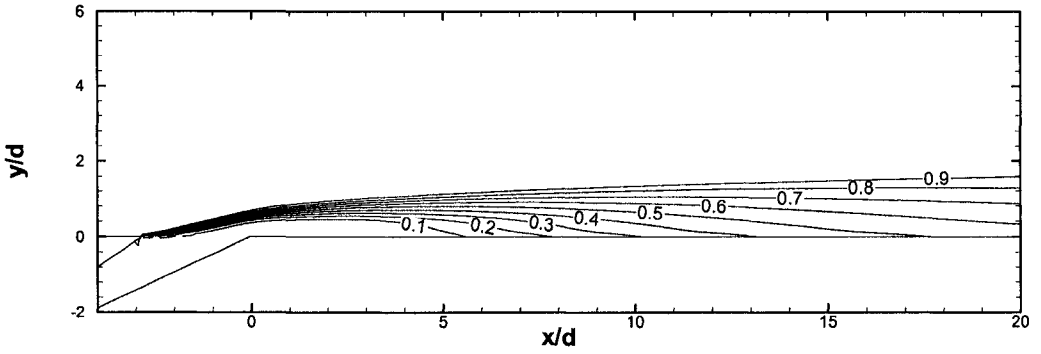

(c) Steady

Fig. 5.15 Instantaneous, time-averaged and steady nondimensional temperature (θ) distributions at centerplane (m = 1) for the louver scheme.

layer near and downstream of the injection and a longer low temperature region, Fig. 5.15c, the time-averaged result reveals an intensified mixing layer with relatively thicker and more diffused coolant, Fig. 5.15b.

Figure 5.16 shows the instantaneous, time-averaged and steady distribution of the adiabatic film cooling effectiveness on the test surface at the blowing ratio of 1 for the louver scheme. The instantaneous result shows the highly disturbed distribution in the spanwise direction. The film is locally broken up even at the core of the downstream region not far from the jet exit. That allows the hot fluid to tuck in close to the wall, locally diminishing the adiabatic film cooling effectiveness. In the time-averaged result, Fig. 5.16b, it can be seen that the film cooling effectiveness of the unsteady result is laterally more uniform than that of the steady result, Fig. 5.16c, and the cooling effectiveness is symmetric in the spanwise direction, as expected.

Q-criterion ($q = (|\Omega_{ij}|^2 - |S_{ij}|^2)/2$) had been used to identify coherent vortical structures in the literature recently. It indicates the balance between the rotation rate and the strain rate. Positive Q isosurfaces identify areas where the strength of rotation surpasses the strain, thus making those surfaces eligible as vortex envelopes (Dubief and Delcayre [105]). A snapshot of typical coherent vortical structures of the cylindrical jet is shown in Fig. 5.17, in which a weak horseshoe vortex, counter-rotating vortex pair (CVP), inner vorticies (vortex tubes), and downstream hairpin coherent structures, can be identified by the Q-criterion. Inner vortices, part of vortex tubes, issued from the coolant injection hole play an important role in the jet mixing process and the jet liftoff phenomena in the near downstream region.

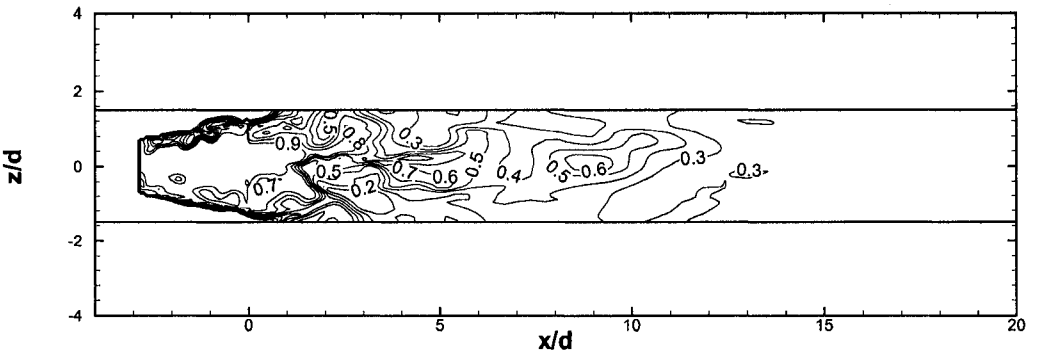

(a) Instantaneous

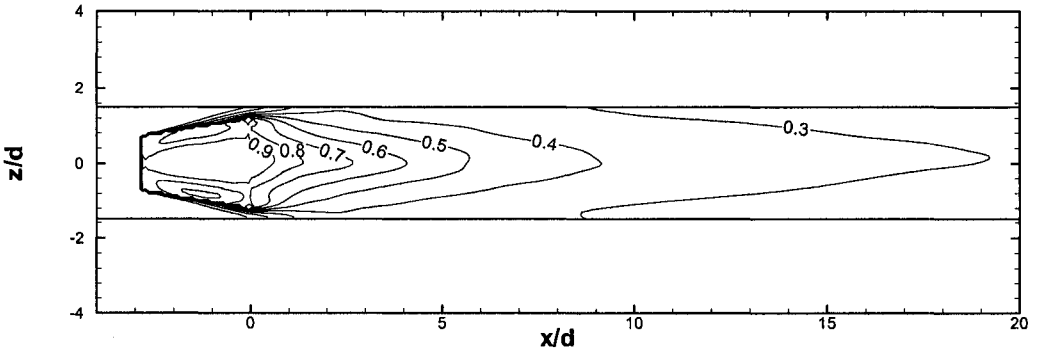

(b) Time-averaged

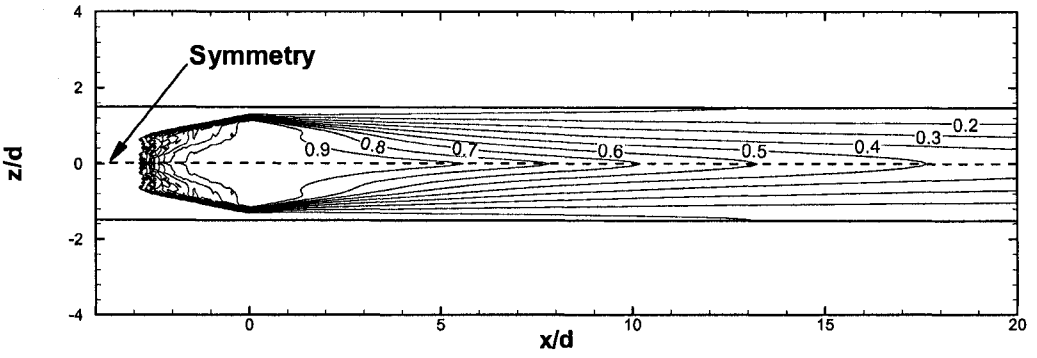

(c) Steady

Fig. 5.16 Instantaneous, time-averaged, and steady effectiveness distribution on the test surface (m = 1).

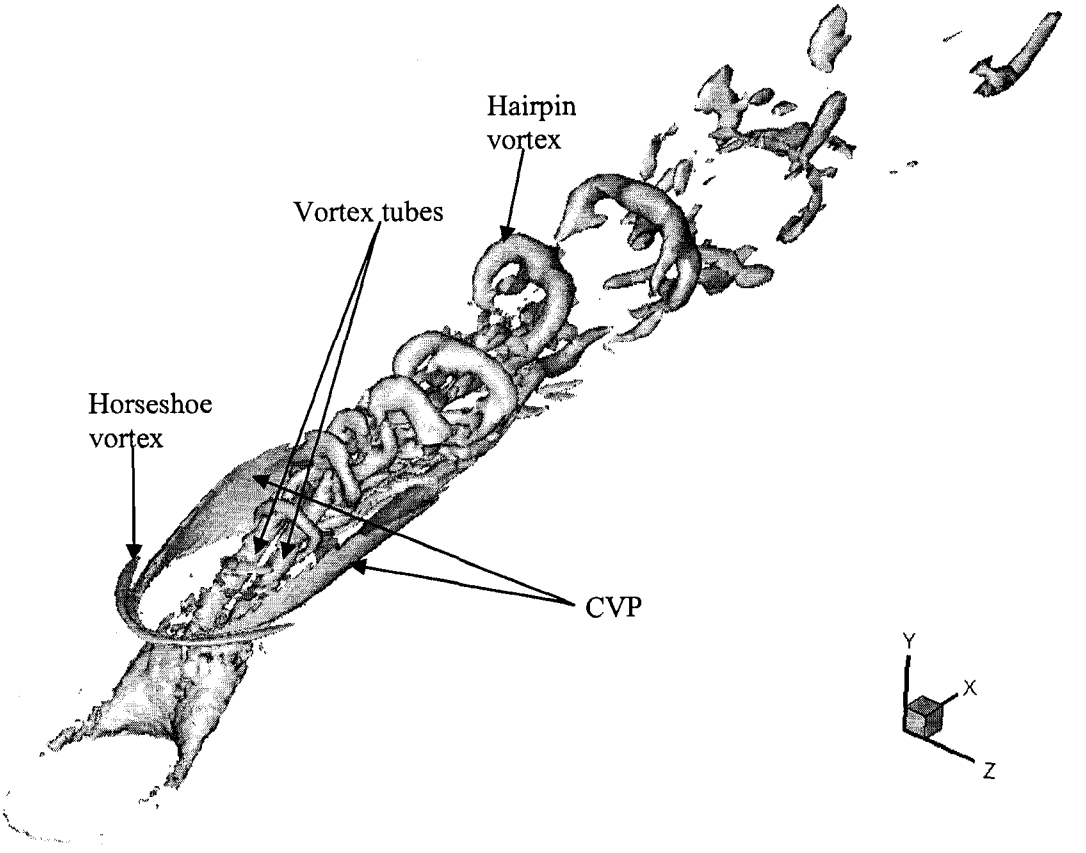

Fig. 5.17 Typical coherent structures in the inclined cylindrical jet in a crossflow.

To clearly observe the coherent structures of the film cooling flow for the louver scheme, the vorticity field at the center plane is plotted in Fig. 5.18. The roller vortices can be clearly identified in this figure. A time sequence of the coherent structures is shown in Fig. 5.19. The coherent structures are represented as a positive isosurface of Q-criterion (Q = 1). In the louver scheme, the coolant issued from the plenum impinges on the wall perpendicularly, is then redirected from vertical to horizontal direction, and finally goes through an increasing cross-sectional area and an inclined path. The primary roll-up vortices due to the impingement of a vertical jet can be seen in the contours of span-wise vorticity component ω_z, Fig. 5.18. The vertical jet is a little tilted due to the bend. The inclined vortical flow is disturbed when passing through the flared and inclined path. The shear layer and roller vortices (negative vorticity patches) originate from the leading edge of the jet exit. These roller vortices begin early to be shed over the jet exit. Thus, the hairpin coherent structure occurs from the middle of the jet exit region, Fig. 5.19. The hairpin coherent structure is identified as the primary large-scale structure as in the case of the cylindrical jet. The large-scale roll-up vortical structures are dissipated through the bended and flared path. In contrast to the case of the cylindrical jet, the inner vortex tubes and horseshoe vortex do not appear in the case of the louver cooling scheme. The hairpin vortex structures for the louver cooling scheme, Fig. 5.19a, are significantly smaller than those of the cylindrical jet, Fig. 5.17. They also break up and are dissipated earlier shortly after injection for the louver cooling scheme. Therefore, the jet liftoff is avoided and no significant hot spots were observed for the louver scheme at the same blowing ratio of 1.

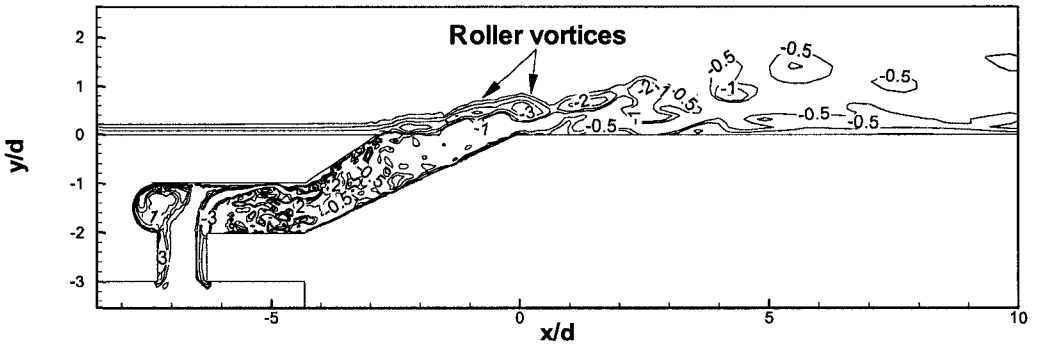

Fig. 5.18 Instantaneous pictures of the normalized vorticity, ω_z at centerplane for the louver scheme at m = 1.

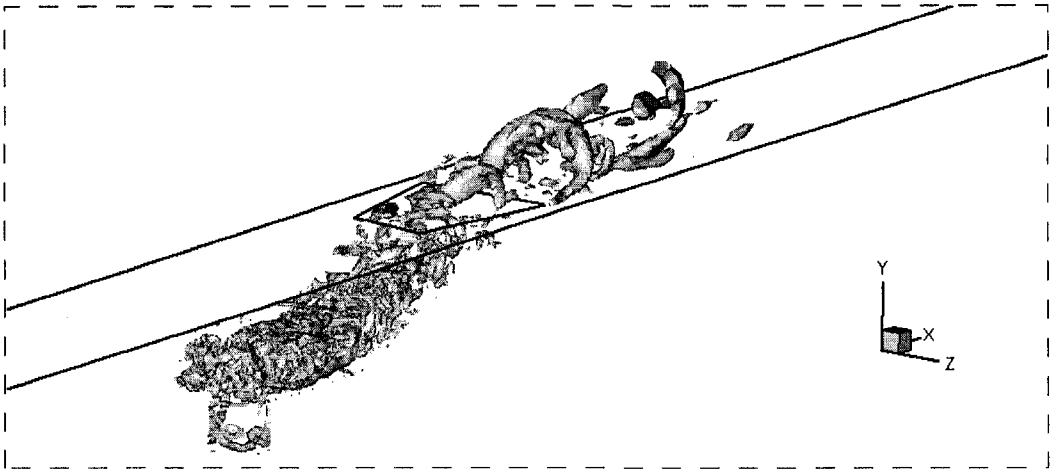

(a) at an instant, τ_0

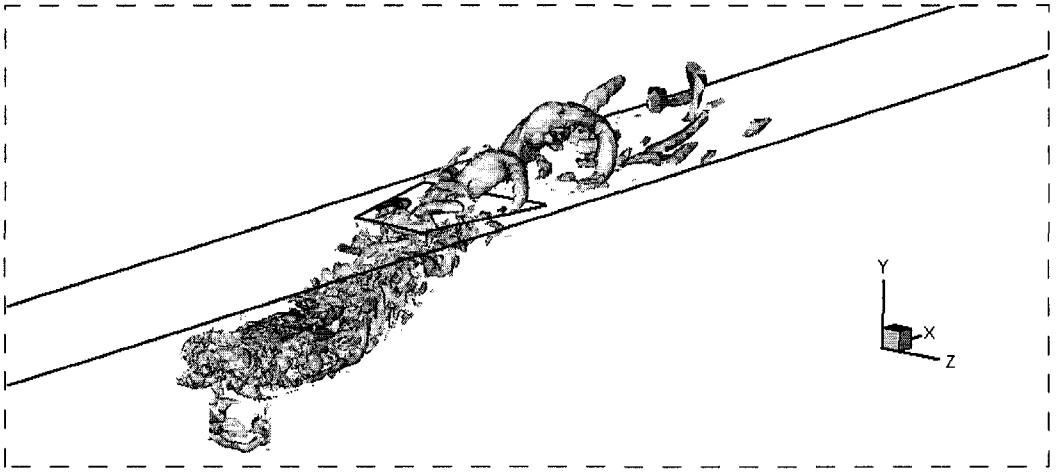

(b) at $\tau_0 + 0.8$

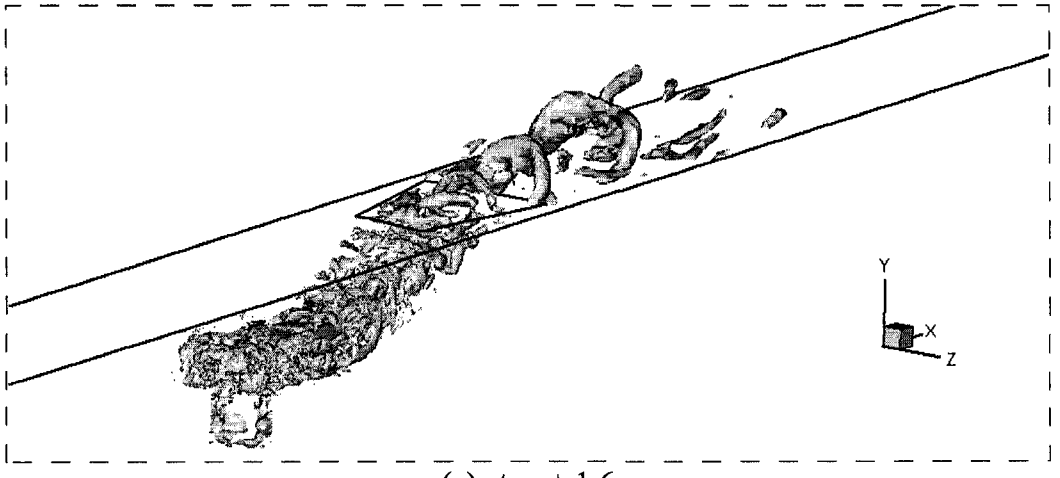

(c) at $\tau_0 + 1.6$

Fig. 5.19 Snapshots of the coherent structures for the louver scheme (m = 1).

To identify the turbulent frequency spectrum of the vortical structures and mixing phenomenon, Fast Fourier Transform (FFT) analyses were conducted using the time variant velocity components (u, v, w) at different locations. Figure 5.20 and 5.21 show the FFT frequency spectrum for the velocity components at several points. For the cylindrical jet, one distinct dominant frequency is observed at the coolant exit plane, Fig. 5.20a. However, several distinct peaks can be observed for the louver scheme, Fig. 5.20c, due to more complex geometry than the cylindrical hole. The vortical structures are dissipated and the turbulent fluctuation increases through the louver scheme, Fig. 5.19. It causes a broad band of peaks at lower as well as at higher frequencies for the cases of both m = 0.5 and m = 1.0. However, as mentioned before, the case of high blowing ratio of 1 shows higher unsteadiness and, consequently, has higher amplitude than that of the low blowing ratio of 0.5 case. The low dominant frequencies, Fig. 5.21c, for the high blowing ratio of 1 are believed to be related to the unsteady motions of the large scale coherent vortical structures. The different magnitudes of the velocity components, shown in Fig. 5.20 and 5.21, support the statement of anisotropic turbulence in the wake region.

5.3 Summary

In this chapter, the performance of the louver cooling scheme was studied by carrying out unsteady state numerical simulations using a Realizable k-ε based DES turbulence model. As a validation, an unsteady analysis was first performed for a traditionally cylindrical hole on a flat plate. A comparison with the experimental data shows that the jet liftoff was captured in the numerical prediction. The prediction of the lateral spreading of the jet after injection was also more realistic in the DES unsteady analysis than that of the steady

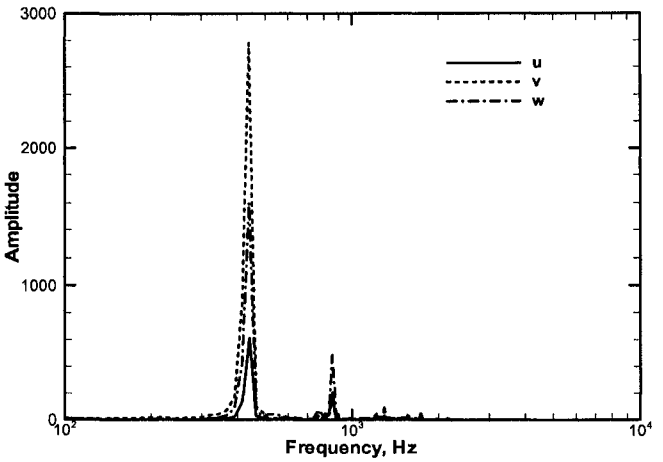

(a) circular hole, m = 1.0

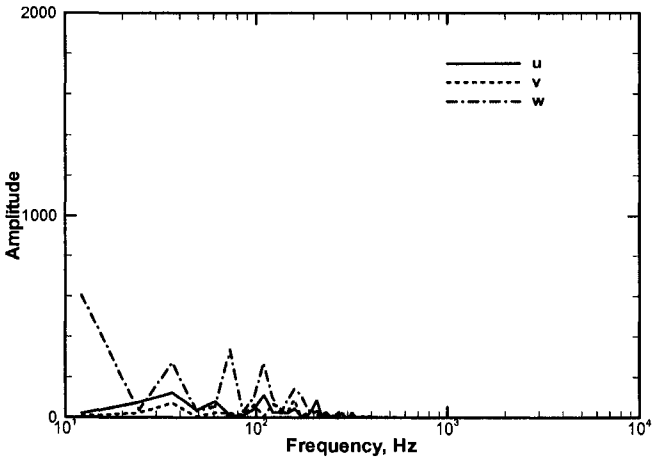

(b) louver scheme, m = 0.5

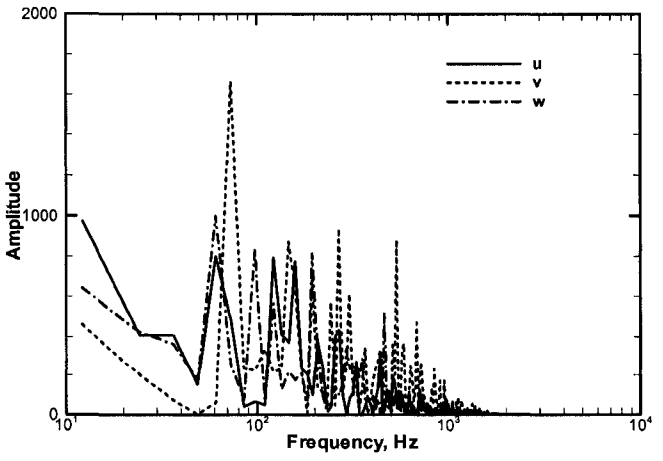

(c) louver scheme, m = 1.0

Fig. 5.20 FFT spectrum of time variant velocity components (u, v, w) at jet exit plane.

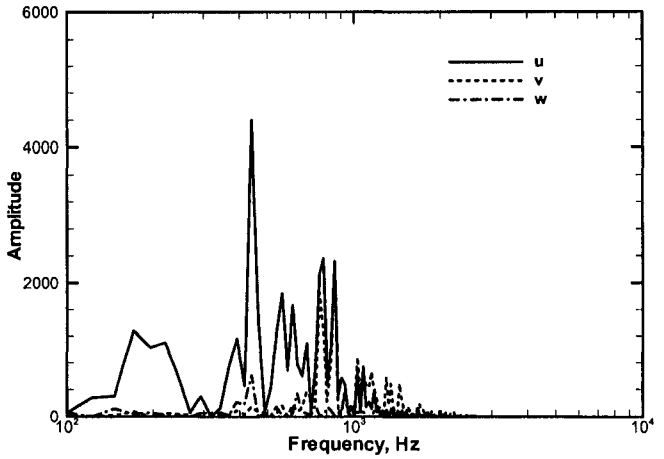

(a) at (3d, 1d, 0), circular hole, m = 1.0

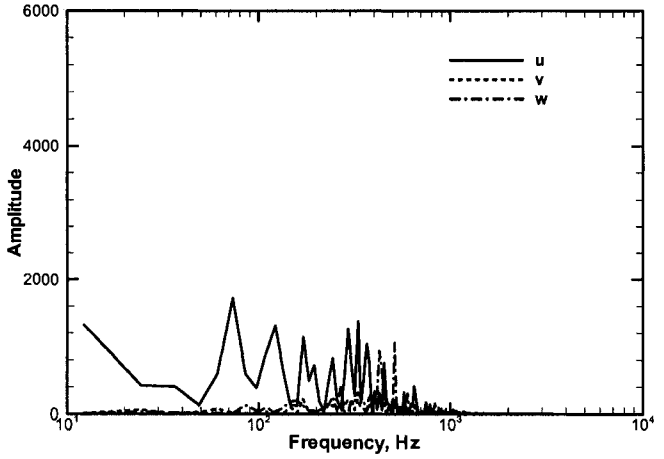

(b) at (3d, 0.5d, 0.5d), louver scheme, m = 0.5

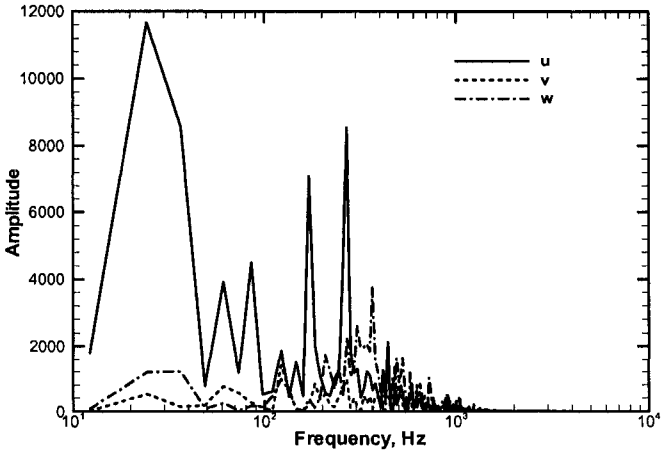

(c) at (3d, 0.5d, 0.5d), louver scheme, m = 1.0

Fig. 5.21 FFT spectrum of time variant velocity components (u, v, w) in downstream.

analysis. More important about unsteady analysis is that the strong fluctuations and unsteadiness of the interaction between the jet and the mainstream can be wholly captured, particularly the coolant fluctuation and the vortical structures in the spanwise direction which will be impossible to capture in steady analysis.

1. The unsteady analysis captured the jet liftoff at high blowing ratios for the cylindrical holes on a flat plate. However, the liftoff effect was exaggerated in the unsteady prediction. Overall, the prediction of the cooling effectiveness by the unsteady analysis is not significantly more accurate than the steady analysis.

2. The unsteady analysis predicted more realistic lateral spreading of the jet than the steady analysis did, which is the biggest advantage of the unsteady analysis over its steady counterpart. In order to capture the unsteadiness and vortical structures of the jet-in-a-crossflow, unsteady analysis is required.

3. Considering the enormous cost in terms of computing resources and the accuracy of the unsteady analysis, unsteady analysis is not recommended for practical industrial applications. The current computing power is still the largest limiting factor preventing unsteady analysis from widespread application.

Chapter 6

Effects of Shock Waves on Film Cooling Performance

In the proceeding two chapters, the louver cooling scheme on a flat plate was analyzed in low speed incompressible flow conditions. In this chapter, the louver cooling scheme on a transonic airfoil was investigated. The focus was the effect of flow compressibility on film cooling performance. The numerical validation was done with a circular hole. Then, the louver cooling scheme on the same airfoil was simulated under the same flow conditions. Specifically, film cooling in supersonic mainstream flow condition was analyzed from a gas-dynamics perspective. The effects of shock wave on film cooling performance were examined in great details. Finally, a theory of coolant-blockage and shaped-wedge similarity was proposed.

6.1 Simulation details

The film cooling configurations studied are shown in Fig. 6.1. Film cooling configurations Fig. 6.1a, 6.1b, and 6.1c were based on Furukawa and Ligrani [106] and configuration Fig. 6.1d was the louver scheme to be tested numerically on the same airfoil for a comparison. The first three film cooling configurations on an airfoil were tested in a wind tunnel and local film cooling effectiveness and Mach number were measured during a steady state flow condition in a blowdown-type facility in the experimental study by Furukawa and Ligrani [106]. Mach numbers along the airfoil surface ranged from 0.4 to 1.24, which match values on the suction surface of an airfoil

under operating condition. Film cooling holes were located near the passage throat of the air flow passage. A single row of holes was employed on the suction surface with the density ratios about 1.4 - 1.6 over a range of blowing ratios. The detailed geometries of the test section of the experimental study were presented in Fig. 6.2 and Fig. 6.3. They showed the detailed computational domain along with the boundary conditions. To save computational resources, only half of the test section was modeled. The chord length of the airfoil was 7.62 cm. The diameter of the circular hole was 0.680mm oriented 30 degrees toward the airfoil surface. The length of the hole was 5.5 diameter with a pitch/diameter ratio of 3.5. Total condition, a pressure of 196.1 kPa and a temperature of 300 K, at the upstream inlet was specified and static atmospheric condition was applied at the downstream outlet. The plenum inlet was a constant mass flow inlet. Periodic boundary condition was applied on the two faces in the span-wise direction. All the other walls were adiabatic with a no-slip boundary condition. Different blowing ratios were achieved by keeping the mainstream condition constant and changing the mass flow rate at the plenum inlet. Those conditions were based on Furukawa and Ligrani [106] and Jackson et al. [41].

The Reynolds number based on the chord length is 1.8×10^6 at the nose of the airfoil and 3.2×10^6 at the throat. The Realizable k-ε turbulence model in combination with the standard wall functions was selected to carry out the simulations using the CFD solver Fluent 6.3 provided by Fluent Inc. The wall functions approach was chosen to avoid having to use a very fine mesh close to the walls to fully resolve the boundary layer. Thus, smaller meshes could be used with more efficient computation and faster and better convergence.

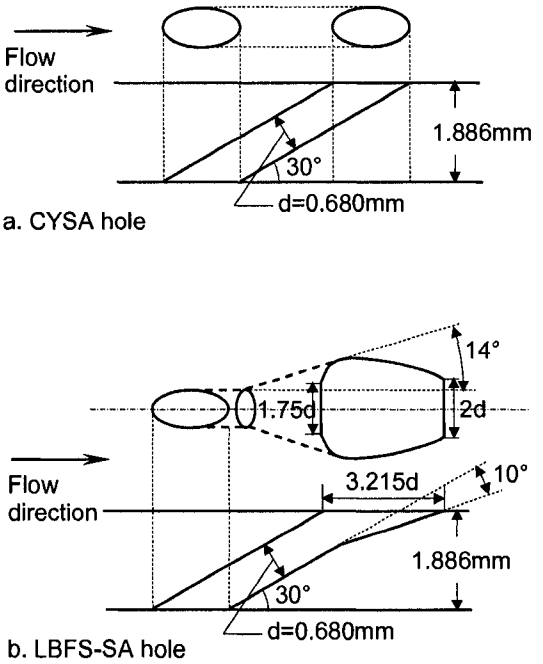

Fig. 6.1 Geometries of the cooling schemes (a. b. c. reproduced from [106]).

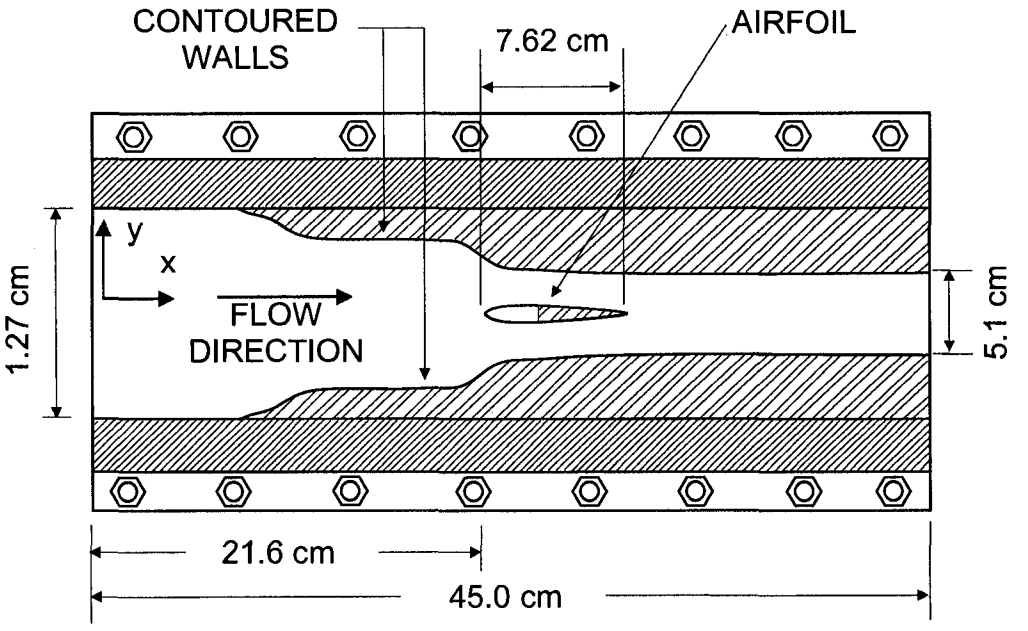

Fig. 6.2 Schematic of the test section (reproduced from [106]).

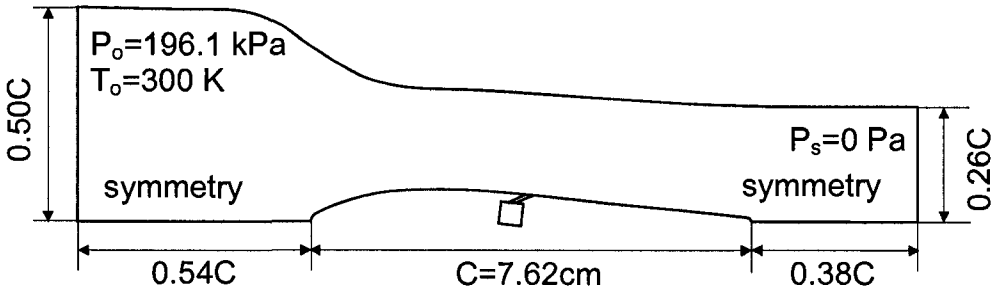

Fig. 6.3 Computational domain based on the test section (not to scale).

Turbulence intensity of the flow at the inlet was set at 0.5% as in the experimental study. A total temperature of 150K at the plenum inlet was specified, which gives a range of coolant to mainstream density ratios around 1.3-2.0 depending on the blowing ratios. For the circular film hole on a flat plate case with a 35° inclined angle, the mainstream velocity is 20m/s corresponding to a Mach number of less than 0.05. Therefore, fluid compressibility can be neglected. The density of the working fluid air was defined as incompressible. The mainstream part of the computational domain for the flat plate case is a rectangle of 20d × 60d with 20d in the upstream of the film hole exit. The temperatures at the mainstream and plenum inlets were specified at 300K and 150K, respectively, which gives a coolant to mainstream density ratio of 2.

The grids contain between 0.8 and 1.5 million cells which took roughly 24 hours of computing time to reach convergence using a workstation with a CPU of 3 GHz and a RAM of 3 GB. In this study, multi-block structured mesh was used, which means a structured mesh was created wherever possible. The majority of cells are concentrated in the boundary layer regions close to wall surfaces as well as the jet exit area. In CFD simulation, it is highly important to ensure an efficient use of grid/cells, a critical factor determining the accuracy of numerical results. Besides residuals going down several orders of magnitude, mass and energy were also checked to ensure they were conserved throughout the computational domain before declaring convergence. Steady state flow condition was assumed for all the cases in the numerical simulations. A second order discretization scheme was used in solving the flow, turbulence, and energy differential equations.

6.2 Results and discussion

All the studies of this louver cooling scheme so far have been done on a flat plate under incompressible flow conditions. It is known that the flow will behave quite differently under supersonic conditions than under subsonic or incompressible conditions. The airfoil presented by Furukawa and Ligrani [106], in which three cooling schemes were tested in a wind tunnel, was chosen to test the performance of the louver cooling scheme. Shock wave dynamics analysis was also done to understand the transonic film cooling phenomenon. Firstly, simulations of the flow without film cooling hole were performed and the prediction of Mach numbers were compared with the available experimental data. Then, the simulations of a circular hole at different blowing ratios were carried out and predictions of cooling effectiveness were compared with the experimental data. These two steps were used to validate the numerical procedures. Finally, the louver cooling scheme on the transonic airfoil was tested and its performance compared with the other three cooling configurations.

6.2.1 Mach number distribution

The calculated Mach number distribution on the center plane without film cooling hole is shown in Fig. 6.4. It can be seen that the Mach number increases from 0.4 at the nose to 1 in the middle then 1.35 at the passage exit with an oblique shock wave at the trailing edge. It is evident that no shock wave occurs within the passage between the leading edge and the trailing edge of the airfoil when film cooling jet is absent. It also can be seen that the Mach number at the location of jet exit is between 1.05 and 1.1, which matches the experimental data [106] of 1.07 very well. Figure 6.5 shows the agreement between the

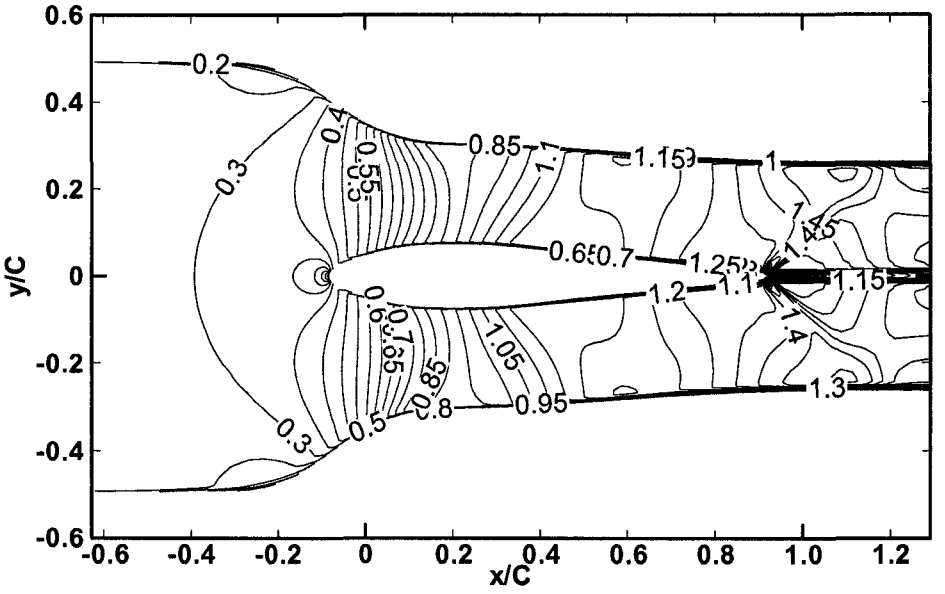

Fig. 6.4 Contours of Mach number on the cross section without film cooling hole.

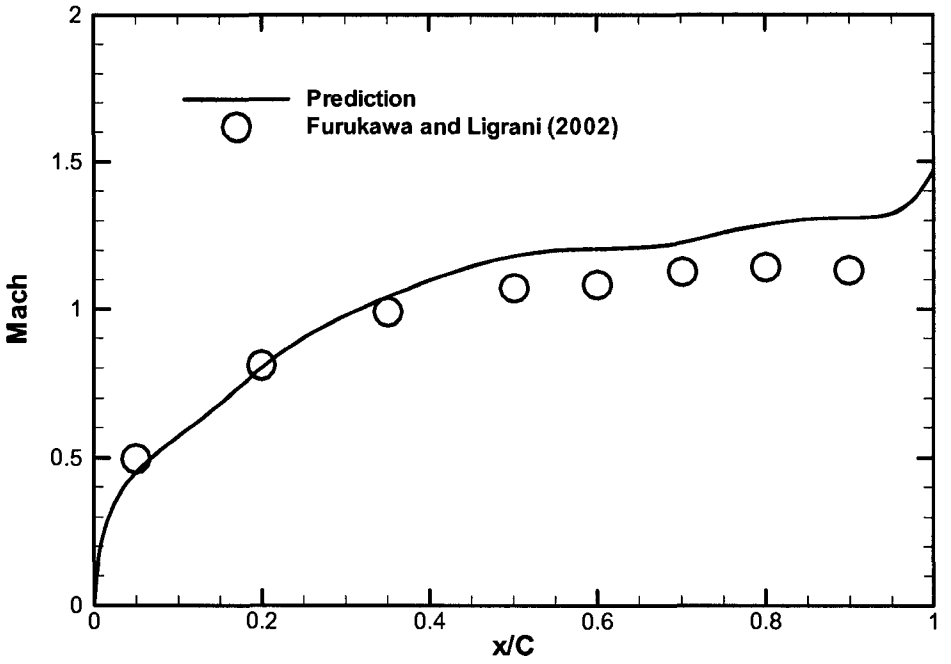

Fig. 6.5 Mach number distribution around the airfoil surface without film cooling hole.

prediction and the experimental data for the value of the Mach number along the airfoil surface. This indicated that the geometries and boundary conditions shown in Fig. 6.3 are appropriate with reasonable accuracy.

6.2.2 Comparison of laterally averaged cooling effectiveness

Figure 6.6 and Fig. 6.7 show the comparison of laterally averaged cooling effectiveness at two different moderately low blowing ratios between the louver cooling scheme and other shaped holes as well as the circular hole. For the circular hole case, near total agreement between the predictions and experimental data exists, indicating that the simulation consistently predicts the right levels of cooling effectiveness at different blowing ratios. The louver cooling scheme provides the highest cooling effectiveness among the three configurations compared, namely circular hole with simple angle (CYSA), layback-fan-shaped hole with simple angle (LBFS-SA), and layback-fan-shaped hole with compound angle (LBFS-CA). The hole's geometries are shown in Fig. 6.1. An interesting phenomenon is that the difference in laterally averaged effectiveness between the circular hole and the louver scheme increases with blowing ratios while that difference between the louver scheme and the other two shaped hole schemes, LBFS-SA and LBFS-CA, decreases with increasing blowing ratio. This can be explained as the cooling effectiveness for the circular hole decreases with blowing ratio after the jet lifts off from the surface at high blowing ratios. The jet liftoff can be avoided or delayed for shaped holes since the jet momentum is reduced by the expanded exit before coolant injection. The advantages of the louver scheme were more noticeable at a low blowing ratio, Fig. 6.6, than at a high blowing ratio, Fig. 6.7.

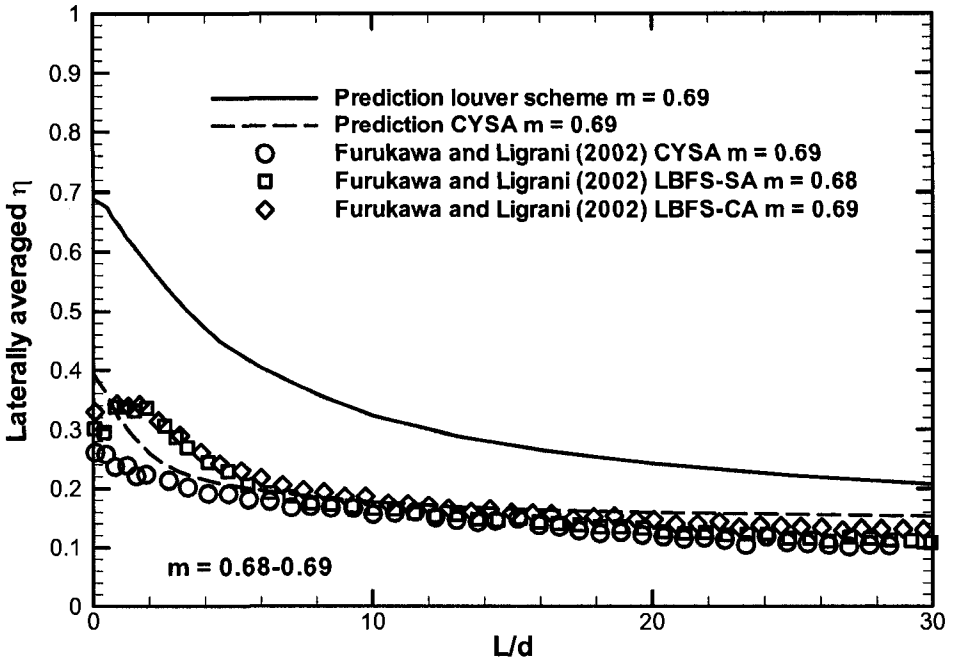

Fig. 6.6 Laterally averaged η for different cooling configurations at blowing ratio of 0.69.

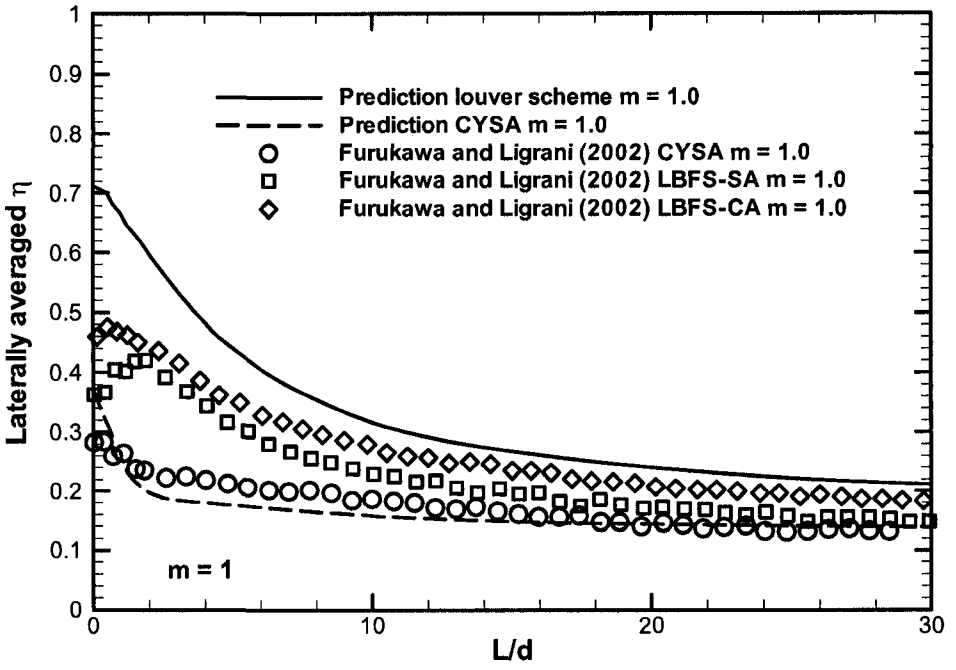

Fig. 6.7 Laterally averaged η for different cooling configurations at blowing ratio of 1.

Figure 6.8 shows the comparison of laterally averaged effectiveness for the circular hole and the louver scheme at different high blowing ratios on the airfoil. Cooling effectiveness decreases dramatically with blowing ratios when the blowing ratios are higher than 1 for both the circular hole and the louver scheme. This is in contrast to what happens at low blowing ratios where effectiveness slowly increases with blowing ratio as shown in Fig. 6.6 and Fig. 6.7. In general, the louver scheme still gives higher laterally averaged effectiveness than the circular hole scheme. However, the effectiveness difference between the two schemes becomes less as blowing ratio is increased. At very high blowing ratios, namely blowing ratios of 2 and 3, the cooling protection provided by the two schemes decreases quickly with blowing ratio and becomes almost ineffective. The louver cooling scheme is only effective in the area of L/d less than 6. In addition to the traditional jet liftoff, such as what happens with a circular jet on a flat plate at blowing ratio of 1 under incompressible flow conditions, the shock wave generated as a result of jet-mainstream interaction contributes more in reducing cooling effectiveness, which will be analyzed in detail next.

6.2.3 Curvature effect

Figures 6.9-6.11 present the curvature effect and the comparison of centerline film cooling effectiveness between the circular hole and the louver scheme. At a low blowing ratio of around 0.5 where the circular jets do not lift off from the surface, the advantage of the louver scheme is apparent only at x/d less than 8, beyond which both schemes give the same level of effectiveness, Fig. 6.9. In either scheme, effectiveness is higher on an airfoil surface than on a flat plate due to the favorable pressure gradient created by flow

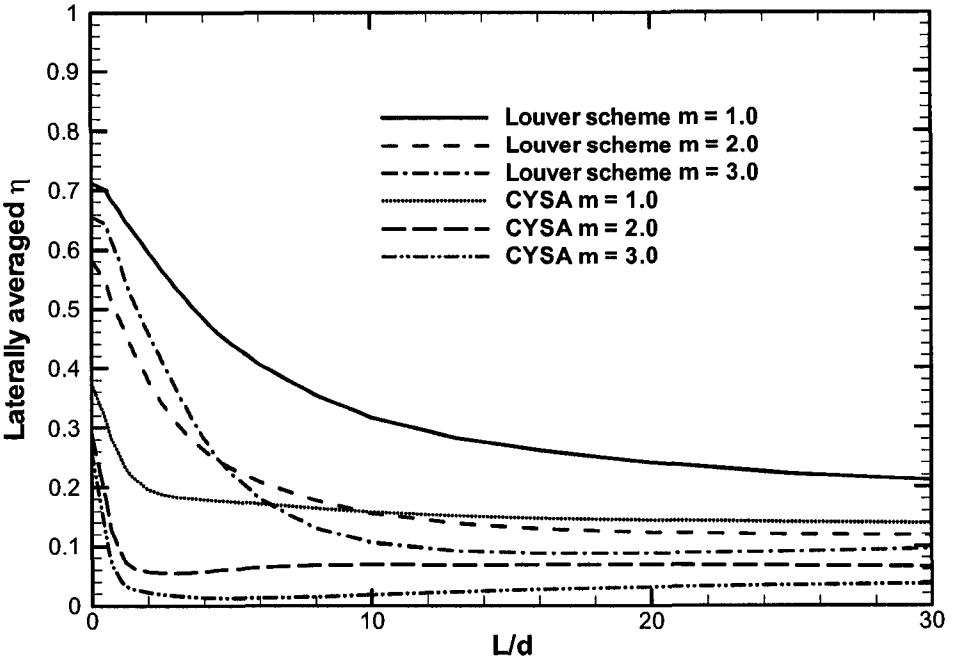

Fig. 6.8 Predicted laterally averaged η at high blowing ratios.

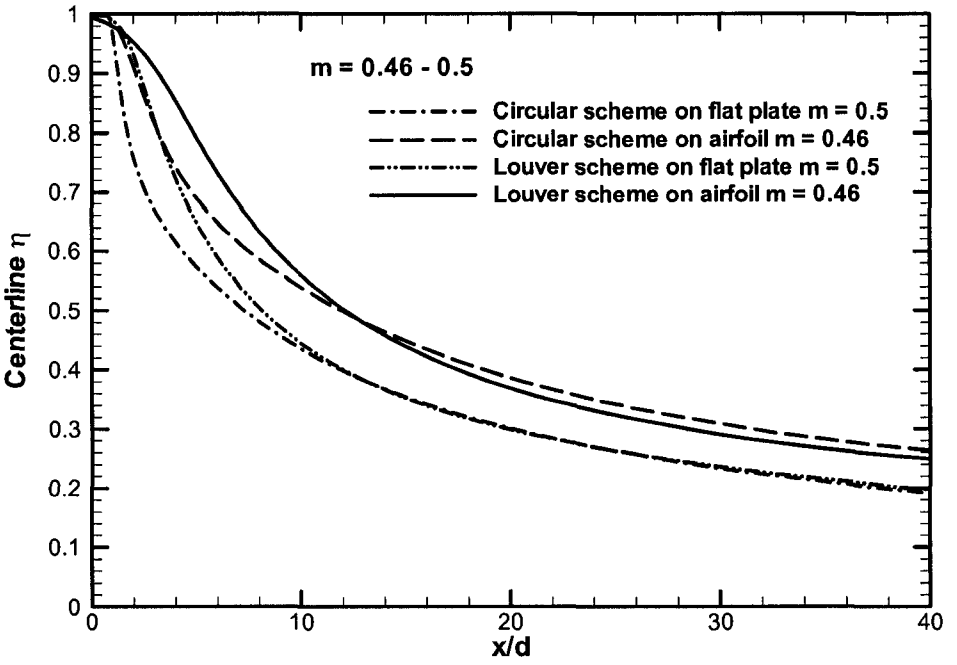

Fig. 6.9 Curvature effect at low blowing ratios.

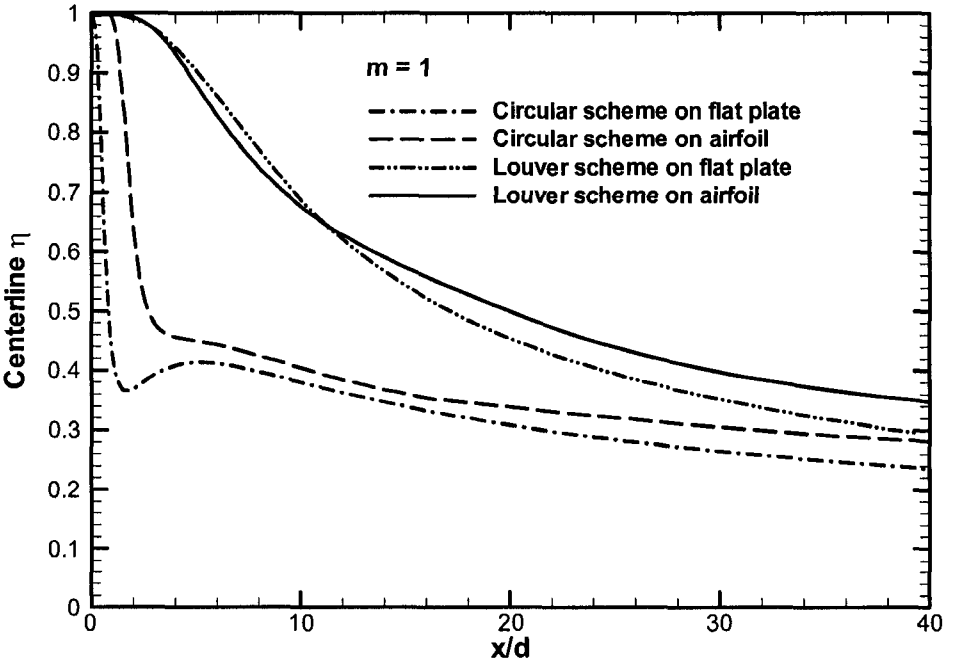

Fig. 6.10 Curvature effect at a moderate low blowing ratio.

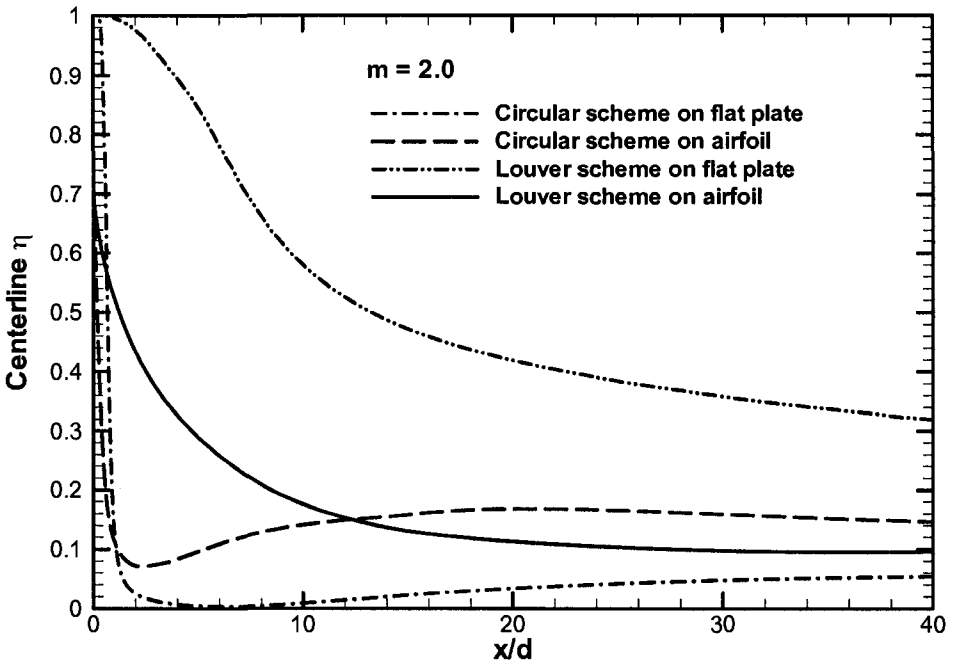

Fig. 6.11 Curvature effect at a high blowing ratio.

acceleration and convex surface on the curved surface. At a higher blowing ratio of 1, Fig. 6.10, for the circular hole case the jet liftoff effect was evident on both the flat plate and the airfoil. The superiority of the louver cooling scheme is clearly demonstrated. As the blowing ratio is raised to 2, Fig. 6.11, dramatic decrease in effectiveness was observed for both cooling schemes on the airfoil. The louver scheme is effective only at x/d less than 8 although jet liftoff does not occur since there is no sudden drop in cooling effectiveness at the centerline. The circular holes lift off of both the flat plate and the airfoil surface completely, leading to poor cooling protection. The liftoff effect on the airfoil for the circular hole is less severe than on the flat plate as a result of favorite pressure gradient created by a curved surface and flow acceleration as already mentioned, Fig. 6.9 and 6.10, therefore, the effectiveness is slightly higher on an airfoil.

6.2.4 Boundary layer velocity profiles

The detailed velocity profiles at different locations along the centerline are shown in Fig. 6.12. For film cooling on the airfoil in transonic flow conditions, Fig. 6.12a shows that at blowing ratio of 1 the circular hole slightly lifts off from the surface due to high coolant momentum and reattachment occurs around L/d of 10. A small separation bubble appears downstream of the injection around L/d from 2 to 6. As the blowing ratio increases to 2, Fig. 6.12b, the separation bubble becomes longer and deeper into the mainstream and reattachment did not occur. The separation bubble dissipates into the mainstream along with the injected coolant and a new fully developed boundary layer forms after L/d of 20 close to the airfoil wall. For the louver scheme on the airfoil, Fig. 6.12c shows that at blowing ratio of 1, no separation bubble occurs due to the reduced momentum because of

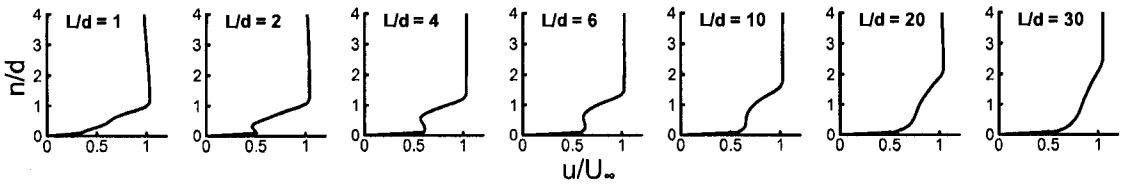

a. Circular hole on the airfoil at m = 1

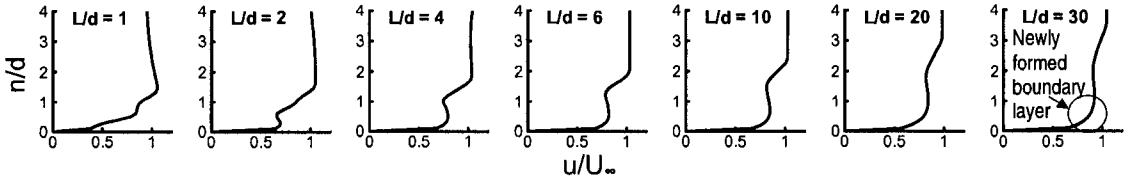

b. Circular hole on the airfoil at m = 2

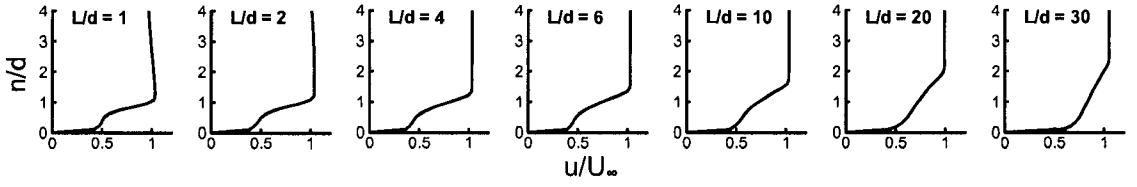

c. Louver scheme on the airfoil at m = 1

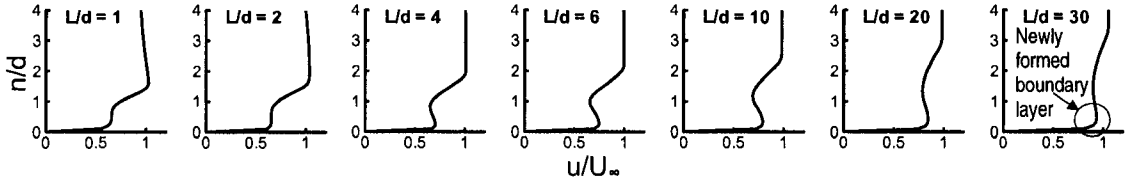

d. Louver scheme on the airfoil at m = 2

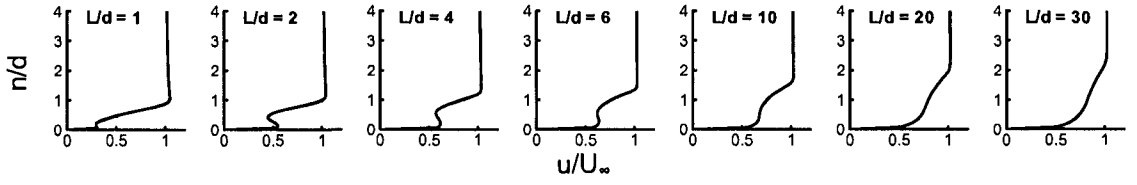

e. Circular hole on a flat plate at m = 1

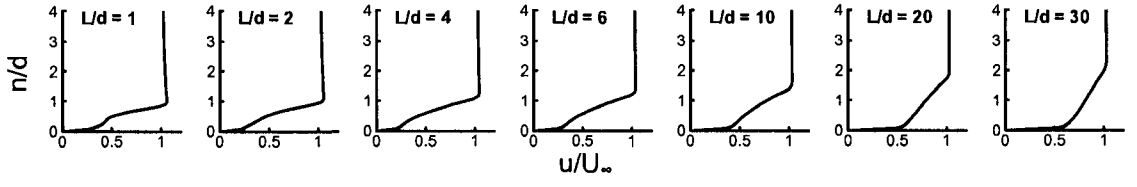

f. Louver scheme on a flat plate at m = 1

Fig. 6.12 Velocity profiles at different locations along the centerline.

the shaping of the exit, though the boundary layer profile was disturbed a little bit. When the blowing ratio increases to 2, Fig. 6.12d, a big separation bubble appears which dissipates into the mainstream. No jet reattachment occurs for the louver scheme, which is similar to what happens to the circular hole case at blowing ratio of 2. To see the difference between high speed and low speed flows, the velocity profiles for both the circular hole and the louver scheme on a flat plate at blowing ratio of 1 are also shown in Fig. 6.12e and 6.12f, respectively. At a low speed when the flow can be considered as incompressible, the circular hole also lifts off from the surface at blowing ratio of 1, Fig. 6.12e. Nonetheless, the separation takes place a little earlier and the bubble is a little thinner and closer to the wall. A comparison between Fig. 6.12c and 6.12f reveals that at blowing ratio of 1 there is no fundamental difference between on a curved airfoil and on a flat plate for the louver cooling scheme except that the boundary layer is a little thinner on a flat plate than on the airfoil.

6.2.5 Effects of shock wave structures

Figure 6.13 and 6.14 show the Mach number distribution on the center-plane with film cooling for the circular hole and the louver scheme cases, respectively. At a low blowing ratio of 0.46, Fig. 6.13a and 6.14a, an oblique shock wave is clearly observed right before the leading edge of the jet exit. This oblique shock emanating from the leading edge of the jet exit reaches the top wall and is reflected back to the bottom surface, known as a regular reflection. A series of expansion waves, also known as an expansion fan, are found around the center of the hole exit right above the shear layer formed by the injected coolant. As the blowing ratio increases, the oblique shock becomes stronger. At blowing

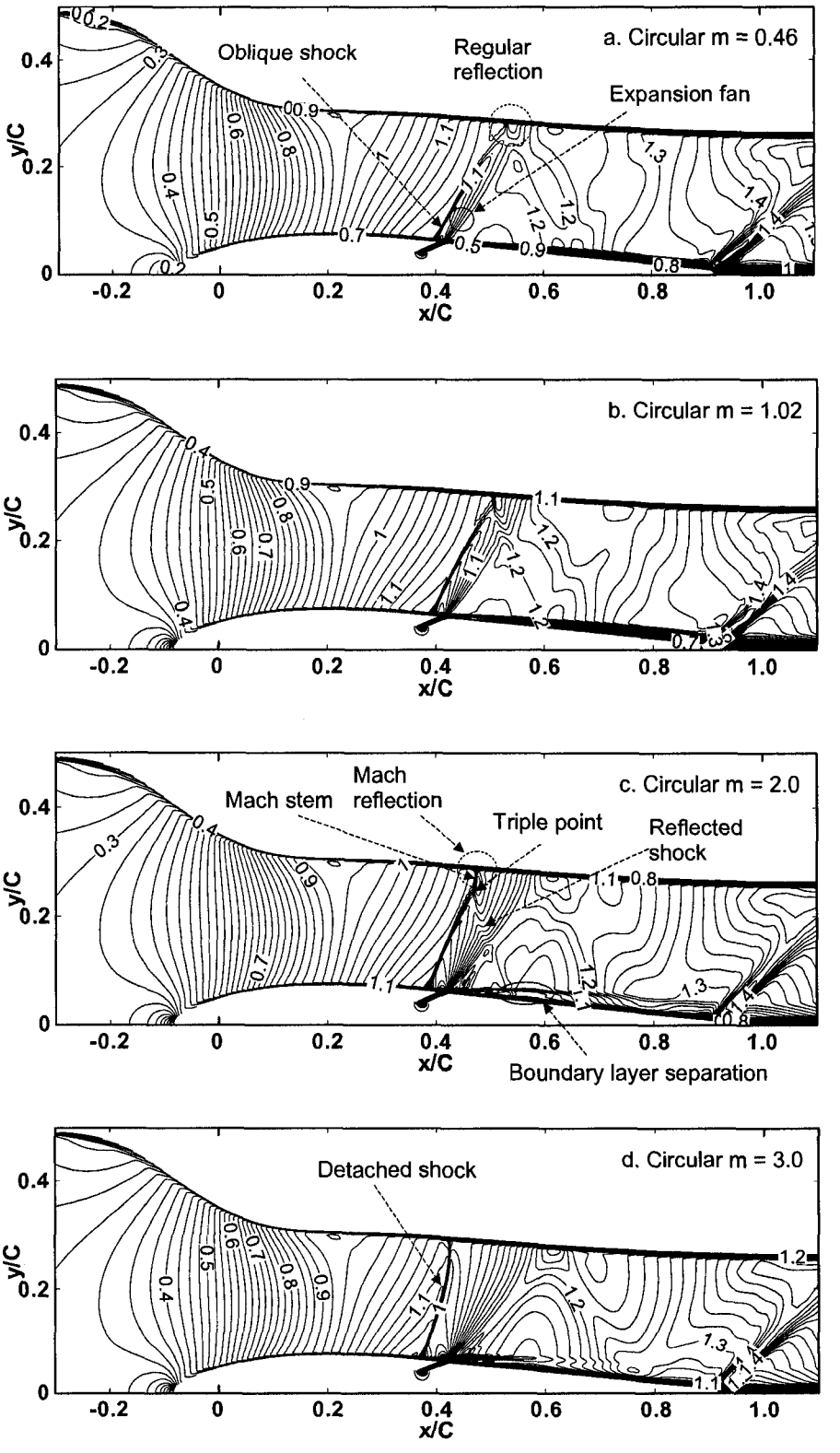

Fig. 6.13 Mach number distribution for the circular hole case at different blowing ratios.

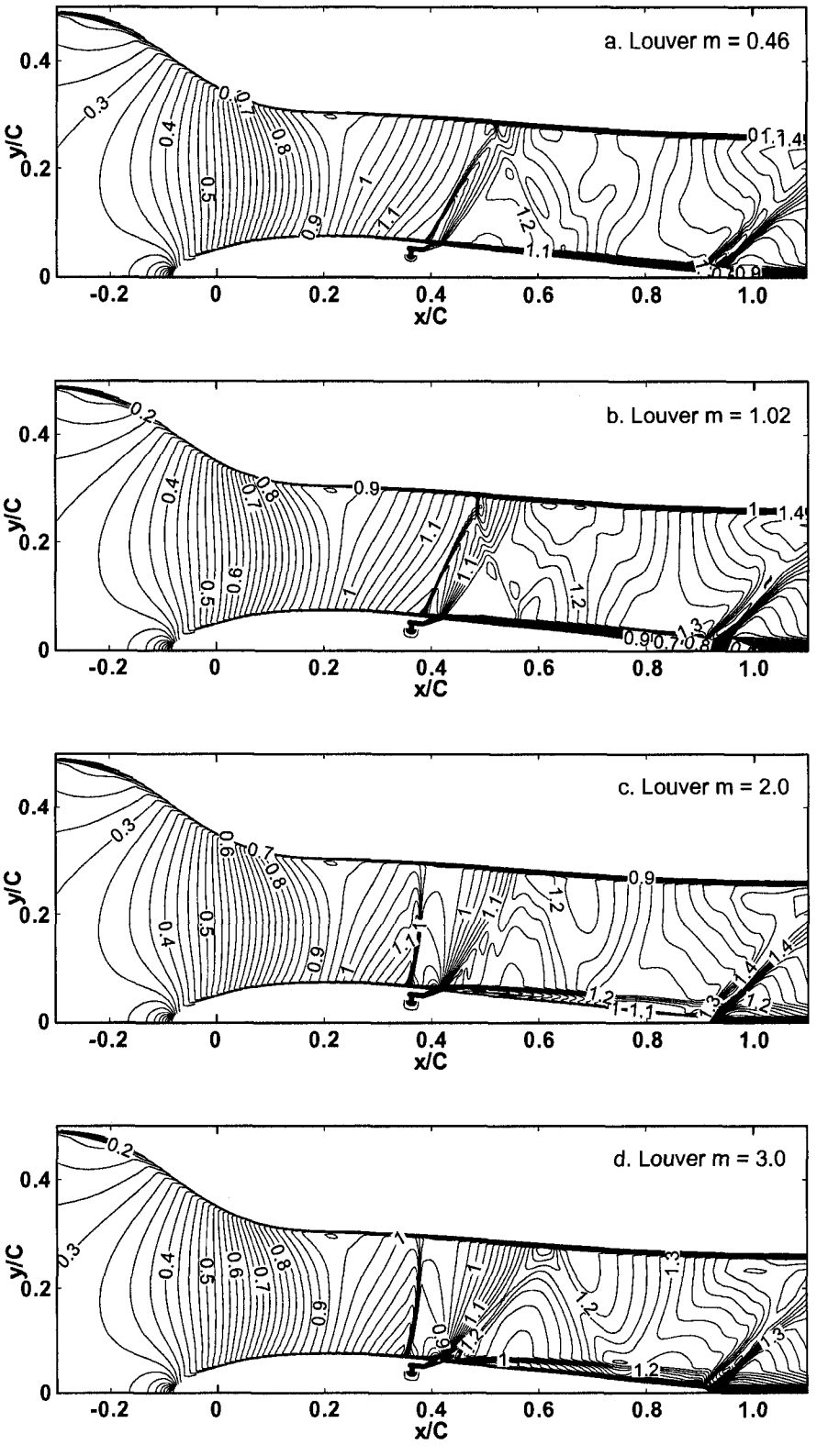

Fig. 6.14 Mach number distribution for the louver scheme at different blowing ratios.

ratio of 2 for the circular hole, Fig. 6.13c, and a blowing ratio of 1 for the louver cooling scheme, Fig. 6.14b, a so-called Mach reflection results which consists of three shock waves intersecting at a single point, known as the triple point. Still, at a higher blowing ratio of 3, Fig. 6.13d, 6.14d, the shock in front of the jet exit is so strong that it detaches completely from the leading edge of the hole exit as a detached shock wave, or a bow shock. Comparing the shock structures at the same blowing ratios between the circular hole and the louver scheme shows that under the same flow conditions the louver scheme causes a slightly stronger shock wave structure than the circular hole does, Fig. 6.13a and 6.14a, and Fig. 6.13c and 6.14c. At the blowing ratio of 1.0, the louver scheme causes a longer Mach stem on the top wall than circular hole, Fig. 6.13b and 6.14b, which means stronger shock structures and shock interactions for the louver scheme. At the same blowing ratio of 2, the shock associated with the louver scheme becomes detached shock, Fig. 6.14c, while attached oblique shock occurs with the circular hole, Fig. 6.13c.

The contours of coolant at a constant temperature after injection are shown in Fig. 6.15 by plotting Mach number on the iso-surface of constant temperature of 200K. It can be seen that the coolant forms a narrower band for the circular hole than for the louver scheme as shown in the top views in Fig. 6.15a and 6.15c. On the other hand, the angle the top layer of injected coolant makes with the wall surface – the nose angle – is sharper for the louver scheme, Fig. 6.15b and 6.15d, as expected since the coolant is stretched in the span-wise direction by the exit shaping in the louver scheme. In this sense, the circular hole is like a three dimensional cone and the louver scheme is close to a two dimensional wedge. For the same flow conditions of mainstream Mach number and the same amount of coolant injected, a cone due to the circular hole injection will cause less

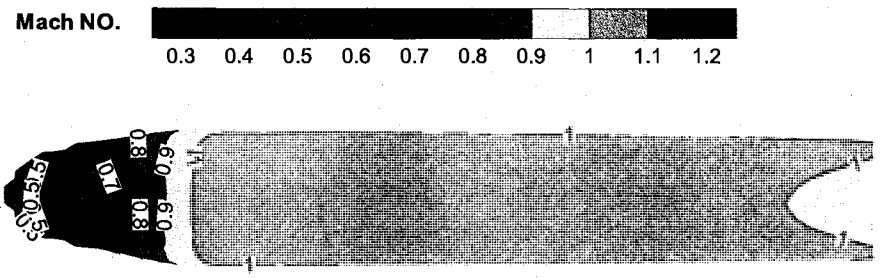

a. Top view for circular hole on the airfoil

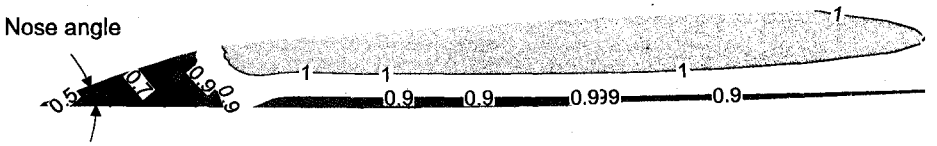

b. Side view for circular hole on the airfoil

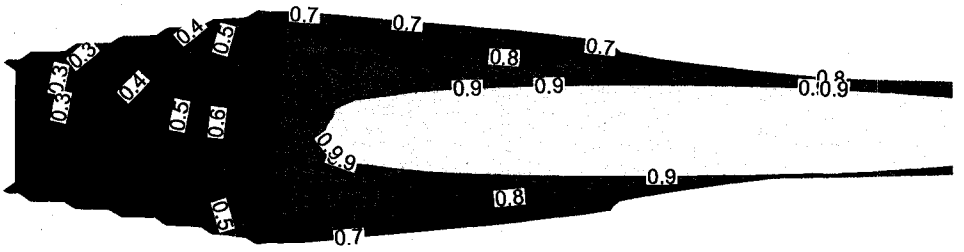

c. Top view for louver hole on the airfoil

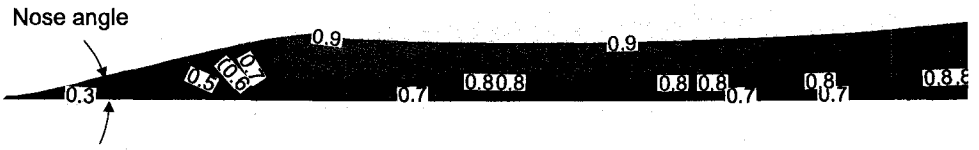

d. Side view for louver hole on the airfoil

Fig. 6.15 Contours of Mach number on iso-surfaces of constant temperature at m = 1.

disturbance to and weaker reaction from the mainstream than a wedge due to the louver scheme injection. From the physics point of view, the flow more easily passes around the sides of the three dimensional cone; the cone thereby presenting less overall disruption to the mainstream.

Figure 6.16 shows the schematics of a shaped wedge in a supersonic flow. Unlike in subsonic or incompressible flow conditions where the mainstream can sense the presence of an obstacle before reaching it, and therefore, adjust itself to allow gradual changes in flow properties with continuous streamlines, in supersonic flow, the mainstream can not sense the presence of an obstacle, shock waves result by which the flow adjusts rapidly to the obstacle through discontinuous changes in fluid properties. The presence of a coolant injection in a supersonic flow generates the effect of a supersonic flow past a wedge. The interaction between the mainstream and the injected coolant can be simplified as a shaped wedge with a rounded top sitting on the surface as shown in Fig. 6.16a. The wedge shape is based on the streamlines of the injected coolant. The wedge angle θ is related to the blowing ratio: the higher the blowing ratio, the larger the wedge angle, and the stronger the shock wave structures that will be generated. The rounded top acts as a gradual convex turn by which an expansion fan is generated with gradual changes in flow properties. Thus, isentropic expansion can be assumed for the flow going through the expansion fan [107]. Figure 6.16b represents the conditions of low blowing ratios. At small wedge angles associated with low blowing ratios, an attached weak oblique shock occurs at the leading edge of the jet exit. A narrow expansion fan is also observed as shown in Fig. 6.13a and 6.14a. The flow properties across these weak shocks do not change much and the cooling effectiveness on the airfoil is close to that on a flat plate as

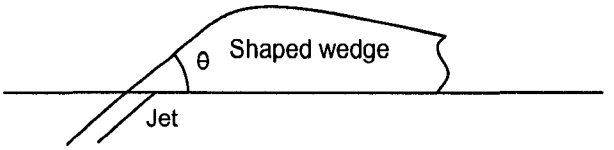

a. Shaped wedge

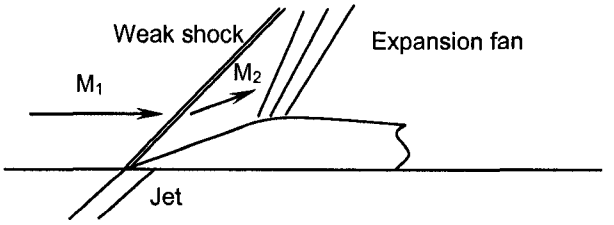

b. Weak shock at low blowing ratios

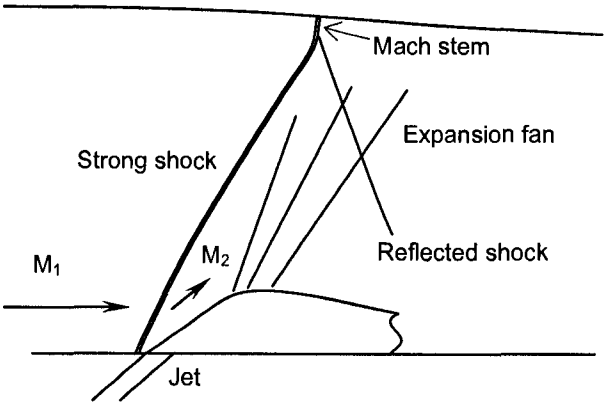

c. Strong shock at high blowing ratios

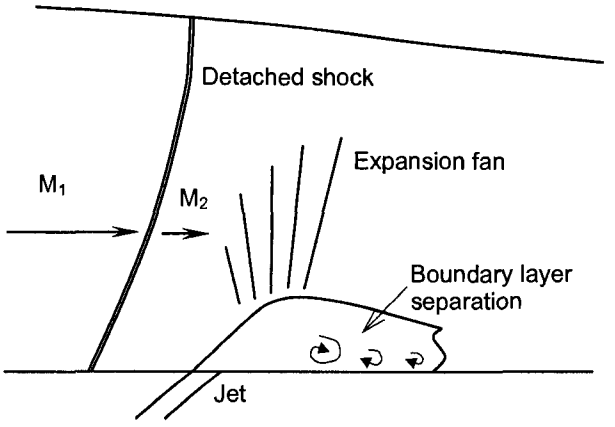

d. Detached shock at very high blowing ratios

Fig. 6.16 Schematic of shock wave structures at different blowing ratios.

shown in Fig. 6.9. The slightly higher cooling effectiveness on the airfoil is the result of a favorable pressure gradient due to the curved surface that a flat plate does not have.

Under the same mainstream flow condition and Mach number, as the blowing ratio increases, the wedge angle becomes larger, resulting in a stronger, still attached, oblique shock and a wider expansion fan, Fig. 6.16c. The strong oblique shock emanating from the leading edge reaches the top surface where Mach reflection occurs [108]. The length of the Mach stem increases with blowing ratios. Immediately after the Mach stem, the flow becomes subsonic, Fig. 6.13c and 6.14b. After the strong oblique shock wave, the flow is deflected upward by a finite angle, usually in the direction parallel to the wedge surface, and the magnitude of the velocity is also suddenly reduced from supersonic to subsonic, leading to more jet liftoff in addition to the traditional liftoff at higher blowing ratios and reduced cooling effectiveness. Particularly, in the vicinity of the leading edge after the shock the magnitude of the flow velocity is the lowest, typically in the subsonic flow regime. The flow accelerates to supersonic again across the ensuing expansion fan. But the small turning angle due to the expansion fan can not make up the loss. Overall, the difference in film cooling effectiveness between on a flat plate and on the airfoil at a high blowing ratio is less than that at a lower blowing ratio for the same cooling scheme, Fig. 6.9 and 6.10. The advantages of the louver cooling scheme are more pronounced at moderately high blowing ratios, Fig. 6.10.

When the blowing ratio is too high, detached shock wave developed, Fig. 6.16d. The supersonic flow is reduced to subsonic flow immediately after the detached shock because the detached shock behaves more like a normal shock. After the detached shock, the flow goes through a wide expansion fan through which the flow becomes supersonic

again. The detached shock and expansion fan drastically change the flow field. Take blowing ratio of 3 as an example, as shown in Fig. 6.17, the static pressure increases by as much as 35% across the compressive detached shock, then decreases by 30% across the ensuing expansion fan. These sudden changes of pressure within a short distance cause the boundary layer separation, Fig. 6.13c, 6.13d, 6.14c, and 6.14d, more pronouncedly Fig. 6.12b and 6.12d, resulting in poor cooling protection and injected coolant dissipating into the mainstream. This coolant dissipation due to boundary layer separation should be distinguished from the traditional jet liftoff caused by the high jet momentum at high blowing ratios. In the traditional jet liftoff, the high momentum of the jet at high blowing ratios is solely responsible for the reduced cooling effectiveness. Once the boundary layer separates from the airfoil surface due to the shock waves, the injected coolant could not stick to the airfoil surface as it does when there is no boundary layer separation. Consequently, most of the coolant is dissipated into the mainstream no matter how much coolant is injected and how small the normal momentum of the jet is. In other words, jet reattachment does not occur once shock wave induced boundary layer separation takes place. This is totally different from what happens for film cooling under subsonic or incompressible flow conditions where there is no shock wave induced boundary layer separation.

6.3 Summary

The flow behaviors of film cooling in transonic or supersonic flows are quite different from those in subsonic or incompressible flows. The convex surface on the airfoil in combination with flow acceleration due to compressibility of the fluid creates a favorable

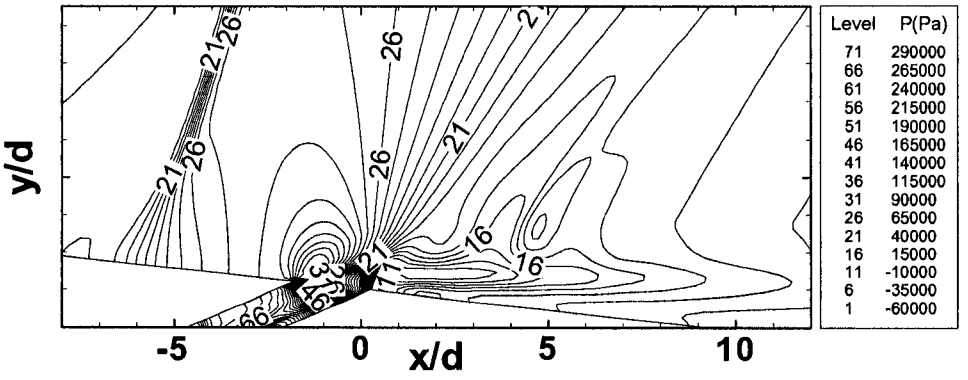

a. Circular hole

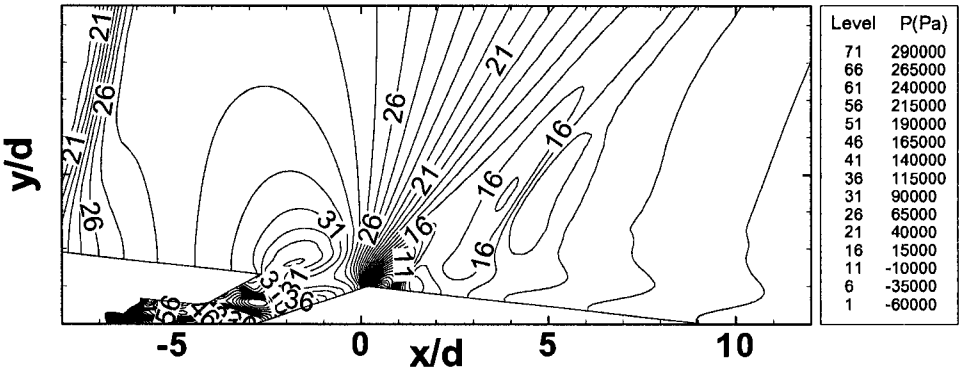

b. Louver scheme

Fig. 6.17 Static pressure distribution around the jet exit at m = 3.

pressure gradient, which presses the injected coolant closer to the targeted surface. When the blowing ratio is low and the oblique shock generated by the interaction between the jet and the mainstream stays attached, usually a weak shock, the cooling effectiveness is generally higher on a convex airfoil surface than on a flat plate. Shock waves were also found to be reflected back and forth between the upper and lower walls as weaker shocks depending on how strong the original shock wave is. The working fluid going through the oblique shock waves is compressed and the subsequent increased pressure may also help push the coolant toward the airfoil surface, thereby increasing the cooling effectiveness. However, when the blowing ratio is too high, a strong detached shock occurs which drastically changes the flow field. As a result, the boundary layer separates from the wall and the coolant becomes ineffective. The proposed coolant-blockage and shaped-wedge similarity qualitatively explains this phenomenon and sheds light on the physics of supersonic film cooling. The main outcomes may be summarized as follows.

1. In transonic or supersonic mainstream flow conditions, the blockage effect of the injected coolant makes the jet act like a shaped wedge. Under the same mainstream flow condition, the higher the blowing ratio, the larger the wedge angle and the stronger the shock waves that are generated.

2. When the oblique shock due to the coolant injection is weak and stays attached to the leading edge of the jet exit, a higher blowing ratio usually provides a higher cooling effectiveness than a low blowing ratio. When the shock becomes detached, the cooling effectiveness is drastically reduced due to the boundary layer separation caused by shock waves regardless of cooling configurations.

3. The louver cooling scheme provides higher cooling effectiveness than the circular hole and the fan-shaped hole. The difference of laterally averaged effectiveness between the louver cooling scheme and the fan-shaped hole is reduced as blowing ratio increases.

4. Using extremely high blowing ratios should be avoided for any cooling schemes when the flow field in the mainstream at the location of the hole is supersonic, particularly for shaped holes, because at very high blowing ratios, a detached shock along with other strong shock wave structures causes boundary layer separation, rendering the coolant virtually ineffective.

The focus of this study is the cooling effectiveness on the airfoil surface. Therefore, the cells were mostly concentrated on the airfoil surface in the boundary layer areas and the jet exit area. As a result, the detailed shock wave structures may not have been resolved fully, particularly the shock wave reflections and interactions. It should be noted that this is only the first attempt to study the shock wave effects on the film cooling performance from a new perspective. There is conflicting information in the literature as to whether the resulting shock waves increase the cooling effectiveness or decrease it. Currently, there is no experimental data of cooling effectiveness available in the open literature for holes on a curved surface at very high blowing ratios when detached shock wave occurs. Therefore, experimental work of cooling effectiveness test at higher blowing ratios under transonic or supersonic flow conditions is highly recommended, since low speed effectiveness data do not apply to high speed flow conditions.

Chapter 7

Simulation of a Turbine Stage with Film Holes – Rotational Effects

The focus of this chapter is the rotational effects on film cooling performance. As in the proceeding chapter, the code validation was done with a circular hole on an airfoil. To facilitate the numerical simulation given the current computational resources, a number of simplifications were made to the flow, including equal number of blades for both stator and rotor parts, utilization of zero-shear stress boundary condition, and neglecting the effects of periodic wake passing by the stator blades due to the mixing plane model. Some simplifications were already proved and tested in the literature. Others were validated first before being fully employed, such as the zero-shear boundary condition. As film cooling at the leading edge of an airfoil is different than that at other area of an airfoil, validation was presented first, followed by analysis of the louver cooling scheme at the same locations. It should be noted that the conclusions of this chapter would not be applicable to film cooling in areas other than the leading edge of an airfoil.

7.1 Numerical methodology and validation

The Ahn et al. [16] was chosen as the benchmark case for the validation of CFD code. In the study, 16 circular holes in two rows are machined on a turbine blade surface at the leading edge. All holes are oriented to the span-wise direction with a 30 degrees surface angle. The blade was mounted to the shaft of a three stage turbine and tested in a low

pressure turbine facility. Figure 7.1a and 7.1b show the circular hole tested in Ahn et al. [16] and the louver scheme tested numerically in this work, respectively. Figure 7.1c and 7.1d show the dimensions of the flow passage of the turbine and the location of the computational domain on the blade.

The computational domains were shown in Fig. 7.2 and Fig. 7.3 along with the boundary conditions for the 2d and 3d cases, respectively. To make the simulation more tractable, the domain was simplified. In Zhang and Hassan [52], it was shown that if setup properly, current turbulence models can give accurate numerical predictions with the jet lift-off at high blowing ratios captured accurately. Based on the study, a good mesh should have at least 0.2 to 0.3 million cells per film hole. Wall functions should be employed to avoid using very fine near wall mesh. Considering the large domain, both stator and rotor blades included, and the number of holes involved, 16 holes in total, it is impractical to simulate the whole blades from hub to tip. Therefore, only one period was considered and periodic boundary condition was applied in the span-wise direction. In so doing, part of the coolant flow interaction between neighbouring holes may be lost. But the case of film holes on a flat plate has shown the result is acceptable with reasonable accuracy.

Another simplification made in this work is the assumption of equal number of blades for both stator and rotor domains. In the experiment, there are 58 stator blades and 46 rotor blades for the stage. To make the simulation simpler, the stator section was assumed to have 46 blades. This simplification was proved reasonable in Yang et al. [109]. Based on the authors' previous work [52], the quality of the mesh system is highly important for the simulation results to be accurate. All the cell elements have to be well-distributed in

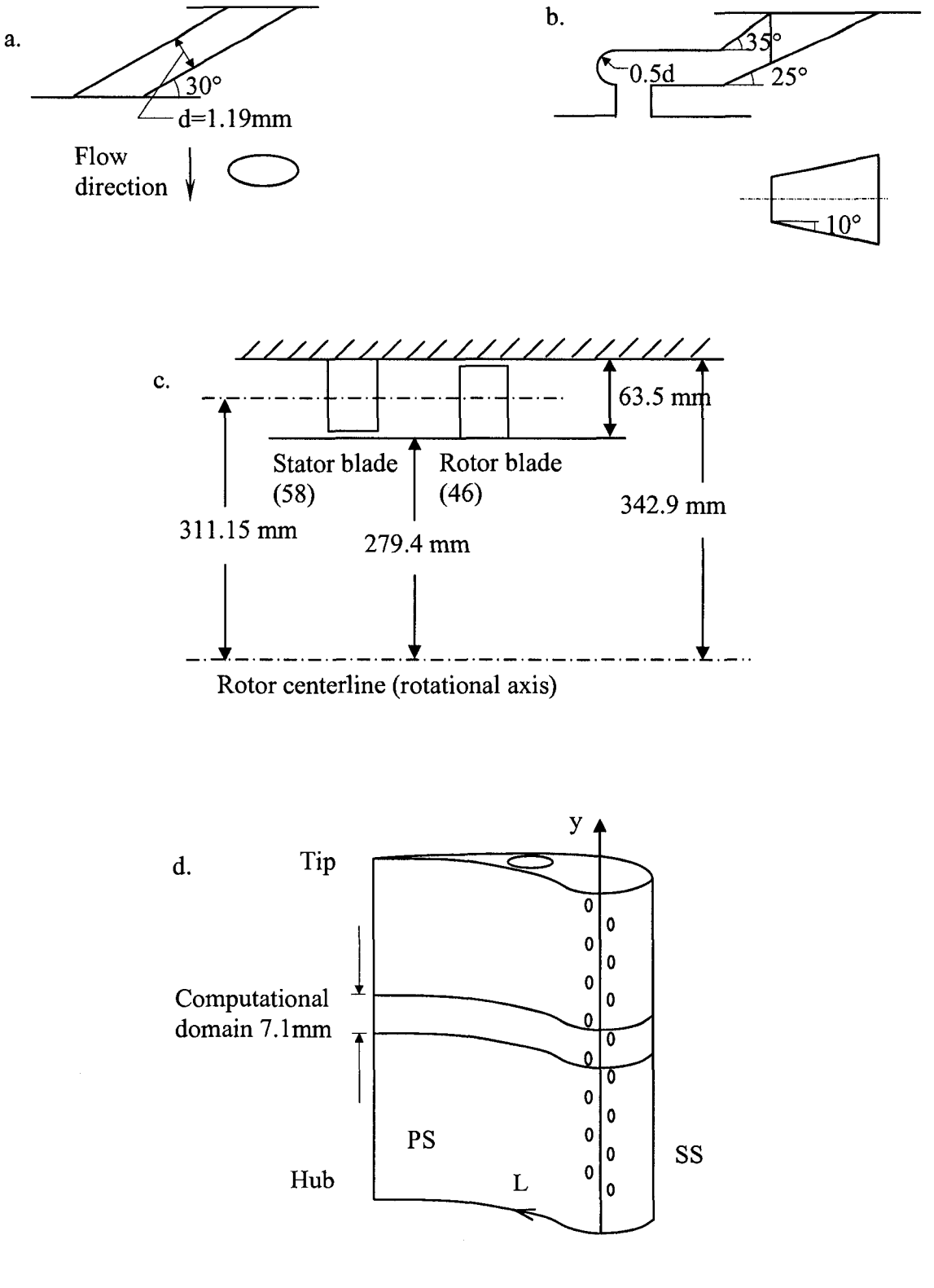

Fig. 7.1 Film hole geometries and turbine blade, a. circular hole; b. louver-cooling scheme; c. first stage schematic; d. film-cooled blade.

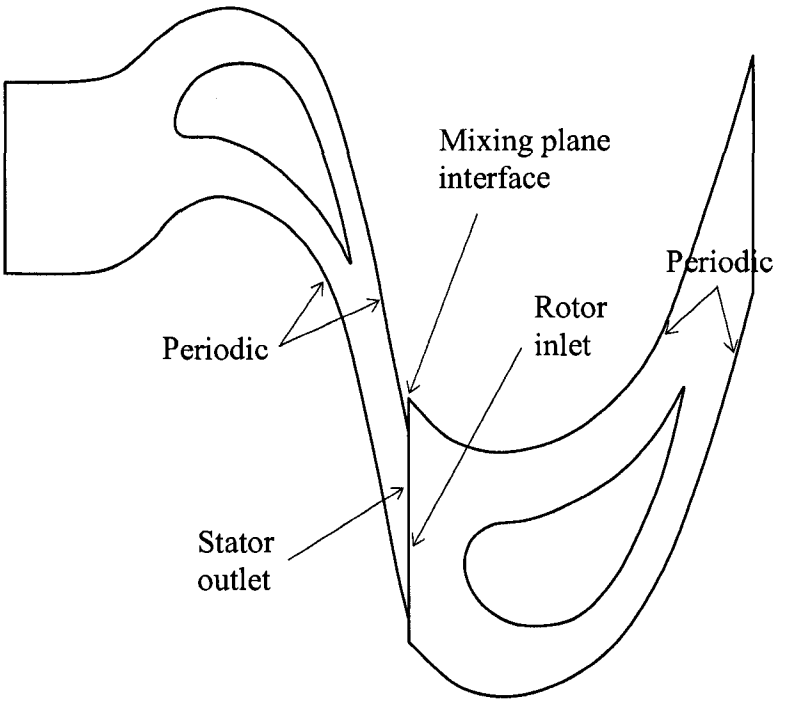

Fig. 7.2 Computational domain and boundary conditions for the 2d case.

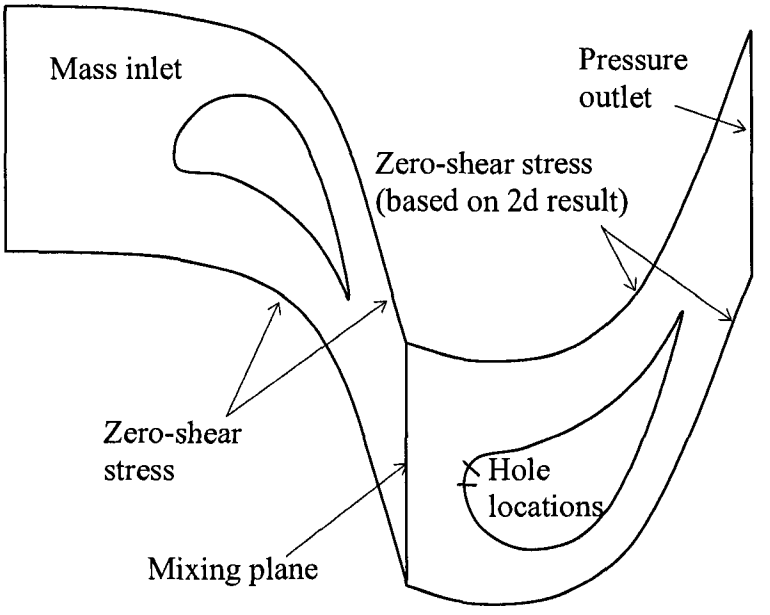

Fig. 7.3 Computational domain and boundary conditions for the 3d case.

the areas with large variable gradients, such as jet exit areas and around blade walls to better resolve the flow field. The two faces separating neighbouring blades in the circumferential direction in the 3d cases were defined as zero-shear stress boundary. This simplification allows better concentration of cells and speeds up the meshing process considerably. Otherwise, two pairs of periodic boundary conditions will force almost half of the cells being poorly positioned and wasted. Firstly, a 2d case, Fig. 7.2, was solved. Then, streamline was found from the 2d solution and used to define the new boundary for the 3d computational domain, Fig. 7.3.

To model the rotation of the rotor blade, the mixing plane approach was adopted. It assumes that the flow field is steady with the rotor-stator interactions being accounted for by approximate means. In the application, there are two fluid zones, the stator blade domain which is stationary and the rotor blade domain which is rotating. The rotating blade renders the whole problem unsteady in nature when viewed from the stationary frame. When viewed from the rotating frame, however, the flow on the rotating blade part can be modeled as a steady-state problem with respect to the rotating frame. To derive the equations for a rotating reference frame, consider a coordinate system which is rotating steadily with an angular velocity $\vec{\omega}$ relative to a stationary frame, as shown in Fig. 7.4. The CFD computation domain for the rotor part is defined with respect to the rotating frame. The position vector $\vec{r}$ denotes an arbitrary point from the origin of the rotating frame in the CFD rotating domain. The fluid velocities from the stationary reference frame can be transformed to the rotating reference frame according to the following relation,

$$\vec{v}_r = \vec{v} - \vec{u}_r \tag{7.1}$$

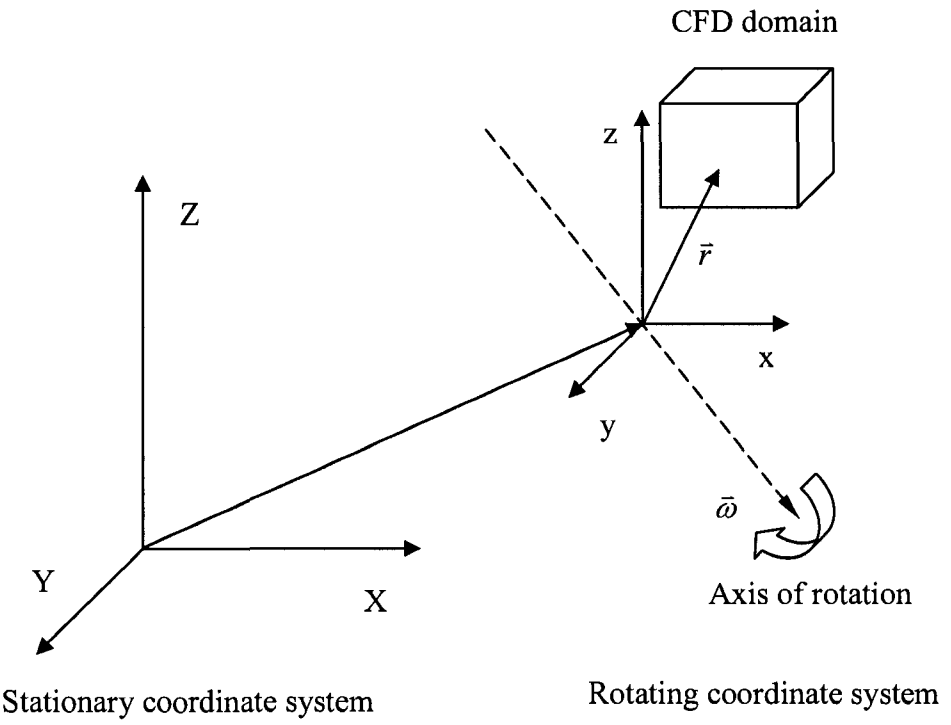

Fig. 7.4 Stationary and rotating reference frames.

where

$$\vec{u}_r = \vec{\omega} \times \vec{r} \,. \tag{7.2}$$

In the above, $\vec{v}_r$ and $\vec{v}$ are the relative velocity and absolute velocity, respectively, and $\vec{u}_r$ is the whirl velocity due to the moving reference frame. Expressing the momentum equations using the relative velocities as dependent variables leads to the relative velocity formulation,

Conservation of mass:

$$\frac{\partial \rho}{\partial t} + \nabla \cdot \rho \vec{v}_r = 0 \tag{7.3}$$

Conservation of momentum:

$$\frac{\partial}{\partial t}(\rho \vec{v}_r) + \nabla \cdot (\rho \vec{v}_r \vec{v}_r) + \rho(2\vec{\omega} \times \vec{v}_r + \vec{\omega} \times \vec{\omega} \times \vec{r}) = -\nabla P + \nabla \cdot \left\{ \mu \left[\left(\nabla \vec{v}_r + \nabla \vec{v}_r{}^T \right) - \frac{2}{3} \nabla \cdot \vec{v}_r I \right] \right\} \tag{7.4}$$

Conservation of energy:

$$\frac{\partial}{\partial t}(\rho E_r) + \nabla \cdot (\rho \vec{v}_r H_r) = \nabla \cdot \left(k \nabla T + \left\{ \mu \left[\left(\nabla \vec{v}_r + \nabla \vec{v}_r{}^T \right) - \frac{2}{3} \nabla \cdot \vec{v}_r I \right] \right\} \cdot \vec{v}_r \right). \tag{7.5}$$

The momentum equation contains two additional terms due to acceleration, i.e., the Coriolis acceleration $(2\vec{\omega} \times \vec{v}_r)$, and the centripetal acceleration $(\vec{\omega} \times \vec{\omega} \times \vec{r})$. The relative internal energy E_r and relative total enthalpy H_r, also knows as the rothalpy, are defined as followings,

$$E_r = h - \frac{P}{\rho} + \frac{1}{2}\left(v_r^2 - u_r^2\right) \tag{7.6}$$

$$H_r = E_r + \frac{P}{\rho}. \tag{7.7}$$

Based on the above formulation, both the stationary and the rotating domains can be modeled as steady-state problems in their own respective reference frames. In the mixing plane approach, flow field parameters from neighboring zones are spatially averaged at the mixing plane and passed as boundary conditions. The spatial averaged process removes any unsteadiness that results due to circumferential variations in the passage to passage flow field. As the flow is treated as a steady-state problem and a time averaged solution is sought, the mixing plane model is reasonable. At each iteration the flow data at the mixing plane interface are area-weight-averaged in the circumferential direction on both the stator outlet and rotor inlet boundaries. The resultant profiles at the stator domain outlet, functions of radial coordinate, are used to update boundary conditions at the rotor domain inlet. In this particular case, the stator domain outlet was defined as pressure outlet and the rotor domain inlet as pressure inlet.

After a solution was obtained, the cooling effectiveness η was calculated according to the following,

$$\eta = \frac{T_{owo} - T_{of}}{T_{owo} - T_{oj}} \tag{7.8}$$

where

T_{owo} = Total temperature on the airfoil wall from the adiabatic case without cooling holes;

T_{of} = Total temperature on the airfoil wall from the adiabatic case with cooling holes;

T_{oj} = Total temperature of coolant feeding the hole.

It is apparent that two cases, the case with film holes and the case without, have to be solved in order to compute the cooling effectiveness η for each test condition.

The grids contain between 0.5 and 0.8 million cells. The cases were run on a super-computer – an HPC cluster for computation. It took 8 CPUs on the cluster around 20,000 iterations to reach convergence in approximately 20 hours of computing time. It was found that the converging rate with the rotating frame is 5 to 10 times slower than the case without rotating frame. Besides residuals going down several orders of magnitude, mass and energy were checked to ensure they were conserved throughout the domain before declaring convergence.

The maximum Mach number is around 0.3 and compressibility can not be neglected. The density was defined as ideal gas according to the ideal gas law. Multi-block mostly structured meshes were created to fully resolve the flow field. Figure 7.5 shows a mesh used in the study. The domain was decomposed into 31 volumes in total, 12 for the stationary stator domain and 19 for the rotating rotor domain, in order to mesh them one by one using hexahedral cells. A total of 101 patches of boundary conditions were deployed for the whole computational domain. Most of the cells were clustered around the two jet exit areas as well as boundary layers along the airfoil surface. Since there is no hole on the stator blade, only six nodes were used in the span-wise direction to reduce the number of cells in meshing the stator domain. In the rotor domain, 50 nodes were used in the span-wise direction in order to fully resolve the flow field of the jet-in-a-cross flow. By so doing, the size of the grid was controlled to be less than 1 million cells. Figure 7.5b and 7.5c shows the mesh structures close to the jet exit areas for the circular hole and the louver scheme, respectively.

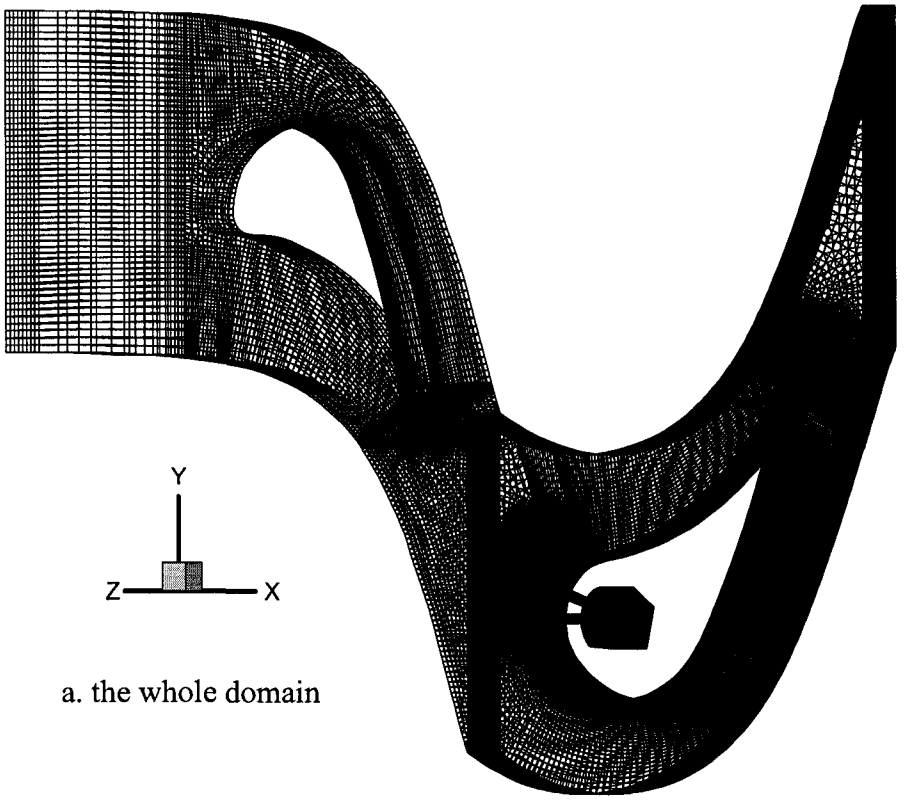

a. the whole domain

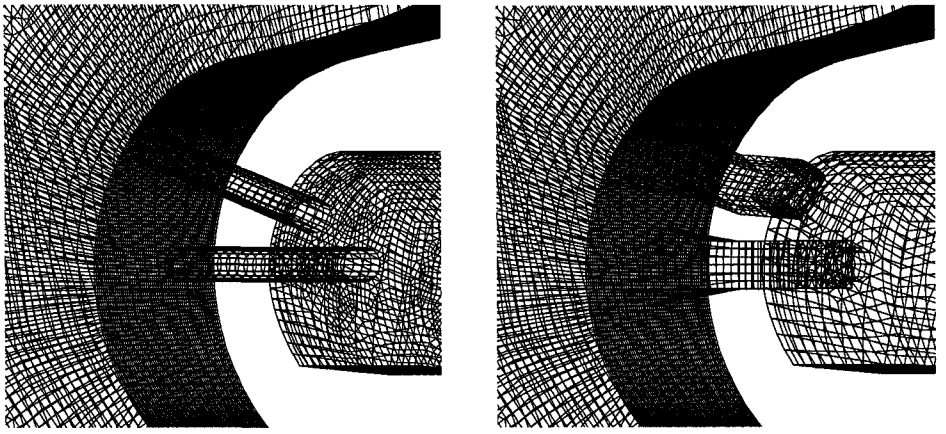

b. the circular hole

c. the louver scheme

Fig. 7.5 Mesh structures – a multi-block mostly structured mesh for the case of 2400 rpm at m = 1.

Figure 7.6 and Fig. 7.7 shows the distribution of Mach number for the 3000rpm case at the cross section without film holes. Acceptable agreement of Mach distribution exists between Fig. 7.6, two dimensional case with periodic boundary condition, and Fig. 7.7, three dimensional case with zero-shear stress boundary condition on the two faces in the circumferential direction. The Mach number around the rotor blade surface between the two dimensional and three dimensional cases is further compared in Fig. 7.8. The difference between the two curves is insignificant and is considered acceptable for engineering applications. It should be noted that whenever the rotational speed is changed, the streamlines will change. Therefore, a new streamline has to be found in a two-dimensional case solution to define the new boundary in a three-dimensional case for the two faces between neighboring blades in the circumferential direction. Thus, cases at different rotational speeds have slightly different domain shapes, which means geometry preparation, mesh generation, and boundary definition have to be done at each rotational speed. Although there is more work involved in this approach, the reduced size of grid and better cell distribution may be well worth the extra efforts. A smaller grid makes the case run faster and with better convergence. This approach has proved to be more rigorous and less likely to run into convergence problems.

To validate the simplification of periodic boundary condition into the zero-shear stress boundary condition in the circumferential direction, two pairs of mesh were generated. Both are three dimensional cases. One has periodic boundary conditions in the circumferential direction and other has the zero-shear stress boundary condition in the same direction. All the other boundary conditions were kept the same for both cases. The difference in the laterally averaged cooling effectiveness is so insignificant that the two

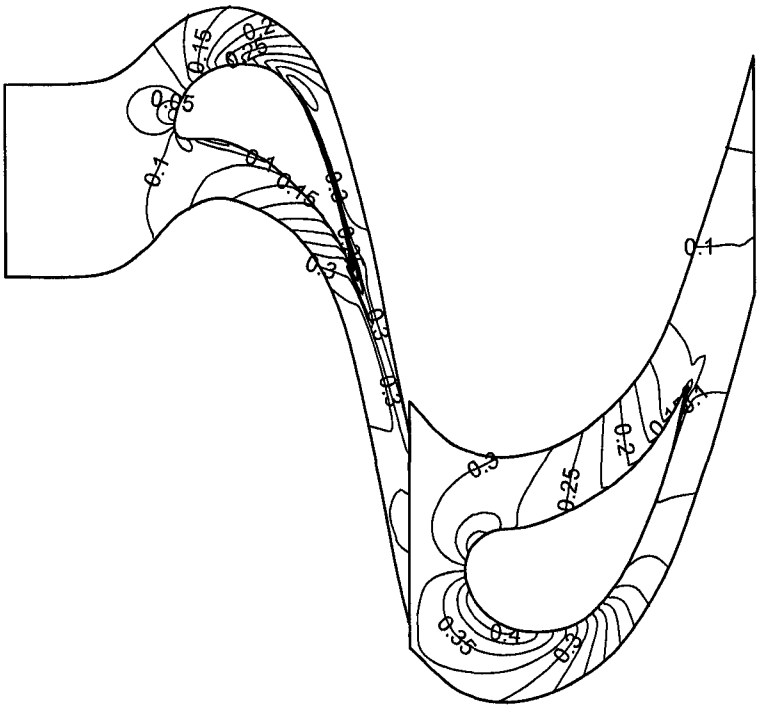

Fig. 7.6 Mach distribution at the cross section for the 2d case.

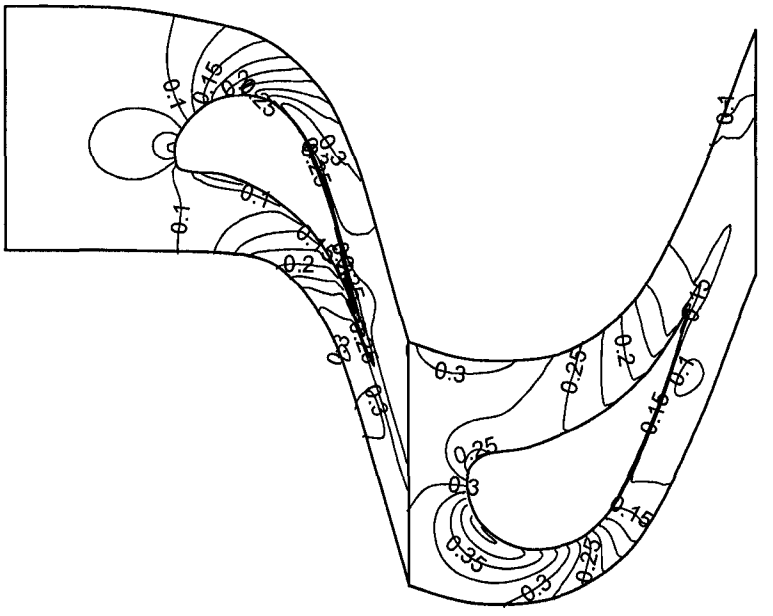

Fig. 7.7 Mach distribution at the cross section for the 3d case.

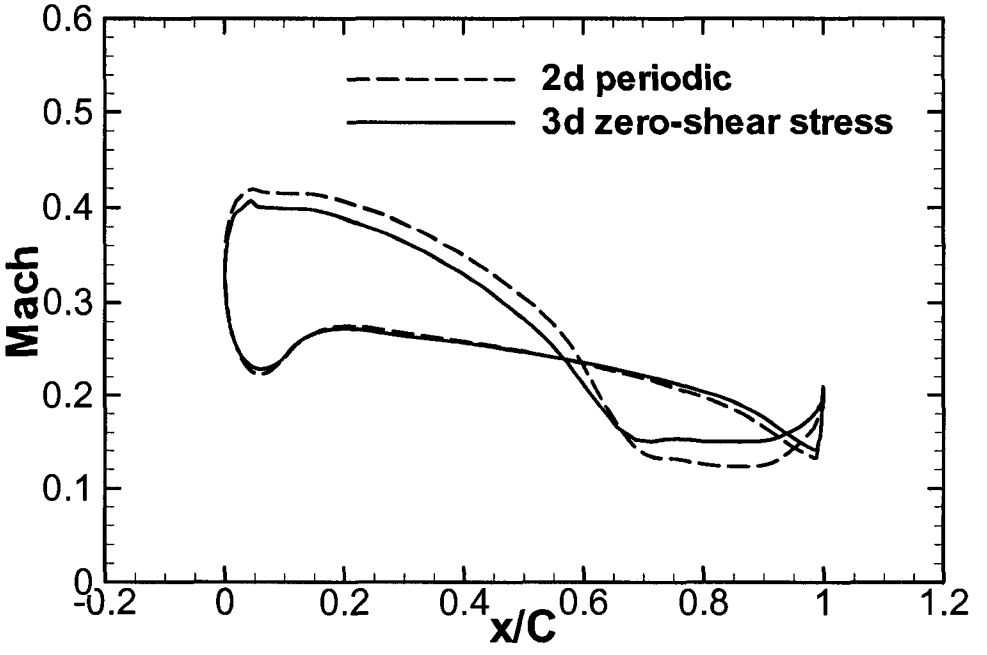

Fig. 7.8 Mach distribution on centerline.

curves almost coincide, as shown in Fig. 7.9. When run on 8 CPUs on a computer cluster, the cases with periodic boundary condition require at least 50% more iterations – around 30,000 – to reach convergence while the sizes of grids for both cases were at the same level. For this reason, all the results for the cases presented below, including three rotational speeds at three blowing ratios for each were from the zero-shear stress boundary condition cases.

Figure 7.10 shows a qualitative comparison of cooling effectiveness on the rotor blade surface at the leading edge between the numerical prediction and the experimental results. The contours are for the two holes at the mid-span of the blade for the blowing ratio of 1 and at the design rotational speed of 2550rpm. The numerical model seems to under-predict the lateral spreading of coolant a little, which could be explained as end-wall effects. For a real turbine blade in the experiment, the high pressure on the pressure side (PS) due to a relatively low speed tends to push streamlines toward the tip of the blade, at the extreme, some fluid close to the tip wall on the pressure side may be able to navigate to the low pressure suction side (SS). This sweeping effect in addition to the compound angle causes more coolant lateral spreading. In the numerical simulation, with only two center holes at the mid-span considered with periodic boundary condition, this end-wall effect is lost.

7.2 Results and discussion

7.2.1 Comparison of laterally averaged cooling effectiveness

To further validate the CFD methodology, predictions of laterally averaged cooling effectiveness at different blowing ratios and different rotational speeds for the circular

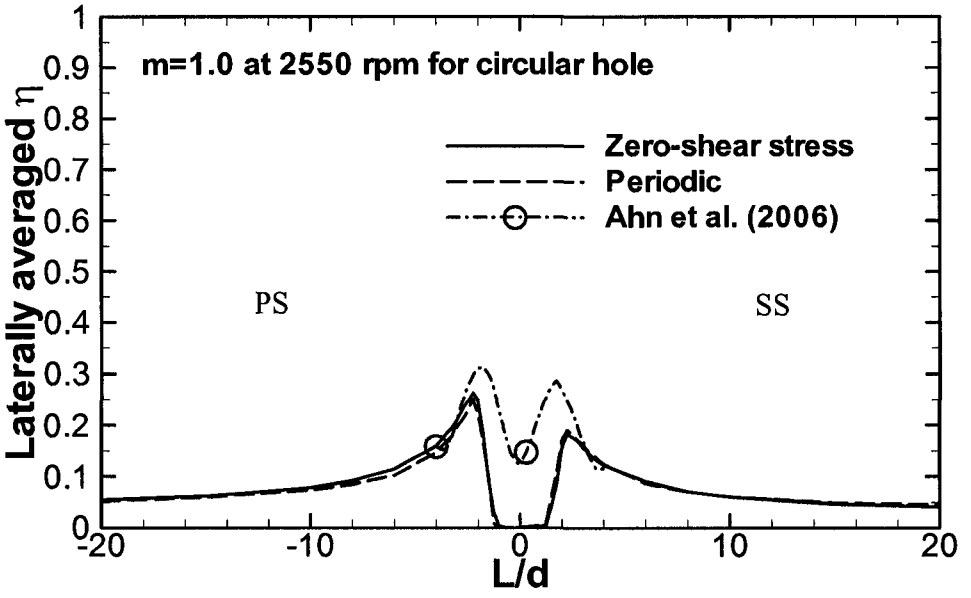

Fig. 7.9 Effectiveness prediction for different boundary conditions.

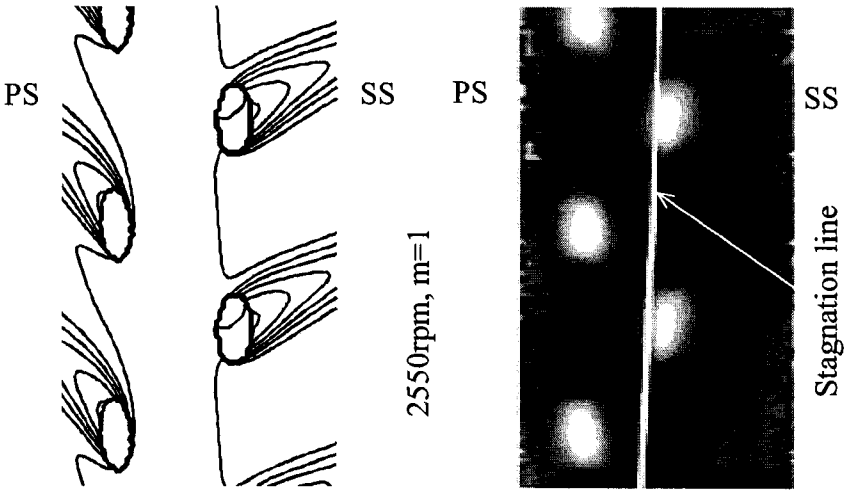

a. numerical b. experimental, Ahn et al. [16]

Fig. 7.10 Effectiveness contours – qualitative comparison.

hole are compared with the experimental data in Fig. 7.11 – 7.14. It can be seen that the numerical prediction agrees with the experimental data at high blowing ratios, Fig. 7.11 and Fig. 7.12. However, the mathematical model considerably under-predicted the cooling effectiveness at a low blowing ratio of 0.5, regardless of rotational speed, Fig. 7.13 and Fig. 7.14. At the very leading edge area close to the stagnation point, around L/d from -2 to 2, the laterally averaged cooling effectiveness was also under-predicted, which can be construed as a result of mismatch of data between the numerical results of this work and the experimental work. The predicted cooling effectiveness data in this work, shown in these figures, were laterally averaged for one period, one hole only at the mid-span as shown in Fig. 7.1d: while the experimental data were for the whole blade from tip to hub of the blade including all the eight holes. At a constant rotational speed, the stagnation line around the airfoil leading edge is not perfectly aligned parallel to the radial direction. Instead, it tilts a little to the clock-wise direction due to the rotational effect as illustrated in Fig. 7.10. Consequently, the coolant issued by the holes close to the hub on the pressure side may partly go to the suction side, or coolant issued by the holes close to the tip on the suction side may partly go to the pressure side, or both depending on the rotational speed and blowing ratio. This leads to a higher level of cooling effectiveness around the leading edge area when the data were span-wise averaged for the whole blade span with all eight holes included. Although for the two holes at the mid-span, the coolant issued by either side holes goes to their correspondent side perfectly, as they are intended to, leaving the area in between totally exposed to the hot mainstream, Fig. 7.10.

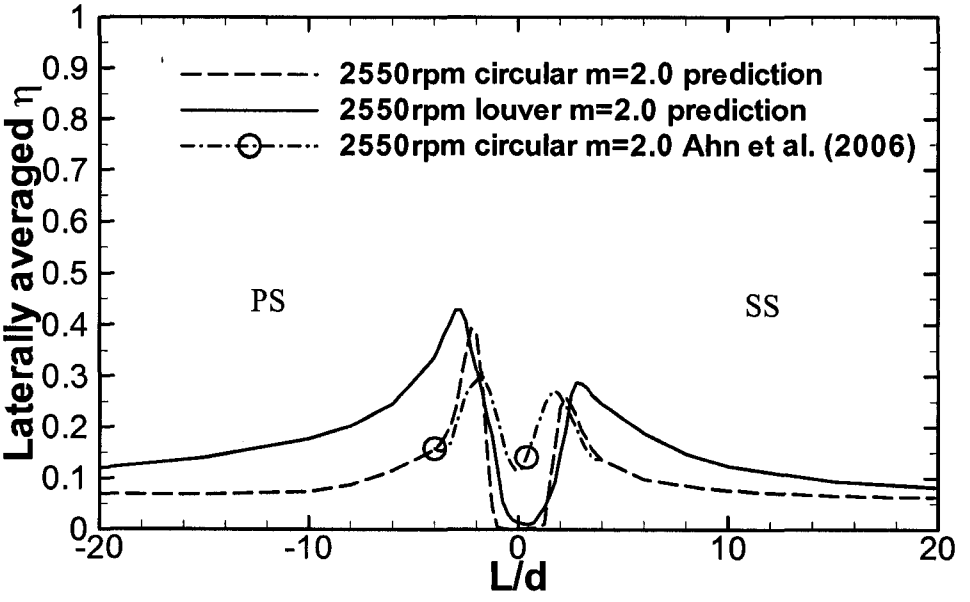

Fig. 7.11 Laterally averaged effectiveness at 2550 rpm and m = 2.

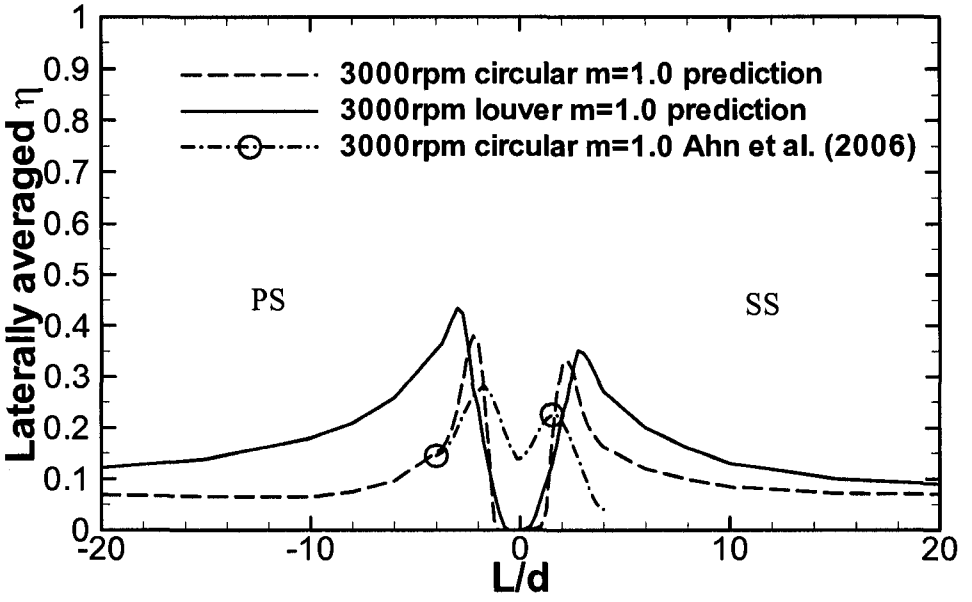

Fig. 7.12 Laterally averaged effectiveness at 3000 rpm and m = 1.

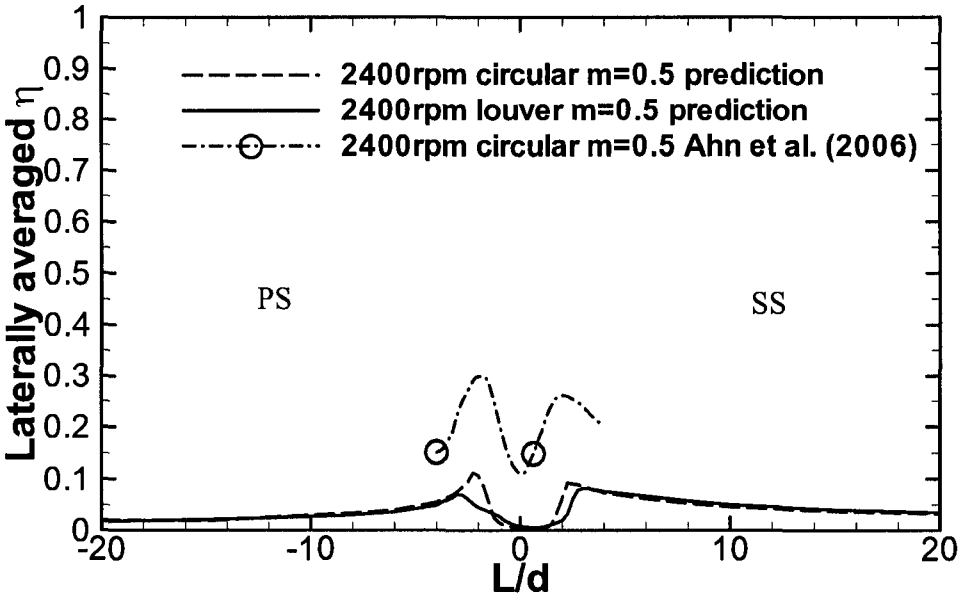

Fig. 7.13 Laterally averaged effectiveness at 2400 rpm and m = 0.5.

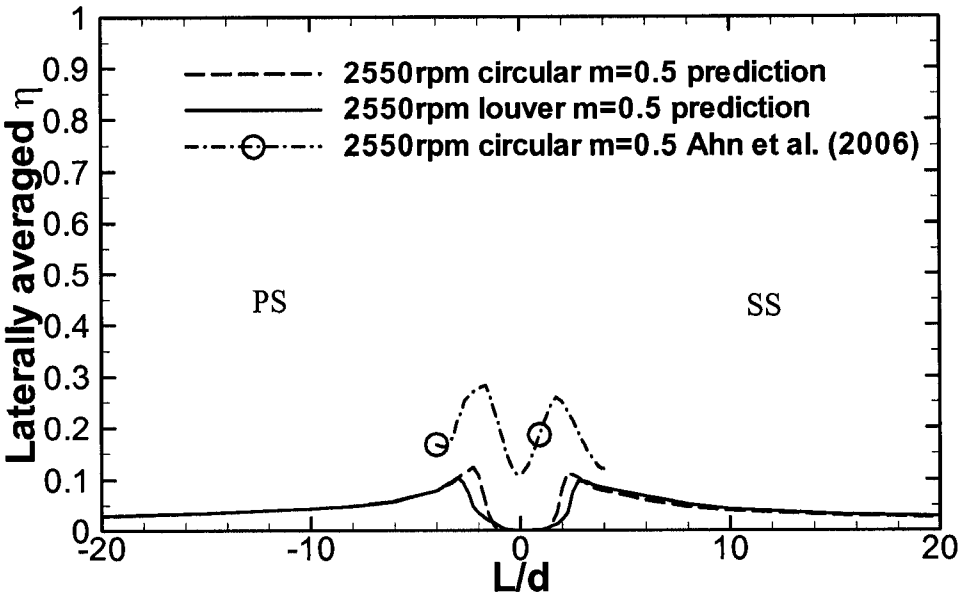

Fig. 7.14 Laterally averaged effectiveness at 2550 rpm and m = 0.5.

Also shown in Fig. 7.11 – 7.14 are the predictions of cooling effectiveness for the louver scheme. At low blowing ratios, Fig. 7.13 and Fig. 7.14, both the louver and circular holes produce same level of cooling effectiveness according to the numerical prediction. At high blowing ratios, Fig. 7.11 and Fig. 7.12, the louver scheme outperforms the circular hole with a higher level of cooling effectiveness. Both the experimental data and the numerical predictions confirm that the cooling effectiveness is higher on the pressure side than on the suction side at the leading edge, in contradiction to non-leading edge film cooling on a turbine blade. In the literature, film cooling effectiveness away from the leading edge is usually higher on the suction side than on the pressure side under the same conditions due to a favourable pressure gradient keeping the coolant close to the airfoil surface on the suction side. This abnormal cooling phenomenon at the leading edge has to do with the impinging mainstream. Normally, the mainstream flow direction is parallel to the cooled surface as opposed to the leading edge where the mainstream flow direction is perpendicular to the surface. The impinging effect of the mainstream is to push the coolant against the wall, preventing it from lifting off of the surface even at high blowing ratios. Hence, high blowing ratios are associated with higher levels of cooling effectiveness.

7.2.2 Effects of blowing ratio

Figure 7.15 – 7.18 shows the effects of blowing ratio. For the circular hole at a below design rotational speed, Fig. 7.15, the higher the blowing ratio, the higher the level of cooling effectiveness. For the circular hole at an above design rotational speed, Fig. 7.16, a higher blowing ratio results in a lower level of cooling effectiveness due to severe jet

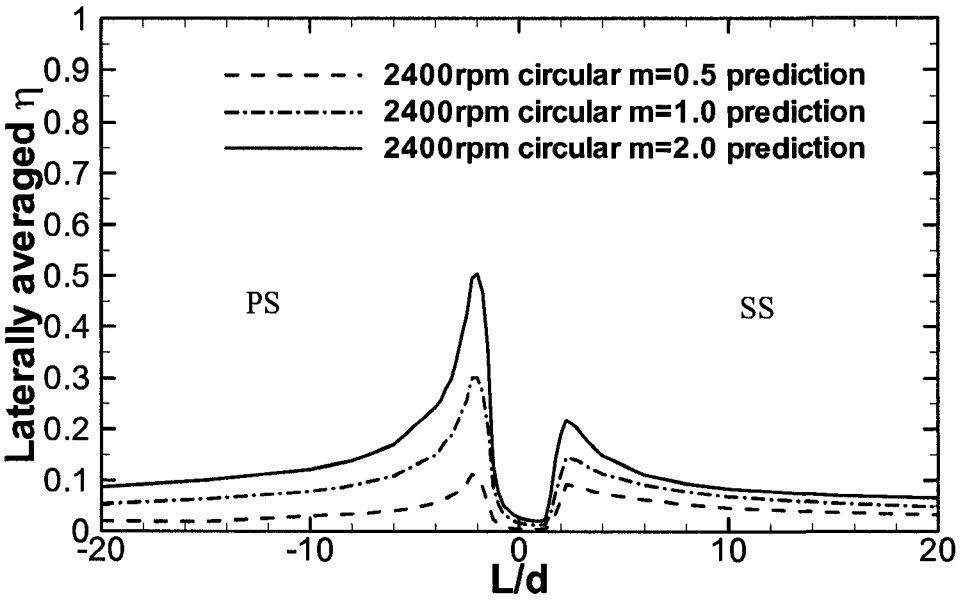

Fig. 7.15 Effects of blowing ratio for the circular hole at below design rotational speed.

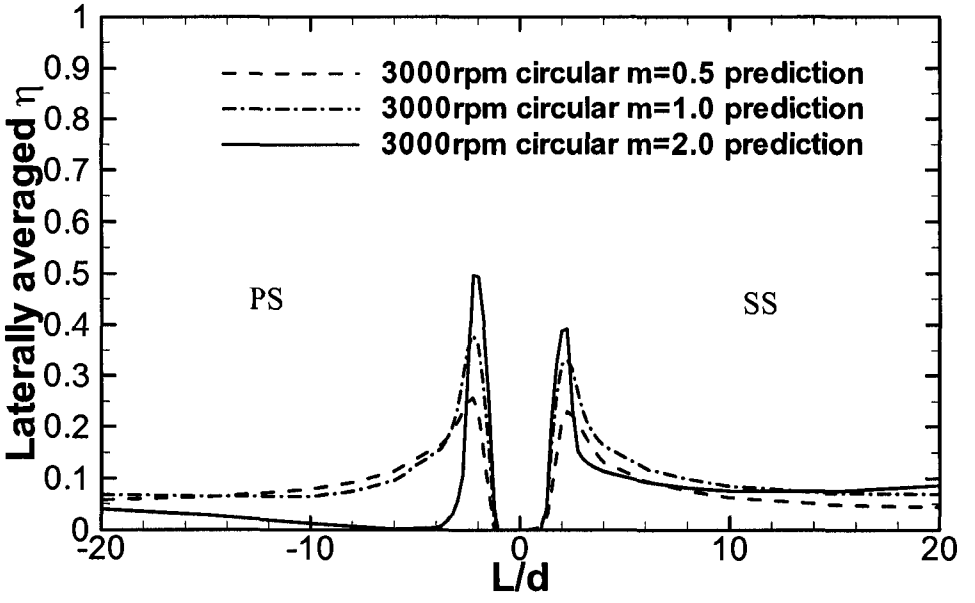

Fig. 7.16 Effects of blowing ratio for the circular hole at above design rotational speed.

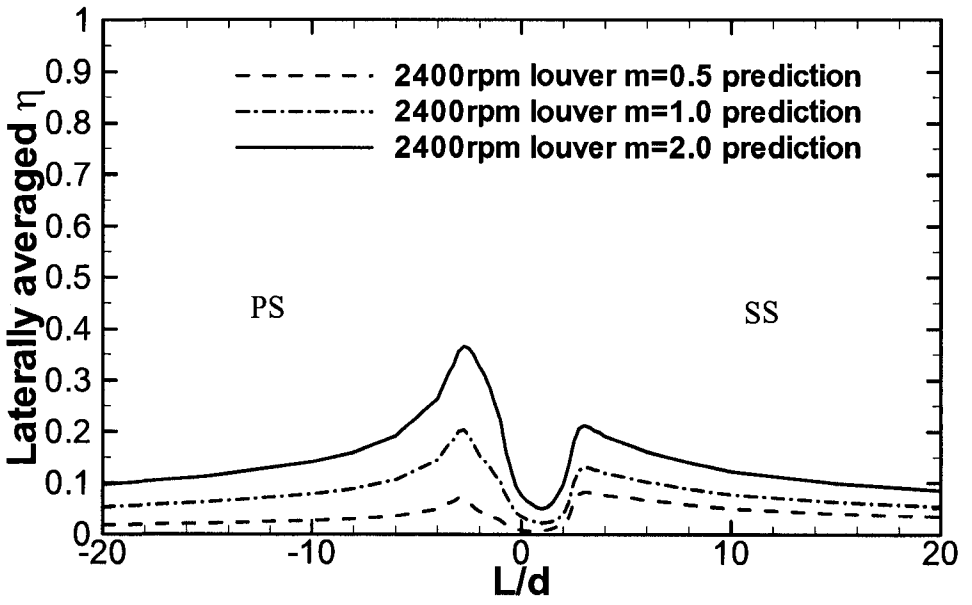

Fig. 7.17 Effects of blowing ratio for the louver scheme at below design rotational speed.

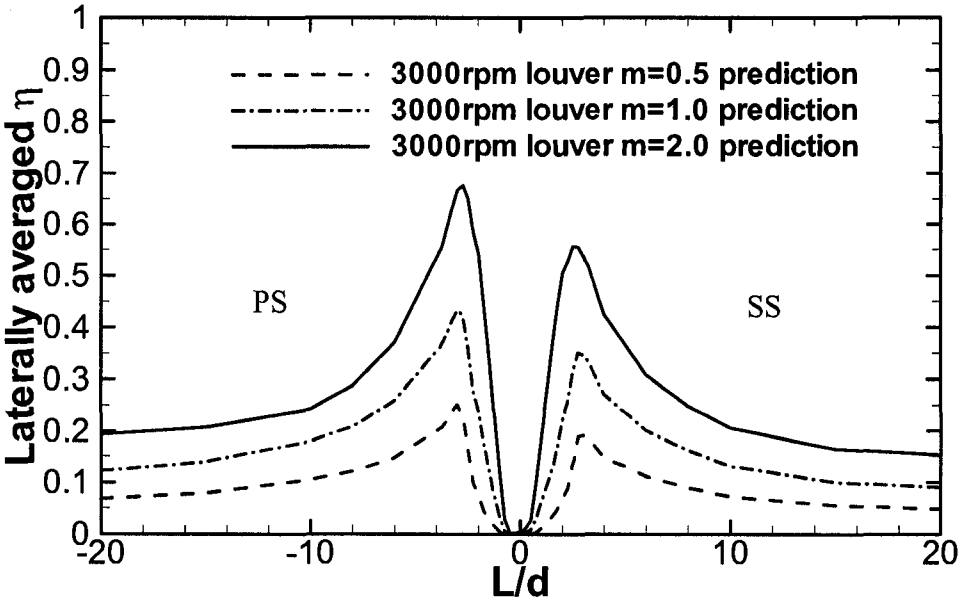

Fig. 7.18 Effects of blowing ratio for the louver scheme at above design rotational speed.

penetration, either on the pressure side or on the suction side. This is possibly a result of shifting incidence angle due to a higher rotational speed. For the louver scheme, as shown in Fig. 7.17 and Fig. 7.18, laterally averaged cooling effectiveness increases with blowing ratio regardless of rotational speed, whether below or above the design speed. Based on this point, the louver cooling scheme is quite beneficial when deployed at the leading edge. Other shaped holes with an expanded exit may also provide similar benefits as well, in comparison with the traditional circular hole.

7.2.3 Effects of rotational speed

To show the effect of rotational speed on cooling effectiveness, data are plotted in Fig. 7.19 – 7.22. For the circular hole at a low blowing ratio, Fig. 7.19, cooling effectiveness increases with rotational speed while the reverse is true at a high blowing ratio, Fig. 7.20. At a low blowing ratio, the jet did not lift off and the blowing ratio is the dominant factor in determining the level of cooling effectiveness, and a higher rotational speed causes the coolant to spread more on the airfoil surface after injection. At a high blowing ratio, jets are more prone to lift off from the surface and the shifting incidence angle associated with the rotational speed is the dominant factor in determining the level of cooling effectiveness. A small amount of incidence angle shifting caused by the rotational speed will lead to severe jet penetration resulting in considerably lower levels of cooling effectiveness. For the louver cooling scheme, as jet liftoff is avoided, a higher rotational speed leads to more lateral coolant spreading and a higher level of cooling effectiveness, Fig. 7.21 and Fig. 7.22.

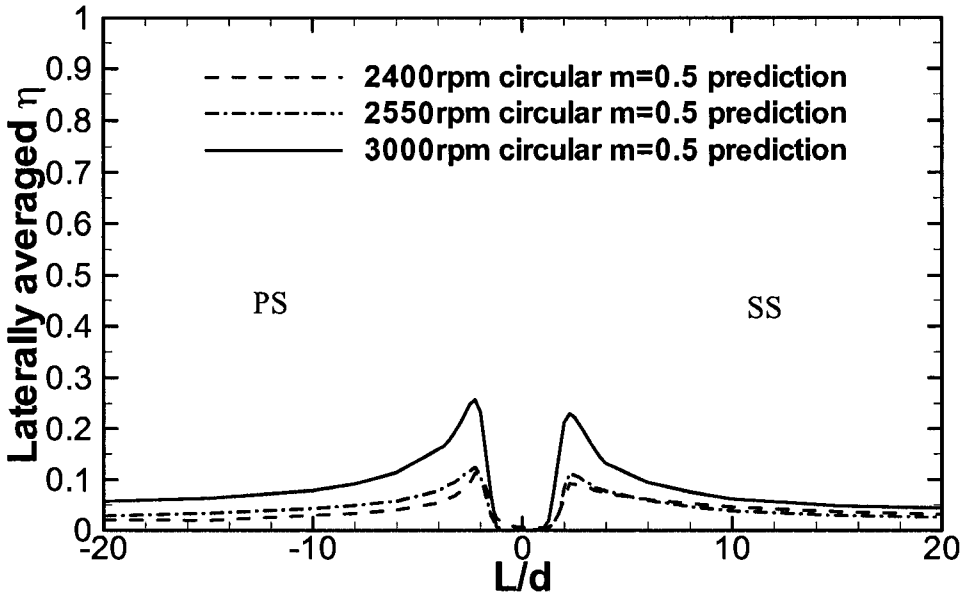

Fig. 7.19 Effect of rotational speed for the circular hole at a low blowing ratio.

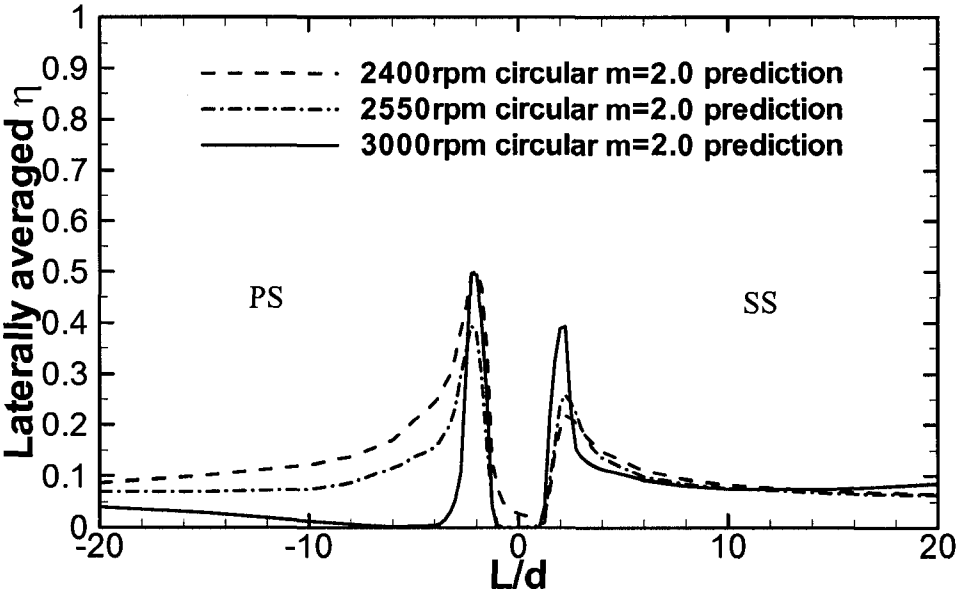

Fig. 7.20 Effect of rotational speed for the circular hole at a high blowing ratio.

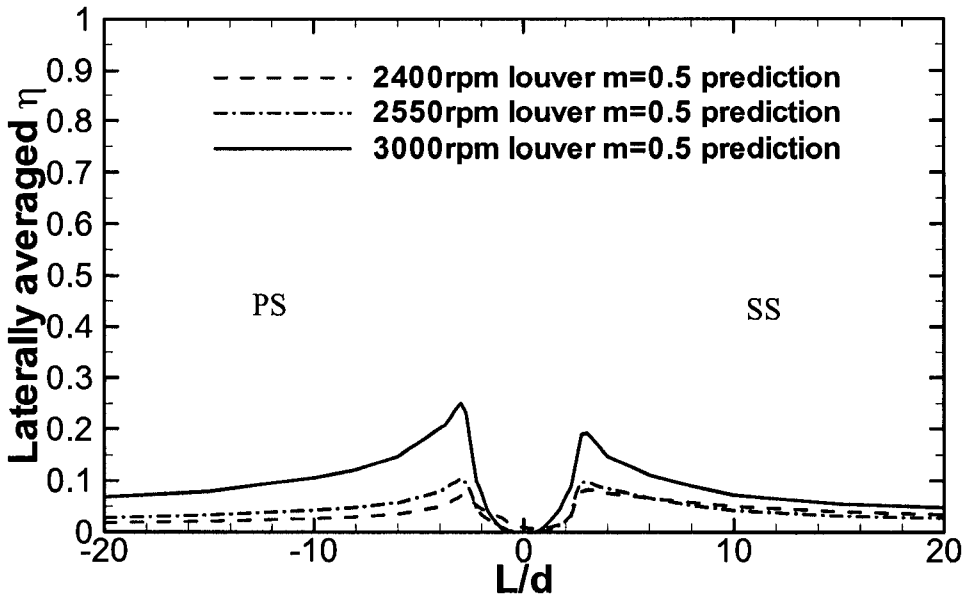

Fig. 7.21 Effect of rotational speed for the louver scheme at a low blowing ratio.

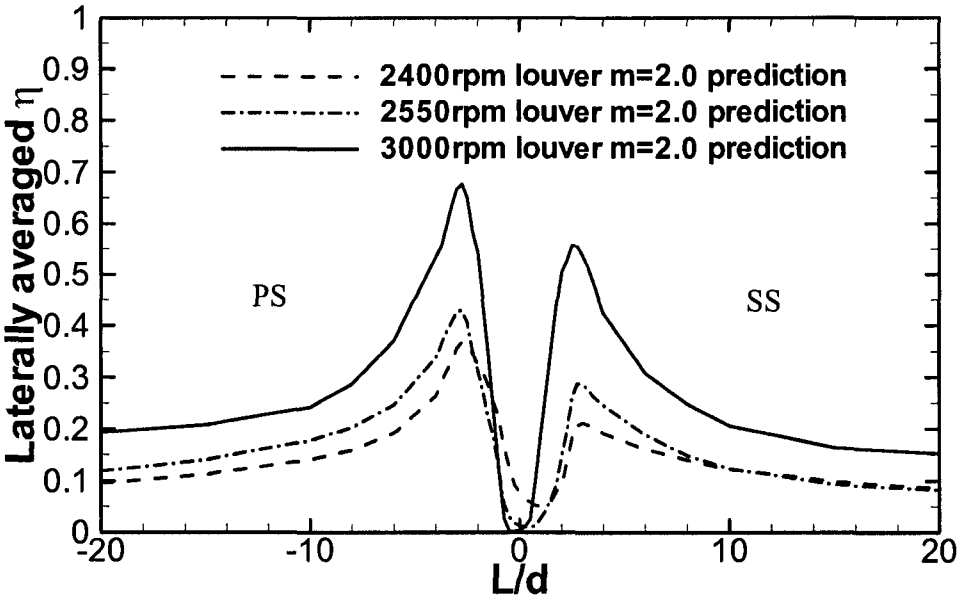

Fig. 7.22 Effect of rotational speed for the louver scheme at a high blowing ratio.

7.2.4 Local adiabatic cooling effectiveness

Contours of cooling effectiveness are plotted in Fig. 7.23 for the case of 3000rpm on the pressure side. Comparison between the circular hole and the louver scheme under the same blowing ratio shows that for the louver scheme, coolant spreads wider after injection with a more uniform cooling effectiveness. For the circular hole, the downstream area that is covered by coolant becomes narrower as blowing ratio increases. The maximum cooling effectiveness increases when the blowing ratio increases from 0.5 to 1, then drops sharply when the blowing ratio increases to 2 because of the severe jet liftoff. For the louver scheme, the downstream area that is covered by the coolant becomes much wider as the blowing ratio increases. The maximum cooling effectiveness increases with blowing ratio, indicating that jet penetration does not occur. Contrary to the circular hole, the higher the blowing ratio for the louver scheme, the more uniform the cooling effectiveness distribution, which is the desirable effect. A similar trend was also found for the suction side. Therefore, the louver scheme is perfectly suited for higher blowing ratio applications.

For a clear comparison in the span-wise direction between the circular hole and the louver scheme, the local cooling effectiveness is presented in Fig. 7.24. At a low blowing ratio of 0.5, the two schemes were predicted to have roughly the same level of cooling effectiveness from x/d of 4 to 15. The point of maximum cooling effectiveness for the circular hole is slightly shifted to the right side in comparison to the louver cooling scheme. As the blowing ratio increases, the distance between the peak values of cooling effectiveness for the two schemes grows, although more shifting occurs for both schemes. The same amount of coolant is injected under the same blowing ratio conditions for both

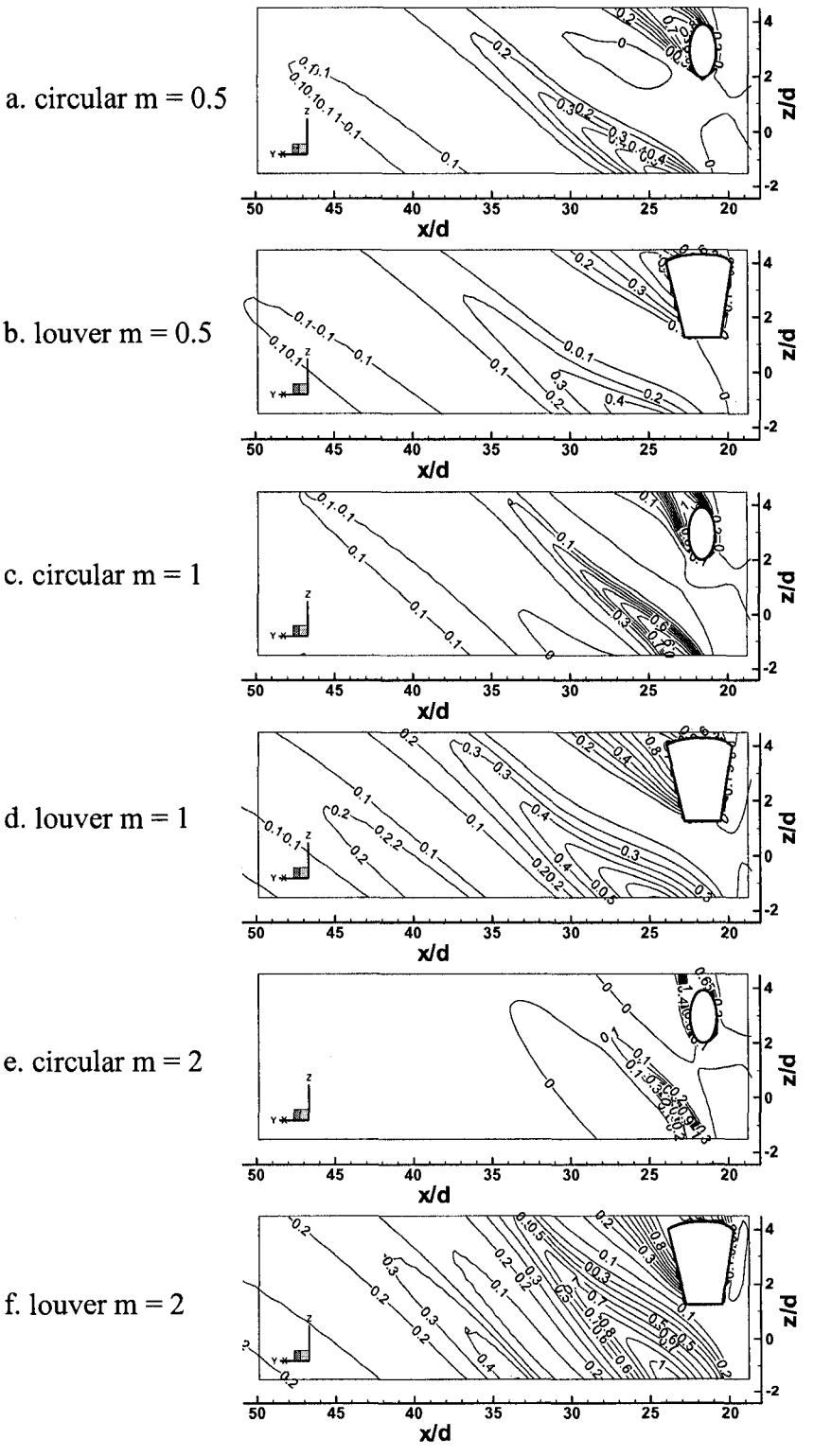

Fig. 7.23 Contours of η on the pressure side for the 3000 rpm cases.

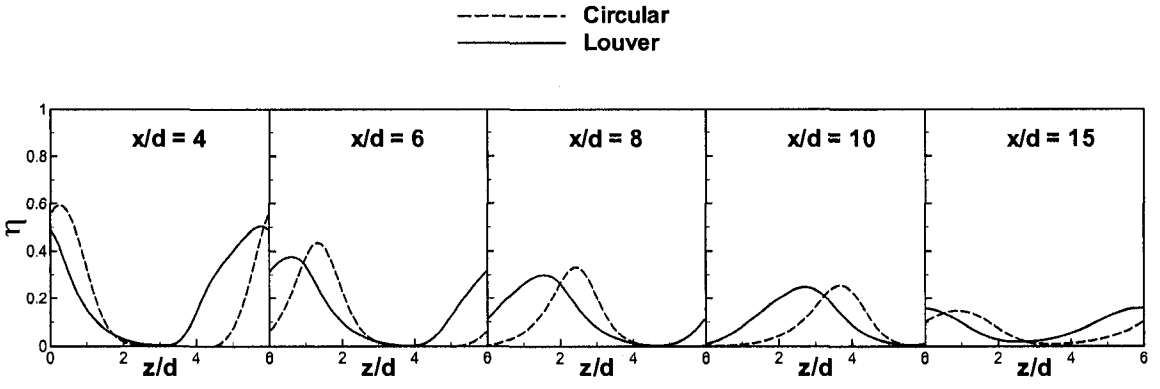

a. m = 0.5

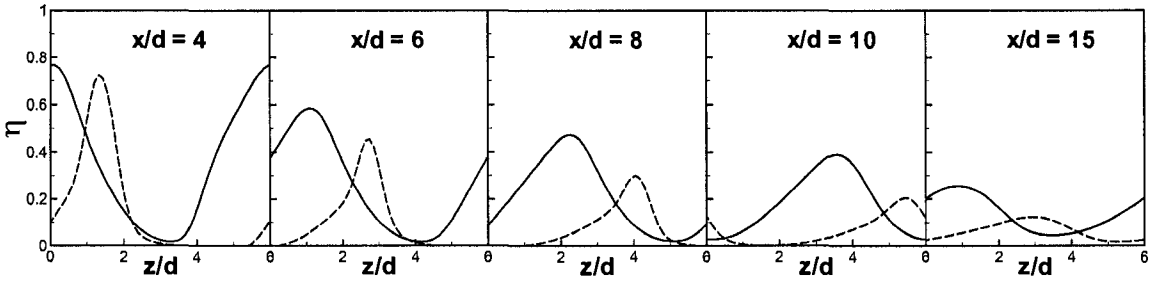

b. m = 1

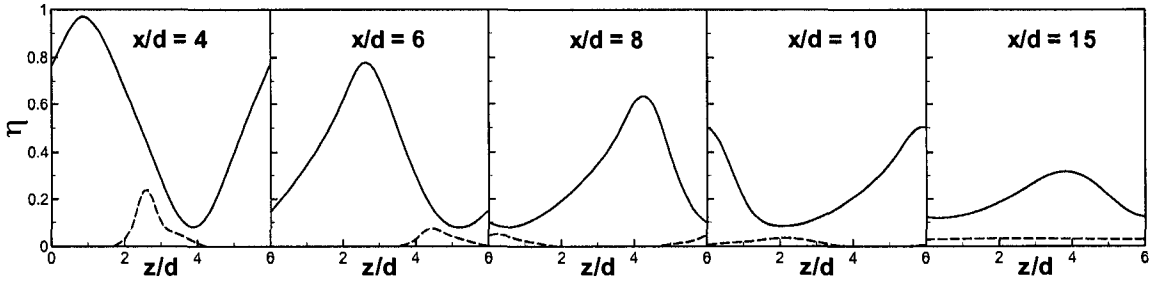

c. m = 2

Fig. 7.24 Comparison of η in the span-wise direction at 3000 rpm on the pressure side.

the circular hole and the louver cooling scheme. Consequently, the momentum of the coolant from the circular hole is more concentrated in comparison with the louver cooling scheme with an exit expansion, which makes the coolant from the circular hole travel further than that from the louver scheme in the span-wise direction before its momentum is overcome by the mainstream. Although the coolant from the circular hole spreads faster and further in the span-wise direction than the coolant from the louver scheme does, the level of laterally averaged cooling effectiveness is much lower for the circular hole than for the louver cooling scheme as already mentioned, since a severe jet penetration occurs for the circular hole at high blowing ratios. The higher the blowing ratio, the wider the difference in the level of cooling effectiveness between the two cooling schemes as shown in the figure.

7.2.5 Comparison of streamlines

Figure 7.25 shows the comparison of streamlines at different blowing ratios and different rotational speeds between the circular hole and the louver scheme. When the rotational speed is below design condition at 2400rpm, the stagnation line shifts toward the pressure side of the blade in comparison to the design condition. As a result, some of the coolant from the pressure side for the louver scheme goes to the suction side after injection instead of to the pressure side as it is intended to do, Fig. 7.25b. As the rotational speed increases slightly above the design speed to 3000rpm, the stagnation line shifts closer to the suction side, somewhere between the two holes. Thus, the coolant issued from the pressure side hole goes to the pressure side and coolant from the suction side goes to the suction side, Fig. 7.25c and Fig. 7.25d. The shifting of the stagnation line toward the

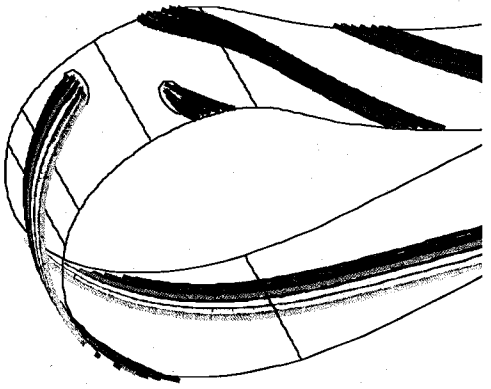

a. 2400rpm m = 0.5 circular

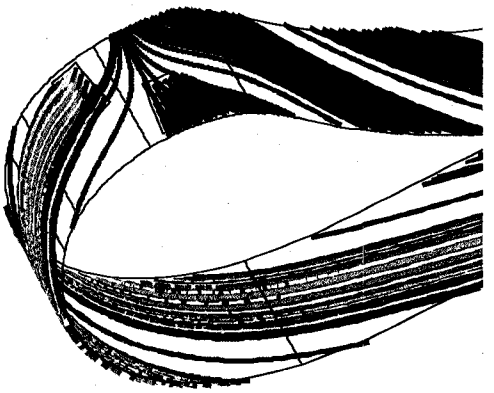

b. 2400rpm m = 0.5 louver

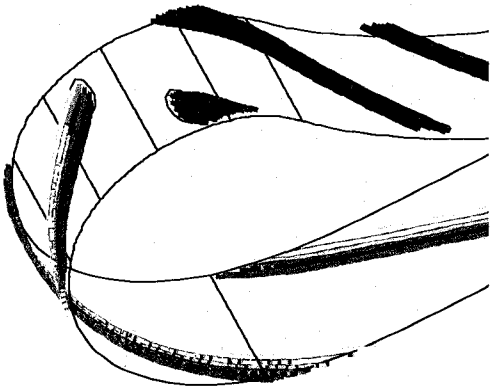

c. 3000rpm m = 0.5 circular

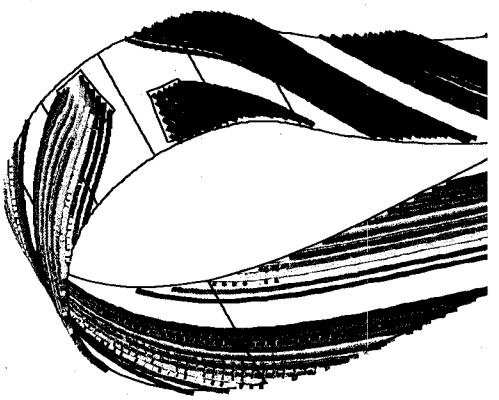

d. 3000rpm m = 0.5 louver

e. 3000rpm m = 2 circular

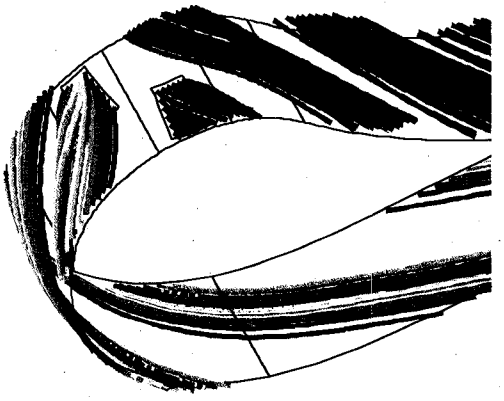

f. 3000rpm m = 2 louver

Fig. 7.25 Streamlines at different blowing ratios and rotating speeds.

suction side as the rotational speed increases changes the deflection angle of the coolant for holes on both sides. But the effect is not equally felt on both sides. At 2400rpm, the stagnation line is closer to the pressure side hole than to the suction side one, and it even cuts through the pressure side louver hole exit, although not the circular hole on the same side. At 3000rpm, slightly above the design speed of 2550rpm, the stagnation line shifts slightly closer to the suction side hole than the pressure side one. For low blowing ratios as coolant does not lift off of the blade surface, increasing rotational speed only increases coolant span-wise spreading, which can be seen by comparing Fig. 7.25a with Fig. 7.25c and Fig. 7.25b with Fig. 7.25d. Thus, higher cooling effectiveness is expected as already shown in Fig. 7.19 and Fig. 7.21.

The momentum of the mainstream can be decomposed into two components, the normal direction to the airfoil surface and the tangential direction. The normal momentum of the mainstream is to press the coolant to the wall and the tangential momentum of the mainstream is to bend the coolant to the wall. As the stagnation line shifts toward the suction side and positive incidence angle becomes negative incidence angle due to an increasing rotational speed, the normal momentum of the mainstream increases and the tangential momentum decreases. As mentioned, at low blowing ratios the jet does not lift off of the surface, even on a flat plat where the mainstream momentum is all tangential. Therefore, the effects of the normal momentum of the mainstream on the jet coolant are insignificant. A decreased tangential momentum will result in the coolant issued from the jet with a 90 degrees compound angle with regard to the mainstream direction spreading more in the span-wise direction. Consequently, more cooling effects are felt on the blade surface with a higher level of cooling effectiveness,

regardless of what cooling scheme it is, Fig. 7.19 and Fig. 7.21. If the higher-than-design rotational speed is kept constant at 3000rpm and blowing ratio increased to 2, Fig. 7.25e and Fig. 7.25f, a dramatic change in the coolant flow behavior occurs for the circular hole in that the coolant shoots off into the mainstream. Although there is more span-wise spreading of the coolant due to an increasing lateral momentum owing to a 90 degrees compound angle, the spreading happens deep in the mainstream instead of on the blade surface. Hence, this is of no help in the cooling of the airfoil blade and the cooling effectiveness drops dramatically, Fig. 7.16. The reduction in cooling effectiveness is less severe on the suction side than on the pressure side, possibly due to a favorable pressure gradient on the suction side pushing coolant toward the airfoil surface and an unfavorable pressure gradient on the pressure side pushing coolant away from the wall, which can be attributed to the curvature effects. These effects are more noticeable for the circular hole than for the louver scheme and at high blowing ratios than at low blowing ratios, particularly when the jet is prone to lift off of the surface.

7.3 Summary

Numerical simulations were carried out for two cooling schemes, a circular hole and a louver cooling scheme, at the leading edge of a rotor blade in a complete turbine stage. A numerical model was created based on a number of simplifications in order to make the meshing process simpler and mesh smaller, so that the CFD cases can be run more efficiently. Multi-block structured meshes with wall functions were employed to further reduce the size of the mesh. It was found that with both the stator and rotor domains it took considerably longer to reach convergence than if the case has only one domain,

either the stator or rotor. Comparisons with experimental data for the circular hole case show that the agreement with the experimental data is generally good. The analysis of film cooling at the leading edge of an airfoil was presented, which sheds light on the physics of film cooling and should prove helpful to the cooling designs of turbine blades. The findings of this study were summarized below.

1. Good agreement exists between prediction and experimental data for the circular hole at higher blowing ratios. At low blowing ratios the model under-predicts the cooling effectiveness.

2. The louver cooling scheme provides higher cooling effectiveness than the circular hole at high blowing ratios. At low blowing ratios, both the circular and the louver scheme give approximately the same levels of cooling effectiveness.

3. For the circular hole, effectiveness increases with blowing ratio at low rotating speeds, and decreases with blowing ratio at high rotating speeds. For the louver scheme, effectiveness increases with blowing ratio regardless of rotating speed.

4. With regard to the cooling effectiveness level, the blowing ratio is the dominant factor at low rotational speeds and the rotational speed is the dominant factor at high blowing ratios for the circular hole. For the circular hole at low blowing ratios, effectiveness increases with rotating speed while at high blowing ratios, the reverse is true. For the louver scheme as jet liftoff is avoided, effectiveness increases with rotating speed.

Chapter 8

Conclusions and Recommendations

8.1 Conclusions and contributions

A comprehensive numerical investigation of a louver cooling scheme under different conditions was conducted in this work, including film cooling in a transonic flow and film cooling on a rotating turbine blade. In previous studies, only the louver cooling scheme on a flat plate under incompressible flow conditions was studied. Nevertheless, the predicted data showed very promising performance in the cooling of targeted surface in comparison with other cooling schemes published in the recent literature. The goals of this study are to investigate the louver scheme under more realistic conditions and to provide some useful data for engine designers. Particular attention was paid to the physics aspects of film cooling process in the analysis of the numerical results under different conditions, such as transonic film cooling and rotating film cooling. It is highly unlikely that two designers will come up with the same cooling design. Nevertheless, all laws of physics should be applied equally. Therefore, the data provided in this work may be extrapolated to other similar designs under similar operating conditions. In addition, the analysis of the louver cooling scheme from the physics point of view should prove useful toward the understanding of film cooling process under different conditions, and thus, hopefully, pave the way to a more efficient cooling design of turbine blades in the future.

In the work, the louver cooing scheme was tested under different conditions. Firstly, multiple rows on a flat plate were studied. Secondly, unsteady analysis of the louver cooling scheme of single row on a flat plate was performed. These two efforts were extensions of previous studies. The study of the louver cooling scheme on a flat plate will not be complete without these two parts. Currently, only single row data of the louver cooling scheme on a flat plate exists in the literature. The second part – unsteady analysis of the louver cooling scheme – is really a test of the accuracy of unsteady analysis against the more popular Reynolds Averaged Navier-Stokes approach toward film cooling simulations. It is obvious that the condition is simpler than the first part, being a single row under ideal conditions. On the other hand, there is a fundamental difference between the two parts, namely that unsteady analysis is notoriously much more expensive and even prohibitive, computationally speaking. This part should prove helpful for some engineers and designers who have to decide whether to use unsteady or steady analysis in most practical industrial applications. Thirdly, the louver cooling scheme on a transonic airfoil was tested in part 3. Since part 2 – unsteady analysis – has proved that unsteady analysis was no more accurate than its steady analysis counterpart, particularly in terms of laterally averaged cooling effectiveness, (although it gave more realistic predictions in certain aspects, lateral coolant spreading as an example), only steady analysis was carried out and mainly laterally averaged cooling effectiveness data was presented in part 3. Finally, the louver cooling scheme on a rotating blade was examined in part 4. Part 3 – transonic film cooling – focuses on shock wave interactions and their effects on film cooling performance. In part 4 – rotating film cooling, the investigation was centered on the rotational effects of turbine blades on film cooling performance. These last two parts

are the new frontiers on the subject of film cooling research. The current knowledge on these two aspects of film cooling is very limited.

Following the tradition of CFD research, numerical analysis of the louver cooling scheme under different test conditions in each part was invariably proceeded by a validation in which the predictions were compared with experimental data in the open literature. Since there is no experimental data available for the louver cooling scheme at present, the CFD validation is critical and its importance can not be over-estimated. This is particularly true for the last two parts – the transonic film cooling and rotating film cooling, as the knowledge of these two topics was so limited that only conflicting information existed in the literature. In spite of the fact that every effort has been made to ensure numerical convergence in the CFD analysis based on the author's knowledge and the analysis and results did make sense to a large extent, the numerical data have to be dealt with caution. There might be bugs in any codes that cause some errors in the final solution and have never been detected. Fluent is no exception. Convergence problems were fought right to the end and for no apparent reason no converged solution has ever been successfully obtained for certain cases during the study.

In general, when tested under different operating conditions, whether it being on a flat plate in incompressible flow, on a curved surface in transonic flow, or at the leading edge of a rotating airfoil in subsonic flow conditions, the louver cooling scheme was proved to consistently provide a higher level of cooling effectiveness than the circular hole. The louver cooling scheme also more or less outperformed other shaped cooling schemes proposed recently in the literature. The advantages of the louver cooling scheme were more noticeable at a high blowing ratio than at a low blowing ratio. Results of multiple

rows of the louver scheme on a flat plate showed that the two staggered rows of holes provided better surface protection than two inline rows and that deployment of three or more rows of holes closely should be avoided, as more coolant injection beyond two rows would not be very efficient in cooling the surface and would result in a waste of coolant. Unsteady analysis of film cooling proved to be very expensive in terms of computing resources and no more accurate than steady analysis. The prediction of the lateral spreading of coolant, however, was more realistic in the unsteady analysis than that of the steady analysis.

The process of film cooling is different on a curved surface than on a flat plate. Convex surface on an airfoil in combination with flow acceleration due to compressibility of the fluid creates a favorable pressure gradient, which presses the injected coolant close to the targeted surface, increasing cooling effectiveness. When the blowing ratio is low and the oblique shock generated by the interaction between the jet and the mainstream stays attached to the leading edge of the film hole exit, cooling effectiveness is generally higher on a convex airfoil surface than on a flat plate. The working fluid going through the oblique shock waves is compressed and the subsequent increased pressure may also push the coolant toward the airfoil surface, leading to a higher level of cooling effectiveness. However, when the blowing ratio is too high, a strong detached shock occurs which drastically changes the flow field. As a result, the boundary layer separates from the wall rendering the coolant ineffective. Under the same transonic or supersonic mainstream flow conditions, the higher the blowing ratio, the stronger the shock waves, and the lower the cooling effectiveness. Therefore, using extremely high blowing ratios

should be avoided for any cooling schemes when the flow field in the mainstream at the location of the hole is supersonic.

The results of rotating film cooling study show that at the leading edge of a rotating blade, the louver cooling scheme behaves quite differently than the circular hole. The rotation of blade had a significant impact on the level of film cooling effectiveness. For the circular hole, effectiveness increased with blowing ratio at below design rotating speeds, and decreased with blowing ratio at above design rotating speeds. For the louver scheme, effectiveness increased with blowing ratio regardless of rotating speed. With regard to the cooling effectiveness for the circular hole, the blowing ratio was the dominant factor at low rotational speeds and the rotational speed was the dominant factor at high blowing ratios. For the circular hole at low blowing ratios, effectiveness increased with rotating speed while at high blowing ratios, the reverse was true. For the louver scheme as jet liftoff was avoided, effectiveness increased with rotating speed.

8.2 Recommendations

Throughout this study, the author struggled against divergence in the CFD simulations continuously. Although commercial software Fluent has proved to be very popular and more powerful with each upgrade, still, there is much room for improvement and more robust and vigorous computing algorithms are called for. It is also possible that the current turbulence modeling was partly responsible for not being able to achieve a converged solution for some cases. Although turbulence remains one the greatest mysteries of science and a breakthrough in the modeling per se is highly unlikely in the foreseeable future, small improvement in the modeling itself would certainly help. More

accurate numerical simulation will not only help test more efficient cooling schemes, but more importantly, it will enable further understanding of film cooling physics as well.

Unsteady analysis of film cooling application is still prohibitively expensive with today's powerful computers. However, its ability to predict a more realistic lateral coolant spreading is very attractive. Any improvement in reducing the cost of computing is highly desirable. An unsteady analysis of the louver cooling scheme on an airfoil and/or on a rotating turbine blade should be studied in the future.

Film cooling studies under transonic or supersonic flow conditions were scarce. More experimental studies of cooling effectiveness under transonic flow conditions on an airfoil are highly needed for the validation of CFD code, especially for shaped holes. In particular, experimental study of the louver cooling scheme on airfoils is highly recommended for providing experimental data. In addition, the benefit of impingement cooling of the louver cooling scheme was not considered in this work and should be taken into account in a conjugate analysis.

Publications out of this work

Journal

Zhang, X. Z., Hassan, I., and Lucas, T., "Louver Cooling Scheme for Gas Turbines: Multiple Rows", AIAA Journal of Thermophysics and Heat Transfer, Vol. 20, 2006, pp. 764-771.

Zhang, X. Z., Kim, S. I., and Hassan. I., "Detached-Eddy Simulation of a Louver-Cooling Scheme for Turbine Blades", AIAA Journal of Propulsion and Power, accepted for publication on 3 May 2008.

Zhang, C. X-Z., and Hassan. I., "Computational Study of the Effects of Shock Waves on Film Cooling Effectiveness", ASME Journal of Engineering for Gas Turbines and Power, accepted for publication on 17 Jun 2008.

Zhang, C. X-Z., and Hassan. I., "Rotational Effects on Film Cooling Performance – Simulation of a Louver Cooling Scheme on a Rotating Turbine Blade", will be submitted to ASME Journal of Engineering for Gas Turbines and Power.

Conference

Zhang, X. Z., Hassan, I., and Lucas, T., "A Louver Cooling Scheme for Gas Turbines – Multiple Rows", 5th International Symposium on Turbulence, Heat and Mass Transfer, Croatia, September 2006.

Zhang, C., and Hassan, I., "Numerical Study of a Novel Cooling Scheme on a Transonic Airfoil", 5th International Conference on Computational Heat and Mass Transfer, Canmore, Alberta, Canada, June 18-22, 2007.

Zhang, C. X-Z., Kim, S. I., Hassan, I. G., "Unsteady Simulations for an Advanced-Louver Cooling Scheme", ASME Turbo Expo 2008: Power for Land, Sea and Air, June 9-13, 2008, Berlin, Germany, ASME paper GT2008-51477.

Kim, S. I., Hassan, I. G., and Zhang, X. Z., "Unsteady Simulation of Film Cooling Flow from an Inclined Cylindrical Jet", 2007 ASME-JSME Thermal Engineering and Summer Heat Transfer Conference, July 8-12, 2007, Vancouver, BC, Canada, ASME paper HT2007-32401.

Zhang, X-Z. C., and Hassan, I., "Computational Study of the Effects of Shock Waves on Film Cooling Effectiveness" will be presented at the ASME Turbo Expo 2009, June 8-12, 2009, Orlando, FL, USA.

Zhang, X-Z. C., and Hassan, I., "Rotational Effects on Film Cooling Performance – Simulation of a Louver Cooling Scheme on a Rotating Turbine Blade", will be presented at the ISABE 2009, 19th International Society for Air Breathing Engines Conference, September 7-11, 2009, Montreal, Canada.

References

[1] Bunker, R. S, "A Review of Shaped Hole Turbine Film-Cooling Technology", Journal of Heat Transfer, Vol. 127, 2005, pp. 441-453.

[2] Goldstein, R. J., Eckert, E. R. G., and Ramsey, J. W., "Film Cooling with Injection through Holes: Adiabatic Wall Temperatures Downstream of a Circular Hole", Journal of Engineering for Power, Series A, Vol. 90, 1968, pp. 384-395.

[3] Sen, B., Schmidt, D. L., Bogard, D. G., "Film Cooling With Compound Angle Holes: Heat Transfer", Journal of Turbomachinery, Vol. 118, 1996, pp. 800-806.

[4] Sinha, A. K., Bogard, D. G., and Crawford, M. E., "Film-Cooling Effectiveness Downstream of a Single Row of Holes with Variable Density Ratio", Journal of Turbomachinery, Vol. 113, 1991, pp. 442-449.

[5] Goldstein, R. J., and Jin, P., "Film Cooling Downstream of a Row of Discrete Holes with Compound Angle", Journal of Turbomachinery, Vol. 123, 2001, pp. 222-230.

[6] Pedersen, D. R., Eckert, E. R. G., and Goldstein, R. J., "Film Cooling with Large Density Difference Between the Mainstream and the Secondary Fluid Measured by the Heat-Mass Transfer Analogy", Journal of Heat Transfer, Vol. 99, 1977, pp. 620-627.

[7] Cho, H. H., Kang, S. G., and Rhee, D. H., "Heat/Mass Transfer Measurement Within a Film Cooling Hole of Square and Rectangular Cross Section", Journal of Turbomachinery, Vol. 123, 2001, pp. 806-814.

[8] Sargison, J. E., Guo, S. M., Oldfield, M. L. G., Lock, G. D., and Rawlinson, A. J., "A Converging Slot-Hole Film-Cooling Geometry – Part 2: Transonic Nozzle Guide Vane Heat Transfer and Loss", Journal of Turbomachinery, Vol. 124, 2002, pp. 461-471.

[9] Chen, P-H, Ding, P-P, and Ai, D., "An improved data reduction method for transient liquid crystal thermography on film cooling measurements", International Journal of Heat and Mass Transfer, Vol. 44, 2001, pp. 1379-1387.

[10] Ahn, J., Jung, I. S., and Lee, J. K., "Film cooling from two rows of holes with opposite orientation angles: injection behavior and adiabatic film cooling effectiveness", International Journal of Heat and Fluid Flow, Vol. 24, 2003, pp. 91-99.

[11] Vogel, G., Graf, A. B. A., Wolfersdorf J., and Weigand, B., "A Novel Transient Heater-Foil Technique for Liquid Crystal Experiments on Film-Cooled Surfaces", Journal of Turbomachinery, Vol. 125, 2003, pp. 529-537.

[12] Ekkad, S. V., and Han, J-C., "A transient liquid crystal thermography technique for gas turbine heat transfer measurements", Meas. Sci. Technol., Vol. 11, 2000, pp. 957-968.

[13] Lee, H-W, Park, J. J., and Lee, J. S., "Flow visualization and film cooling effectiveness measurements around shaped holes with compound angle orientations", International Journal of Heat and Mass Transfer, Vol. 45, 2002, pp. 145-156.

[14] Jung, I. S., Lee, J. S., and Ligrani, P. M., "Effects of Bulk Flow Pulsations on Film Cooling with Compound Angle Holes: Heat Transfer Coefficient Ratio and Heat Flux Ratio", Journal of Turbomachinery, Vol. 124, 2002, pp. 142-151.

[15] Jessen, W., Schroder, W., and Klaas, M., "Evaluation of jets effusing from inclined holes into crossflow", International Journal of Heat and Fluid Flow., Vol. 28, 2007, pp. 1312-1326.

[16] Ahn, J., Schobeiri, M. T., Han, J-C, and Moon, H-K, "Film Cooling Effectiveness on the Leading Edge Region of a Rotating Turbine Blade with Two Rows of Film Cooling Holes Using Pressure Sensitive Paint", Journal of Heat Transfer, Vol. 128, 2006, pp. 879-888.

[17] Mhetras, S., Narzary, D., Gao, Z., and Han, J-C., "Effect of a Cutback Squealer and Cavity Depth on Film-cooling Effectiveness on a Gas Turbine Blade Tip", Journal of Turbomachinery, Vol. 130, 2008, pp. 1-13.

[18] Gao, Z., Narzary, D. P., and Han, J-C, "Film cooling on a gas turbine blade pressure side or suction side with axial shaped holes", International Journal of Heat and Mass Transfer, Vol. 51, 2008, pp. 2139-2152.

[19] Schulz, A., "Infrared thermography as applied to film cooling of gas turbine components", Meas. Sci. Technol., Vol. 11, 2000, pp. 948-956.

[20] Baldauf, S., Schulz, A., and Wittig, S., "High-Resolution Measurements of Local Heat Transfer Coefficients from Discrete Hole Film Cooling", Journal of Turbomachinery, Vol. 123, 2001, pp. 749-757.

[21] Li, X., Gaddis, J. L., and Wang, T., "Mist/Steam Heat Transfer in Confined Slot Jet Impingement", Journal of Turbomachinery, Vol. 123, 2001, pp. 161-167.

[22] Li, X-C, and Wang, T., "Simulation of Film Cooling Enhancement with Mist Injection", Journal of Heat Transfer, Vol. 128, 2006, pp. 509-519.

[23] Nasir, H., Acharya, S., and Ekkad, S., "Improved film cooling from cylindrical angled holes with triangular tabs: effect of tab orientations", International Journal of Heat and Fluid Flow, Vol. 24, 2003, pp. 657-668.

[24] Dittmar, J., Schulz, A., and Wittig, S., "Assessment of Various Film-Cooling Configurations Including Shaped and Compound Angle Holes Based on Large-Scale Experiments", Journal of Turbomachinery, Vol. 125, 2003, pp. 57-64.

[25] Colban, W., Gratton, A., Thole, K. A., and Haendler, M., "Heat Transfer and Film-Cooling Measurements on a Stator Vane with Fan-Shaped Cooling Holes", Journal of Turbomachinery, Vol. 128, 2006, pp. 53-61.

[26] Colban, W., and Thole, K., "Influence of hole shape on the performance of a turbine vane endwall film-cooling scheme", International Journal of Heat and Fluid Flow, Vol. 28, 2007, pp. 341-356.

[27] Miao, J-M, and Wu, C-Y, "Numerical approach to hole shape effect on film cooling effectiveness over flat plate including internal impingement cooling chamber", International Journal of Heat and Mass Transfer, Vol. 49, 2006, pp. 919-938.

[28] Gritsch, M., Schulz, A., and Wittig, S., "Adiabatic Wall Effectiveness Measurements of Film-Cooling Holes With Expanded Exits", Journal of Turbomachinery, Vol. 120, 1998, pp. 549-556.

[29] Sargison, J. E., Guo, S. M., Oldfield, M. L. G., Lock, G. D., and Rawlinson, A. J., "A Converging Slot-Hole Film-Cooling Geometry – Part 1: Low-Speed Flat-Plate Heat Transfer and Loss", Journal of Turbomachinery, Vol. 124, 2002, pp. 453-460.

[30] Taslim, M. E., and Khanicheh, A., "Film Effectiveness Downstream of a Row of Compound Angle Film Holes", Journal of Heat Transfer, Vol. 127, 2005, pp. 434-440.

[31] Okita, Y., and Nishiura, M., "Film Effectiveness Performance of an Arrowhead-Shaped Film-Cooling Hole Geometry", Journal of Turbomachinery, Vol. 129, 2007, pp. 331-339.

[32] Rutledge, J. L., Robertson, D., and Bogard, D. G., "Degradation of Film Cooling Performance on a Turbine Vane Suction Side due to Surface Roughness", Journal of Turbomachinery, Vol. 128, 2006, pp. 547-554.

[33] Guo, S. M., Lai, C. C., Jones, T. V., Oldfield, M. L. G., Lock, G. D., and Rawlinson, A. J., "Influence of Surface Roughness on Heat Transfer and Effectiveness for a Fully Film Cooled Nozzle Guide Vane measured by Wide Band Liquid Crystals and Direct Heat Flux Gages", Journal of Turbomachinery, Vol. 122, 2000, pp. 709-716.

[34] Li, X-C, and Wang, T., "Computational analysis of surface curvature effect on mist film cooling performance", Proceedings of the ASME Turbo Expo, Vol. 4, Part A, 2007, pp. 433-443.

[35] Waye, S. K., and Bogard, D. G., "High-Resolution Film cooling Effectiveness Comparison of Axial and Compound Angle Holes on the Suction Side of a Turbine Vane", Journal of Turbomachinery, Vol. 129, 2007, pp. 202-211.

[36] Ethridge, M. I., Cutbirth, J. M., and Bogard, D. G., "Scaling of Performance for Varying Density Ratio Coolants on an Airfoil with Strong Curvature and Pressure Gradient Effects", Journal of Turbomachinery, Vol. 123, 2001, pp. 231-237.

[37] Al-Hamadi, A. K., Jubran, B. A., and Theodoridis, G., "Turbulence intensity effects on film cooling and heat transfer from compound angle holes with particular application to gas turbine blades", Energy Convers. Mgmt, Vol. 39, 1998, pp. 1449-1457.

[38] Mayhew, J. E., Baughn, J. W., and Byerley, A. R., "The effect of freestream turbulence on film cooling adiabatic effectiveness", International Journal of Heat and Fluid Flow, Vol. 24, 2003, pp. 669-679.

[39] Saumweber, C., Schulz, A., and Wittig, S., "Free-Stream Turbulence Effects on Film Cooling With Shaped Holes", Journal of Turbomachinery, Vol. 125, 2003, pp. 65-73.

[40] Coulthard, S. M., Volino, R. J., and Flack, K. A., "Effect of Jet Pulsing on Film Cooling – Part I: Effectiveness and Flow-Field Temperature Results", Journal of Turbomachinery, Vol. 129, 2007, pp. 232-246.

[41] Jackson, D. J., Lee, K. L., Ligrani, P. M., and Johnson, P. D., "Transonic Aerodynamic Losses Due to Turbine Airfoil, Suction Surface Film Cooling", Journal of Turbomachinery, Vol. 122, 2000, pp. 317-326.

[42] Medic, G., and Durbin, P. A., "Toward Improved Film Cooling Prediction", Journal of Turbomachinery, Vol. 124, 2002, pp. 193-199.

[43] Garg, V. K., "Heat transfer on a film-cooled rotating blade using different turbulence models", International Journal of Heat and Mass Transfer, Vol. 42, 1999, pp. 789-802.

[44] Keimasi, M. R., and Taeibi-Rahni, M., "Numerical Simulation of Jets in a Crossflow Using Different Turbulence Models", AIAA Journal, Vol. 39, 2001, pp. 2268-2277.

[45] Guo, T-T, Liu, J-H, Li, S-H, and Xu, Z., "Large eddy simulation of film cooling", Proceedings of the Chinese Society of Electrical Engineering, Vol. 27, 2007, pp. 83-87.

[46] Rozati, A., and Tafti, D. K., "Large-eddy simulation of leading edge film cooling: Analysis of flow structures, effectiveness, and heat transfer coefficient", International Journal of Heat and Fluid Flow, Vol. 29, 2008, pp. 1-17.

[47] Renze, P., Schroder, W., and Meinke, M., "Large-eddy simulation of film cooling flows at density gradients", International Journal of Heat and Fluid Flow, Vol. 29, 2008, pp. 18-34.

[48] Martini, P., Schulz, A., Bauer, H-J., Whitney, C. F., "Detached Eddy Simulation of Film Cooling Performance on the Trailing Edge Cutback of Gas Turbine Airfoils", Journal of Turbomachinery, Vol. 128, 2006, pp. 292-299.

[49] Bell, C. M., Hamakawa, H., and Ligrani, P. M., "Film cooling From Shaped Holes", Journal of Heat Transfer, Vol. 122, 2000, pp. 224-232.

[50] Yu, Y., Yen, C. H., Shih, T. I. P., and Chyu, M. K., "Film Cooling Effectiveness and Heat Transfer Coefficient Distributions Around Diffusion Shaped Holes", Journal of Heat Transfer, Vol. 124, 2002, pp. 820-827.

[51] Immarigeon, A., and Hassan, I., "An advanced impingement/film cooling scheme for gas turbines – numerical study", International Journal of Numerical Methods for Heat & Fluid Flow, Vol. 16, 2006, pp. 470-493.

[52] Zhang, X. Z., and Hassan. I., "Film Cooling Effectiveness of an Advanced-Louver Cooling Scheme for Gas Turbines", Journal of Thermophysics and Heat Transfer, Vol. 20, 2006, pp. 754-763.

[53] Zhang, X. Z., and Hassan, I., "Numerical investigation of heat transfer on film cooling with shaped holes", International Journal of Numerical Methods for Heat & Fluid Flow, Vol. 16, 2006, pp. 848-869.

[54] Schmidt, D. L., Sen, B., and Bogard, D. G., "Film Cooling With Compound Angle Holes: Adiabatic Effectiveness", Journal of Turbomachinery, Vol. 118, 1996, pp. 807-813.

[55] Thole, K., Gritsch, M., Schulz, A., and Wittig, S., "Flowfield Measurements for Film-Cooling Holes With Expanded Exits", ASME Journal Of Turbomachinery, Vol. 120, 1998, pp. 327-336.

[56] Gritsch, M., Colban, W., Schar, H., and Dobbeling, K., "Effect of Hole Geometry on the Thermal Performance of Fan-Shaped Film Cooling Holes", Journal of Turbomachinery, Vol. 127, 2005, pp. 718-725.

[57] Makki, Y. H., and Jakubowski, G. S., "An Experimental Study of Film Cooling from Diffused Trapezoidal Shaped Holes", AIAA Paper AIAA-86-1326, 1986.

[58] Rhee, D. H., Lee, Y. S., and Cho, H. H., "Film Cooling Effectiveness and Heat Transfer of Rectangular-shaped Film Cooling Holes," ASME Paper No. GT-2002-30168, 2002.

[59] Giebert, D., Gritsch, M., Schulz, A., and Wittig, S., "Film-Cooling from Holes with Expanded Exits: A Comparison of Computataional Results with Experiments", ASME Paper 97-GT-163, 1997.

[60] Hyams, D. G., and Leylek, J. H., "A Detailed Analysis of Film-Cooling Physics: Part III – Streamwise Injection with Shaped Holes," Journal of Turbomachinery, Vol. 122, 2000, pp. 122-132.

[61] Bohn, D., Ren, J., and Kusterer, K., "Conjugate Heat Transfer Analysis of Film Cooling Configurations with Different Hole Geometries", ASME Paper GT2003-38359, 2003.

[62] Jubran, B. A., and Maiteh, B. Y., "Film cooling and heat transfer from a combination of two of simple and/or compound angle holes in inline and/or staggered configuration", Heat and Mass Transfer, Vol. 34, 1999, pp. 495-502.

[63] Ligrani, P. M., Wigle, J. M., Ciriello, S., and Jackson, S. M., "Film-Cooling From Holes With Compound Angle Orientations: Part 1 – Results Downstream of Two Staggered Rows of Holes With 3d Spanwise Spacing", Journal of Heat Transfer, Vol. 116, 1994, pp. 341-352.

[64] Yuen, C. H. N., and Martinez-Botas, R. F., "Film Cooling Characteristics of Rows of Round Holes at Various Streamwise Angles in a Crossflow: Part I. Effectiveness", International Journal of Heat and Mass Transfer, Vol. 48, 2005, pp. 4995-5016.

[65] Yuen, C. H. N., and Martinez-Botas, R. F., "Film Cooling Characteristics of Rows of Round Holes at Various Streamwise Angles in a Crossflow: Part II. Heat Transfer Coefficients", International Journal of Heat and Mass Transfer, Vol. 48, 2005, pp. 5017-5035.

[66] Maiteh, B. Y., and Jubran, B. A., "Effects of pressure gradient on film cooling effectiveness from two rows of simple and compound angle holes in combination", Energy Conversion and Management, Vol. 45, 2004, pp. 1457-1469.

[67] Bergeles, G., Gosman, A. D., and Launder, B. E., "Double-Row Discrete-Hole Cooling: an Experimental and Numerical Study", Journal of Engineering for Power, Vol. 102, 1980, pp. 498-503.

[68] Amer, A. A., Jubran, B. A., and Hamdan, M. A., "Comparison of different two-equaiton turbulence models for prediction of film cooling from two rows of holes", Numerical Heat Transfer, Vol. 21, 1992, pp.143-162.

[69] Fric, T. F., and Roshko, A., "Vortical Structure in the Wake of a Transverse Jet", Journal of Fluid MEchancs, Vol. 279, 1994, pp. 1-47.

[70] Roy, S., Kapadia, S., and Heidmann, J. D., "Film Cooling Analysis Using DES Turbulence Model", ASME Paper GT-2003-38140, 2003.

[71] Kapadia, S., Roy, S., and Heidmann, J., "Detached Eddy Simulation of Turbine Blade Cooling", AIAA Paper AIAA-2003-3632, 2003.

[72] Tyagi, M., and Acharya, S., "Large Eddy Simulation of Film Cooling Flow From an Inclined Cylindrical Jet", Journal of Turbomachinery, Vol. 125, 2003, pp. 734-742.

[73] Wegner, B., Huai, Y., and Sadiki, A., "Comparative Study of Turbulent Mixing in Jet in Cross-Flow Configurations Using LES", International Journal of Heat and Fluid Flow, Vol. 25, 2004, pp. 767-775.

[74] Holloway, D., Walters, D. K., and Leylek, J. H., "Computational Study of Jet-in-Crossflow and Film Cooling Using a New Unsteady-Based Turbulence Model", ASME Paper GT-2005-68155, 2005.

[75] Guo, X., Schroder, W., and Meinke, M., "Large-Eddy Simulations of Film Cooling Flows", Computers & Fluids, Vol. 35, 2006, pp. 587-606.

[76] Ito, S., Goldstein, R. J., and Eckert, E. R. G., "Film Cooling of a Gas Turbine Blade", Journal of Engineering for Power, Vol. 100, 1978, pp. 476-481.

[77] Teng, S., Sohn, D. K., and Han, J-C, "Unsteady Wake Effect on Film Temperature and Effectiveness Distribution for a Gas Turbine Blade", Journal of Turbomachinery, Vol. 122, 2000, pp. 340-347.

[78] Thakur, S. T., Wright, J., and Shyy, W., "Convective film cooling over a representative turbine blade leading-edge", International Journal of Heat and Mass Transfer, Vol. 42, 1999, pp. 2269-2285.

[79] Colban, W., Gratton, A., Thole, K. A., and Haendler, M., "Heat Transfer and Film-Cooling Measurements on a Stator Vane With Fan-Shaped Cooling Holes", Journal of Turbomachinery, Vol. 128, 2006, pp. 53-61.

[80] Lakehal, D., Theodoridis, G. S., and Rodi, W., "Three-dimensional flow and heat transfer calculations of film cooling at the leading edge of symmetrical turbine blade model", International Journal of Heat and Fluid Flow, Vol. 22, 2001, pp. 113-122.

[81] Colban, W., Thole, K. A., and Haendler, M., "Experimental and Computational Comparison of Fan-Shaped Film Cooling on a Turbine Vane Surface", Journal of Turbomachinery, Vol. 129, 2007, pp. 23-31.

[82] Haas, W., Rodi, W., and Schonung, B., "The Influence of Density Difference Between Hot and Coolant Gas on Film Cooling by a Row of Holes: Predictions and Experiments", Journal of Turbomachinery, Vol. 114, 1992, pp. 747-755.

[83] Guo, S. M., Lai, C. C., Jones, T. V., Oldfield, M. L. G., Lock, G. D., and Rawlinson, A. J., "The application of thin-film technology to measure turbine-vane heat transfer and

effectiveness in a film-cooled, engine-simulated environment", International Journal of Heat and Fluid Flow, Vol. 19, 1998, pp. 594-600.

[84] Drost, U., and Bolcs, A., "Investigation of Detailed Film Cooling Effectiveness and Heat Transfer Distributions on a Gas Turbine Airfoil", Journal of Turbomachinery, Vol. 121, 1999, pp. 233-242.

[85] Reiss, H., and Bolcs, A., "Experimental Study of Showerhead Cooling on a Cylinder Comparing Several Configurations Using Cylindrical and Shaped Holes", Journal of Turbomachinery, Vol. 122, 2000, pp. 161-169.

[86] Juhany, K. A., and Hunt, M. L., "Flowfield Measurements in Supersonic Film Cooling Including the Effect of Shock-Wave Interaction", AIAA Journal, Vol. 32, 1994, pp. 578-585.

[87] Ligrani, P. M., Saumweber, C., Schulz, A., and Wittig, S., "Shock Wave-Film Cooling Interactions in Transonic Flows", Journal of Turbomachinery, Vol. 123, 2001, pp. 788-797.

[88] Dring, R. P., Blair, M. F., and Joslyn, H. D., "An Experimental Investigation of Film Cooling on a Turbine Rotor Blade", Journal of Engineering for Power, Vol. 102, 1980, pp. 81-87.

[89] Abhari, R. S., and Epstein A. H., "An Experimental Study of Film Cooling in a Rotating Transonic Turbine", Journal of Turbomachinery, Vol. 116, 1994, pp. 63-70.

[90] Takeishi, K., Aoki, S., Sato, T., and Tsukagoshi, K., "Film Cooling on a Gas Turbine Rotor Blade", Journal of Turbomachinery, Vol. 114, 1992, pp. 828-834.

[91] Weigand, B., and Harasgama, B., "Computations of a Film Cooled Turbine Rotor Blade with Non-Uniform Inlet Temperature Distribution Using a Three-Dimensional Viscous Procedure", ASME paper 94-GT-15, 1994.

[92] Garg, V. K., "Adiabatic Effectiveness and Heat Transfer Coefficient on a Film-Cooled Rotating Blade", Numerical Heat Transfer, Part A, Vol. 32, 1997, pp. 811-830.

[93] Garg, V. K., "Heat Transfer on a Film-Cooled Rotating Blade", International Journal of Heat and Fluid Flow, Vol. 21, 2000, pp. 134-145.

[94] Garg, V. K., "Heat Transfer on a Film-Cooled Rotating Blade Using Different Turbulence Models", International Journal of Heat and Mass Transfer, Vol. 42, 1999, pp. 789-802.

[95] Ahn, J., Schobeiri, M. T., Han, J-C, and Moon, H-K, "Effect of Rotation on Leading Edge Region Film Cooling of a Gas Turbine Blade with Three Rows of Film Cooling Holes", International Journal of Heat and Mass Transfer, Vol. 50, 2007, pp. 15-25.

[96] Leylek, J. H., and Zerkle, R. D., "Discrete-Jet Film Cooling: A Comparison of Computational Results with Experiments", ASME Paper 93-GT-207, 1993.

[97] Walters, D. K., and Leylek, J. H., "A Detailed Analysis of Film Cooling Physics: Part I: Streamwise Injection With Cylindrical Holes", Journal of Turbomachinery, Vol. 122, 2000, pp. 102-112.

[98] Shih, T.-H., Liou, W. W., Shabbir, A., Yang, Z., and Zhu, J., "A New k-ε Eddy-Viscosity Model for High Reynolds Number Turbulent Flows - Model Development and Validation", Computers Fluids, Vol. 24, 1995, pp. 227-238.

[99] Launder, B. E., and Spalding D. B., "The Numerical Computation of Turbulent Flows", Computer Methods in Applied Mechanics and Engineering, Vol. 3, 1974, pp. 269-289.

[100] FLUENT 6.3 Documentation, User's Guide, Chapter – 9, 12, 13. Fluent Inc., 2006.

[101] Zhang, X-Z, "An Advanced-Louver Cooling Scheme for Gas Turbine – Adiabatic Effectiveness and Heat Transfer Performance", MSc. Thesis, Concordia University, 2004.

[102] Kim, S., Zhang, X. Z., and Hassan, I., "Unsteady Simulation of Film Cooling Flow from an Inclined Cylindrical Jet", ASME Paper HT2007-32401, 2007.

[103] Mulugeta, K. B., and Patankar, S. V., "A Numerical Study of Discrete-Hole Film Cooling", ASME Paper 96-WA/HT-8, 1996.

[104] Ferguson, J. D., Walters, D. K., and Leylek, J. H., "Performance of Turbulence Models and Near-Wall Treatments in Discrete Jet Film Cooling Simulations", ASME Paper 98-GT-438, 1998.

[105] Dubief, Y., and Delcayre, F., "On Coherent-Vortex Identification in Turbulence," Journal of Turbulence, Vol. 1, article 011, 2000, pp. 1-22.

[106] Furukawa, T., and Ligrani, P., "Transonic Film Cooling Effectiveness from Shaped Holes on a Simulated Turbine Airfoil", Journal of Thermophysics and Heat Transfer, Vol. 16, 2002, pp. 228-237.

[107] John, J. E. A., Gas Dynamics, Allyn and Bacon, Boston, 1969, pp. 120-123.

[108] Ben-Dor, G., Shock Wave Reflection Phenomena, Springer-Verlag, New York, 1992, pp. 10-16.

[109] Yang, H., Gao, Z., Chen, H. C., Han, J. C., and Schobeiri, M. T., "Prediction of Film Cooling and Heat Transfer on a Rotating Blade Platform with Stator-Rotor Purge and Discrete Film-Hole Flows in a 1-1/2 Turbine Stage", ASME paper GT2007-27069, 2007.

ENCS PRINTING

Laser Printer: HIGHLIGHTER
job id: 84903

user: xuezh_zh
host: SAMBA Authenticated
file: Microsoft Word - ChadPhD_ThesisFinal.doc
Date: Wed Oct 8 10:47:07 EDT 2008
Pages printed: 215
Quota remaining: 1950